



**TURUN  
YLIOPISTO**  
UNIVERSITY  
OF TURKU

A large, cylindrical observatory dome with a corrugated metal exterior and a ribbed dome top, illuminated by the warm light of a sunset. The sky is a mix of blue and orange, with some clouds visible. A metal staircase leads up to a small entrance on the side of the dome.

**GALAXY EVOLUTION  
THROUGH THE LENS OF  
ACTIVE GALACTIC NUCLEI,  
THEIR HOST GALAXIES, AND  
ENVIRONMENTS**  
An observational study

**Maria Babakhanyan Stone**





**TURUN  
YLIOPISTO**  
UNIVERSITY  
OF TURKU

# **GALAXY EVOLUTION THROUGH THE LENS OF ACTIVE GALACTIC NUCLEI, THEIR HOST GALAXIES, AND ENVIRONMENTS**

An observational study

---

Maria Babakhanyan Stone

## University of Turku

---

Faculty of Science  
Department of Physics and Astronomy  
Astronomy  
Doctoral programme in Exact Sciences

## Supervised by

---

Dr. Kari Nilsson  
Finnish Centre for Astronomy with ESO  
(FINCA), University of Turku, Finland

Dr. Jari Kotilainen  
FINCA, University of Turku,  
Finland

Dr. Roberto De Propris  
FINCA, University of Turku, Finland;  
Botswana International University of  
Science and Technology (BIUST),  
Botswana

## Reviewed by

---

Dr. Andrea Merloni  
Max-Planck Institute for Extraterrestrial  
Physics, Germany

Prof. Peter Johansson  
University of Helsinki, Finland

## Opponent

---

Dr. Anna Wolter  
National Institute for Astrophysics (INAF),  
Astronomical Observatory of Brera, Italy

The originality of this publication has been checked in accordance with the University of Turku quality assurance system using the Turnitin OriginalityCheck service.

Cover Image: NOT telescope in La Palma, Spain. Photographer Maria Stone.

ISBN 978-951-29-9720-6 (PRINT)  
ISBN 978-951-29-9721-3 (PDF)  
ISSN 0082-7002 (PRINT)  
ISSN 2343-3175 (ONLINE)  
Painosalama, Turku, Finland, 2024

*Dedicated to my husband James and to my children Angel, Natali, and Archie  
To the memory of my grandmother Maria Skidanova (aka Babo)  
and of my first astronomy teacher Armen Oskanyan*

\*\*\*

I bless your paths and pray for thee,  
with tenderness and love.  
The angels guard your steps, but see,  
the life may still hit hard.  
Then let the echos of my lullabies  
return your soul to joy and peace.  
Hush, jána, hush, just close your eyes —  
and feel again my gentle kiss.

Maria Stone

UNIVERSITY OF TURKU

Faculty of Science

Department of Physics and Astronomy

Astronomy

STONE, MARIA BABAKHANYAN: Galaxy evolution through the lens of active galactic nuclei, their host galaxies, and environments

Doctoral dissertation, 189 pp.

Doctoral programme in Exact Sciences

April 2024

## ABSTRACT

The body of research relayed in this dissertation pertains to investigating the immediate environments of Type I quasars for clues to the formation and evolution of galaxies through observations. The neighboring galaxies are key agents in the local environment around the quasar. Through longslit (Paper I) and multi-object spectroscopy (Paper II), I contributed to the identification of neighboring galaxies within several hundred kiloparsec projected distance of 44 low redshift quasars from the Falomo et al. (2014) catalog of 416 quasars located in the Stripe82 region of the Sloan Digital Sky Survey (SDSS). I found that the quasars and inactive galaxies had a similar number of companion galaxies at low redshifts and that the quasar companions had a moderate star formation rate.

In papers III and IV, I was able to tap into the rich archival data from the Galaxy and Mass Assembly (GAMA) spectroscopic survey to investigate quasar environments at low redshifts using larger statistics (more than 200 quasars). I studied the properties of the bright neighbors within a close volume centered on a quasar and looked at the host galaxy star formation histories. I found that the properties of spectroscopically confirmed bright neighbors around quasars are statistically similar to those of inactive galaxies.

The main conclusion brought to light through this dissertation is that at low-redshift Type I quasar activity is not impacted in a major way by its environment, but instead internal processes within the quasar host galaxy itself are the more probable mechanism for the AGN phenomenon. While it is possible that some major mergers fuel SMBHs at low-redshift, this is not the predominant scenario. Overall, this body of work contributes the crucial observational data to contrast and constrain the theoretical models of how AGN are triggered and their role in the life of the host galaxy as well as a potential impact on galaxies in its vicinity.

**KEYWORDS:** galaxy evolution, quasars, supermassive black holes, active galactic nuclei, active galaxies, star formation, galaxy environments

TURUN YLIOPISTO

Matemaattis-luonnontieteellinen tiedekunta

Fysiikan ja tähtitieteen laitos

Tähtitiede

STONE, MARIA BABAKHANYAN: Galaxy evolution through the lens of active galactic nuclei, their host galaxies, and environments

Väitöskirja, 189 s.

Eksaktien tieteiden tohtoriohjelma

huhtikuu 2024

## TIIVISTELMÄ

Tässä väitöskirjatyössä esitellään havaintotuloksia, jotka liittyvät tyypin I kvasaarien välittömässä ympäristössä sijaitsevien galaksien muodostumiseen ja evoluutioon. Kvasaarien lähigalaksit antavat tärkeää tietoa kvasaarien lähiolosuhteista. Väitöskirjan ensimmäisessä (I) ja toisessa (II) julkaisussa identifioin 44 matalan punasiirtymän “Stripe 82” -kvasaarin (Falomo et al. 2014, yhteensä 416 kvasaaria) lähigalakseja (projisoitu etäisyys muutamia satoja kiloparsekkeja) käyttäen sekä longslit että MOS-spektroskopiaa. Tulokseni mukaan matalan punasiirtymän kvasaareilla ja “tavallisilla” galakseilla on keskimäärin yhtä monta lähigalaksia. Lisäksi havaitsin, että kvasaarien lähigalaksien tähtienmuodostus on melko maltillista.

Väitöskirjan julkaisuissa III ja IV käytin hyväkseni Galaxy and Mass Assembly (GAMA) -tietokannan runsasta materiaalia tutkiakseni matalan punasiirtymän kvasaarien lähiympäristöjä suuremmalla otoksella (yli 200 kvasaaria). Tutkin kirkkaimpien lähigalaksien morfologiaa ja tähtienmuodostushistoriaa ja havaitsin, että spektroskooppisesti vahvistetut kirkkaat lähigalaksit ovat samanlaisia sekä kvasaarien että tavallisten galaksien ympäristöissä.

Väitöskirjan päätulos on, että matalilla punasiirtymillä tyypin I kvasaarien aktiivisuuden käynnistämiseen ei tarvita vuorovaikutusta lähigalaksien kanssa vaan aktiivisuus syntyy emogalaksin sisäisistä mekanismeista. On toki mahdollista, että galaksien sulautuessa yhteen vuorovaikutus käynnistää ytimen aktiivisuuden, mutta tämä ei ole pääasiallinen reitti. Väitöskirjatyön tuloksena on syntynyt havaintoaineistoa, jolla on tärkeä rooli kun tutkitaan aktiivisten galaksiytimien vaikutusta niiden emogalaksien ominaisuuksiin ja kehitykseen sekä niiden mahdollista vaikutusta lähigalakseihin.

ASIASANAT: galaksien kehitys, kvaasarit, supermassiiviset mustat aukot, aktiiviset galaksiytimet, aktiiviset galaksit, tähtienmuodostus, galaksien ympäristöt

# Acknowledgements

Galaxies are spectacular objects. These “island-universes” are considered to be the units of our cosmos. The dimensions and timescales of galaxies are usually beyond our human experiences. However, studying galaxies helps us understand our place in the Universe.

This *magnum opus* summarizes my work on the topic and signifies the culmination of a seven year journey as of April 2024. As with any other such marathon, my success stands on the shoulders of numerous giants, who I would like to acknowledge here, focusing on the positives.

## Babo

One of the two people to whom I dedicate this book (albeit posthumously) is my maternal grandmother Maria Skidanova or *Babo*. Babo had a very tough life, full of unfairness, mistreatment, ungrateful attitude, loneliness, and pain. She lost her father when she was three years old, her mother at the age of 13. She dropped out of the seventh grade to take care of her half-siblings and work. She had abusive step-parents who forced her out of her own house. Her own marriage ended in a divorce after a betrayal, and she raised on her own her children. Even her later years were difficult. And yet, my grandmother is extremely cherished by me because she is one of the few people who loved me for me regardless of anything that I could have ever given her or any accolades I achieved in life.

She had a loving, generous, joyful soul, bringing sunshine along with her, despite it all, and her vivacity and kindness overpowered any imperfections. For example, as other elderly ladies in Armenia sat near their apartment buildings in groups, as we walked by with my grandmother, she would joke, “Are you ladies waiting for your knight on a white horse?” She was a woman of action — not only taking care of her family selflessly, helping out neighbors and relatives without asking anything in return, serving at the church, but also, against tradition, taking charge of her own life. She worked many different jobs, in particular servicing the trains, had her own apartment, was financially independent, was honest, and had strong principles.

Babo supported the educational aspirations of her daughters and granddaughters. In the face of challenges, she was unstoppable and imparted to me also not to sweat the stuff, such as mean things people say — she would advise: “let it go in one ear and out the other, you go and tell them that you have such a grandmother who will



show them, so what?" Many a time, when I had difficulties in moving forward in my PhD program, I felt her cheering for me from the heavens.

#### My first astronomy teacher

Armen Oskanian was my first astronomy teacher. I met him on the first day of my high school, when he was presenting the Astronomy club activity, where I participated for four years. He was an excellent educator and also went above and beyond for the students. He organized night observing sessions and trips to the Byurakan Observatory. He also gave me individual tutoring lessons in my home on various coordinate systems, logarithms, magnitude systems, and so on. He taught me how to read the night sky, the various star names, the myths and stories behind the different constellations and stars. I did not apply myself during the Astronomy club days and did not do my homework. So during my PhD degree, I thought it was a chance for me to apply myself and not make the same mistakes, to try my hardest, giving me peace that I have done what I could. He also was the first person to present to me the concept of quasars. I am extremely thankful for his dedication, time, and teachings.

#### The beginnings

Early 1990s. Yerevan, Armenia. A neighborhood on a hill, at the edge of the city, bordering the nearby villages. A typical afternoon. I pull the children's books on science from the bookshelf, and enjoy reading about the planets, stars, and about interesting lives of astronomers.

A typical evening. I procured some lenses from somewhere and am trying to put them together, observing the various features on the surface of the bright Moon, outside of our balcony on the fifth floor of the rectangular building.

A typical dawn. The sunlight did not break the darkness yet, I am out heading with a bucket towards the grocery shops to stand in line for our family's portion of oil, passing the dark buildings of the neighborhood, exactly the same as the one where I live in, made of bright colored tuff, yet still grayish-black in the night. I meet the curving line of people in coats, it's cold, it's dark, quiet whispers here and there. My gaze lifts up above the darkness around me into the bright night sky. There is a bright star. I recognize that it is the Morning Star, Venus, the planet shining, leading, enticing dreams, bringing hope... I measure in my mind the 40 degrees that it should have from the Sun - the horizon line, as the Sun will soon break that line with powerful rays to give us a new day. I think of the astronomer who wanted to also see the Mercury, but it is so close to the Sun, that he could never do it - will I ever be able to see the Mercury?

A typical morning. I gaze out the window at the large mountain. The sun is rising. I notice that it is rising not from the center of the mountain as before, but at an angle. I wonder why.

Some say people are influenced by their environment. I have been curious about

astronomy since childhood. Was it living in a naturally mountainous area? Was it the fact that the streets were dark at night? Was it the availability of a rich library of books at home? Was it a way of escape? I am grateful that at home I could read and I had freedom to explore my interests.

### Education and experiences before PhD

I am very grateful to all my good teachers and professors before PhD: early school years (my math teacher Silva Surenovna), including the wonderful high school Anania Shirakatsi (my math teacher Mr. Zohrabyan), undergraduate and Masters degree institution San Jose State University (SJSU). During my high school, I also find that my experience of about five years in jazz group “Talisman” with Mr. Karlos Petrosovich was invaluable, as he taught how practice makes perfect, how mastering a skill gives you a sense of pride, how to think out of the box, how to be creative, how interesting it is to travel, and how to enjoy life outside the ivory towers. For example, he used to say, that if you don’t perform well, then you have to walk in front of other people in a shy way, but if you practice and perform well, then you can boldly look in the eyes of your listeners.

Coming to the United States gave me an opportunity to pursue education. In particular, the SJSU gave me an opportunity to pursue higher education in a welcoming and diverse environment, presenting the whole world for my exploration without limits. In my coursework every single teacher there was amazing. I had a multitude of inspiring experiences, such as a week in Death Valley (with astronomer Monica Kress), a trip to the San Diego Wild Park, and visits to the California Science Academy. I got to work in several research labs, including with Dr. Elaine Bryant on extremophile microbial ecology from martian analog environments. While I got numerous scholarships, the education was expensive, and so I also worked sometimes up to four jobs as a student, and am grateful to my extensive on-campus community and friends (especially Ann Baldwin, John Boothby, Maureen Scharberg, Karen Singmaster, Carolus Boekema).

The SJSU educators made the sciences accessible, they explained concepts clearly, made the environment very welcoming. Plus, during my Master’s degree I had the opportunity to spend one year in Paris, France, where I took my first graduate level physics courses in French - it was Quantum Mechanics (or should I say *mécanique quantique*)! During my study abroad year, besides taking physics courses at the amazing University of Pierre and Marie Curie, I had the privilege of taking French language courses in Sorbonne — all this by day. By night I worked full-time in biotech industry to match the US timezone (thanks to my Biocompare family, especially Kristen and Piera). In Paris I got the flavor of what it was like to be a student in Europe — and started wishing to come back to Europe for a longer period of time.

My degree in humanities not only gave me the present of 12 months in Paris, but also a fuller appreciation of what it means to be human on this Earth (Mille mercis

M. Desalvo, Mme Van Hooff, Mme Trudeau). I learned about numerous artists and writers who walked interesting lives and journeys as they found their voice. For example, the celebrated Marcel Proust had to pay the costs out of pocket to publish the masterpiece “À la recherche du temps perdu”.

My Master’s supervisor Dr. Aaron Romanowsky gave me the opportunity to do research in Astronomy, and also organized trips to various observatories in California. He was very patient and sensitive, and also challenged me to think as an independent scientist. My professors Dr. Patrick Hamill and Dr. Ken Wharton made me fall in love even more with every topic in Physics (yes, especially with the Electricity and Magnetism!), and had the brilliance and patience to help me master these topics even though my undergrad degree was in Biology. Dr. Hamill often mentioned the stories of famous astronomers during our courses (e.g., Tycho Brahe, his pet deer, nose, and graduate student Kepler). Outside of school, I am especially thankful to the NASA internships and my mentor Miriam Rodon for sharing about her journey through a doctoral program, which inspired me to have courage to attempt a PhD in Astronomy.

Actually it is my second attempt at a PhD. My first attempt at a PhD was in Dual-Title Ecology and Astrobiology program at Penn State, which ended in a huge fiasco within about a year, rippling into financial debt and other livelihood problems (housing, etc.), not to mention career uncertainty. Nevertheless, this experience gave me some insight into what academia is. It’s very important to have a good supportive environment and network in research, take time off to relax, as well as financial stability. It also above all gave me exposure to several Astronomy courses which reignited my interest in the subject, and I took that time period as an opportunity to start taking baby steps towards the career of my dreams - astronomy, the topic of my passion now. I especially thank Dr. Steinn Sigurdsson for being a great teacher, and for answering my questions about PhD Astronomy programs each time I asked.

I am also thankful to my friends in Pennsylvania, Heather and Minne, as well as all the kind baristas of the Pump Station — you brought fun to my life and I miss you. I am grateful for the kind Debra Weimer for hiring me to contribute to a real estate related project. I am grateful for the quaint local coffee shops, bakeries, creameries, and juicy BBQ places in Pennsylvania, as well as the opportunities I got to visit natural spaces with the Wetlands Ecology class and then on my own, especially to admire birds, all around the nation.

### PhD journey

However, I appreciate greatly that somehow my journey brought me to the career of an astronomer, at the brink of getting a doctoral degree - despite many ebbs and flows of life, including multiple moves across continents and oceans.

On the way to the PhD program (technically the second time) there were so many people who helped me to get there. And so, I found a doctoral program in Astronomy

through Seppo Laine, Dr. Romanowsky's collaborator, which became my PhD home — a community of astronomers near the Tuorla Observatory in Turku, Finland, much further north than I have ever thought I would be at, a place where Santa Claus claims to reside, almost magical (although I have yet to see the northern lights).

The PhD program in itself elucidated to me better what it means to do research. It is a long journey, life happens along the way. It is not one day of work, but many days of small contributions. Some concepts are hard, and the neurons may need a stretch from time to time (or all the time), but I have learned to tackle complex problems and the importance of work-life balance. Some moments are unfair, hopefully in my life I can contribute to improve there.

I am grateful for the opportunity to study galaxies and quasars at the University of Turku (UTU) as a doctoral student, within the research group and guidance of Jari Kotilainen. I appreciate the wisdom, support, advice, navigation, grace, and experience imparted on me from my skilled supervisor, which helped me grow as an independent researcher, and learn more about not forgetting to be human while pursuing science. Jari gave me the opportunity and provided a platform to launch my academic career as an astronomer. I am also grateful for the work, mounds of technical knowledge, and advice from my second supervisor Kari Nilsson. Kari also graciously agreed to lead me through the dissertation process, when Jari stepped away from his duties, and I am grateful for his patience and for working through all the hurdles there. And my third supervisor, Roberto de Propriis, gave me the opportunity to work on several interesting projects, and have provided guidance to shape them into publishable works — important for building a publication-based thesis. I appreciate the student-oriented attitude of Roberto when he works with students, that he always replies to questions about science and career without delays. He also gave me practical advice on developing science questions for independent research.

I am grateful as well to main local and international collaborators: Daniela Bettoni, Renato Falomo, as well as many co-author students and postdocs. I also had a kind mentor in Elina Lindfors. To complete this long-term project, the inspiration and support from everyone in Tuorla Observatory and at the UTU was crucial, which helped to surmount the challenges along the way. Through the doctoral program, my childhood passion for astronomy is shaped into a career.

I would like to thank Kaj Wiik for helping throughout the years with all sorts of software questions, to Mauri Valtonen for always replying to my random astrophysics questions, to Talvikki Hovatta for wisdom on FAS related matters and for opportunity to work on blazar-related research, to Kalle Karhunen for being a nice officemate and helping me patiently with my first observing run at the NOT, to my local co-authors Nischal Acharya and Clare Wethers, to FINCA group of people and our meetings, to my research director Seppo Mattila, and department head Juri Poutanen. I am grateful to all people who taught courses I took: Seppo Mattila, Kari

Nilsson, Roberto de Propriis, Jari Kotilainen, Talvikki Hovatta, Pekka Heinämäki, Sergey Tsygankov, and numerous people who gave shorter lectures and tutorials. Again, I would like to mention FINCA, because the people from FINCA always answered questions related to astronomy careers and I appreciate that.

I would like to thank for funding support the Finnish Cultural Foundation, EDUFI grant, FINCA, UTU. In particular, I am grateful for the opportunity and for the amazing support both from my supervisor, my collaborators, from Nordic Optical Telescope, and from New Technology Telescope staff members, during my observing nights in La Palma and La Silla. Plus, I have had the fortune to interact with brilliant academics outside of the UTU, such as during my service on the Finnish Astronomical Board, and in meetings with Kumpula women of science (University of Helsinki). Especially when writing my thesis, I am grateful that I got support from the UTU library resources and also University of Helsinki and Aalto libraries.

I learned a lot in different areas of astronomy and beyond, and extend a gratitude to all communities (real and virtual) and all entities for making information available, digestible, for creating resources and databases, workshops and programs to make it possible to find solutions to problems during the PhD program - commending accessibility rather than obfuscation, which encouraged exploration and acquisition of a skill or information.

Many amazing points in my PhD include travel to exotic countries: SMBH workshop in Italy, conference in Greece, research experience at ESO in Garching with hosts Paola Andreani and Michele Ginolfi, meeting in Armenia. I presented in conferences and meetings in wonderful institutes and research groups online. I got extensive observing experience. The output of the thesis work is richer with papers beyond the four included in the dissertation.

#### Last year

Judging from the senioritis stress of B.S. and M.S. programs, I am thankful that I reached out for support in the autumn of 2023. The dissertation process continued much longer beyond what I planned, so this support was important not to give up and to manage the stress levels. I am thankful to my church family, to people outside of the department who agreed to listen about my life in meetings, coffee breaks, chats (in no particular order): Katri, Fatemeh, the several mothers support groups, Leena, Viivi, Mia, Sonja, Kaisa. In the department - to my fellow students, especially the 2024 coffee meetings with Jenni, career know-how chats with Johanna (and beyond), to Elina whose door I could knock on at any time. For the dissertation process steps, great thanks to the administrators Sanna Ranto and Eevi Savola for answering questions and for advice. I also appreciate the work and time by the pre-examiners (Prof. Johansson, Dr. Merloni) and the opponent, Dr. Anna Wolter. In the last few months, working with Talvikki Hovatta and Elina Lindfors brought encouragement and joy.

### For my children

Thank you, my dear children, for bringing sunshine to my life, for bringing meaning to days. When I felt down that my career trajectory specifically in the PhD program was not going as fast or that I did not hit it out of the park on certain career achievements, I reflected on how blessed I was from the family side by having you to shine brightly in my life. Many a day, when I felt sad, hugging you brought joy back to me, and the troubles floated away. I enjoyed hearing your little footsteps, when I was sitting at the computer and you came to my desk to get some mommy time.

### For my husband

James, I am so grateful that you have supported my move here to Finland to pursue my career despite numerous unknowns. We managed together through various hardships, some quite bad. Especially in the beginning when our financial situation was not stable and we took it day by day, not knowing where the funds for food would come from and where we would be living. Thank you for going through this with me as an adventure and with a positive attitude. I also felt inspired by your own path in academia, your creativity, communication skills, and ingenuity. After we catch up on sleep, I look forward to chasing some auroras with you.

### Family, friends, caregivers

With all my heart, I am sincerely indebted to my family and friends for enriching my life, as often I was lost in solitary work on my thesis, and especially through pandemic. I am grateful for the grandparents of my kids: Jo Anne, Vahan, and Naira, as well as the doctors and childcare personnel who helped me take care of my children throughout the years.

### For myself

I want to finish by thanking myself for daring to pursue a career in astronomy. I am proud of my creativity, perseverance, talents, and achievements. *Bonne continuation!*

P.S. Despite efforts to catch errors by myself, my colleagues, and supervisors, it is possible that few remain. I claim the full responsibility for them.

April 11th, 2024

*Maria Babakhanyan Stone*



## MARIA BABAKHANYAN STONE

*\*\*aimed at the Solar system, landed amongst galaxies\*\**

As a child, I used to observe from my window the Sun rising out of the mountain and also the Moon at night. In high school, I visited the Byurakan Observatory. One day our teacher shared about quasars and extremely dense matter, a lecture that went way over my head, although its memory stayed with me through life. Little did I know that after going on to study biology in undergrad I would pivot to research extreme singularities in space.

By studying Martian analog environment ecology, I was exposed to astronomy research which re-ignited my childhood passion. After some reflection on life and inspiration from lives of French literary creators, I took baby steps to bend my career trajectory towards astronomy. A marvelous journey unfolded with stops in Paris to study Quantum Mechanics in French, catching up on math and physics graduate coursework in California, researching ultra-diffuse galaxies in the Coma cluster, working at NASA, volunteering at the American Astronomical Society meeting one winter. Gradually I developed the interest and courage to pursue the doctoral study of enigmatic supermassive black holes and specifically how they affected the evolution of galaxies.

Living in Finland as a doctoral researcher has been very rewarding, especially because our family was blessed with two wonderful children, making family time quite cherished. I aim to continue my astronomy research career as a postdoc. For personal enjoyment, I dabble with music, travel, languages, and baking scones.

# Table of Contents

<b>Acknowledgements</b> . . . . .	<b>vi</b>
<b>Table of Contents</b> . . . . .	<b>xiv</b>
<b>Abbreviations</b> . . . . .	<b>xvii</b>
<b>List of Symbols and Constants</b> . . . . .	<b>xxi</b>
<b>List of Original Publications</b> . . . . .	<b>xxiii</b>
<b>1 Introduction</b> . . . . .	<b>1</b>
<b>2 Overview of the formation and evolution of galaxies</b> . . . . .	<b>5</b>
2.1 When did galaxies form? . . . . .	5
2.1.1 The young Universe: from the BB to the era of radiation domination . . . . .	7
2.1.2 From the matter domination epoch to the formation of the first stars . . . . .	8
2.1.3 Continued structure formation till present day . . . . .	9
2.1.4 Main observations defining the present-day Universe . . . . .	10
2.1.5 Galaxy evolution simulations . . . . .	11
2.2 Key concepts in cosmology . . . . .	13
2.2.1 The standard cosmological model . . . . .	13
2.2.2 Laws of physics . . . . .	14
2.2.3 Cosmological principle . . . . .	15
2.2.4 Hubble's law . . . . .	16
2.3 Cosmological distances . . . . .	17
2.3.1 Comoving and proper distances . . . . .	18
2.3.2 Comoving separation between galaxies . . . . .	21
2.3.3 Angular diameter distance and luminosity distance . . . . .	21
<b>3 Observed properties of galaxies</b> . . . . .	<b>24</b>
3.1 Galaxy morphology . . . . .	25
3.1.1 Elliptical galaxies . . . . .	27



3.1.2	Spiral galaxies . . . . .	29
3.1.3	Other morphological types . . . . .	30
3.1.4	Morphologies of very distant galaxies (high redshift) . . . . .	31
3.2	Dynamical features in galaxies . . . . .	32
3.2.1	Velocity dispersion . . . . .	32
3.2.2	Rotational velocity and $v_{\text{rot}}/\sigma$ . . . . .	34
3.3	Surface brightness profiles . . . . .	36
3.4	Scaling relations . . . . .	36
3.4.1	Color-magnitude relation . . . . .	38
3.4.2	Luminosity function . . . . .	39
3.4.3	Tully-Fisher relation for spiral galaxies . . . . .	39
3.4.4	The fundamental plane for elliptical galaxies . . . . .	41
3.5	Star formation . . . . .	43
<b>4</b>	<b>Active Galactic Nuclei . . . . .</b>	<b>48</b>
4.1	Observational signatures of AGN . . . . .	49
4.1.1	AGN types . . . . .	50
4.1.2	Unification theory . . . . .	52
4.2	AGN astrophysics . . . . .	55
4.2.1	Where is the SMBH boundary? . . . . .	55
4.2.2	Accretion of infalling gas . . . . .	57
4.2.3	Eddington luminosity . . . . .	58
4.2.4	BLR and NLR gas cloud velocities . . . . .	59
4.2.5	SED signatures echo AGN structure . . . . .	59
4.3	AGN environment . . . . .	59
4.3.1	AGN host galaxies . . . . .	61
4.3.2	AGN co-evolution . . . . .	61
4.3.3	AGN neighborhoods . . . . .	63
4.3.4	AGN environments at larger scales . . . . .	64
4.4	AGN triggering . . . . .	67
4.4.1	Galaxy interactions . . . . .	68
4.4.2	Secular mechanisms . . . . .	69
4.5	Quasars through time . . . . .	70
<b>5</b>	<b>Observational methods . . . . .</b>	<b>73</b>
5.1	Optical imaging . . . . .	73
5.1.1	Measuring galaxy brightness . . . . .	75
5.2	Spectroscopy . . . . .	77
5.2.1	Estimating the luminosity of an emission line . . . . .	78
5.2.2	Measuring SFR from [O II] emission lines . . . . .	82
5.3	Infrared observations . . . . .	85

5.4	Surveys . . . . .	86
5.4.1	Sloan Digital Sky Survey . . . . .	87
5.4.2	GAMA survey . . . . .	88
5.5	Spectral energy distribution of galaxies . . . . .	88
5.5.1	CIGALE . . . . .	91
5.5.2	Stellar population synthesis . . . . .	91
5.5.3	SED-based properties from GAMA survey . . . . .	93
5.6	Telescopes . . . . .	95
5.6.1	Nordic Optical Telescope . . . . .	95
5.6.2	Gran Tecan . . . . .	96
5.6.3	New Technology Telescope . . . . .	97
<b>6</b>	<b>Summary of the original publications . . . . .</b>	<b>98</b>
6.1	Low-redshift quasars in the SDSS Stripe 82 – II. Associated companion galaxies and signature of star formation . . . . .	98
6.2	Low-redshift quasars in the SDSS Stripe 82 — III. MOS observations . . . . .	99
6.3	Galaxy and Mass Assembly (GAMA): Low-redshift Quasars and Inactive Galaxies Have Similar Neighbors . . . . .	100
6.4	Galaxy and Mass Assembly (GAMA): The Properties of Quasar Host Galaxies, Star Formation Histories, and Stellar Populations. . . . .	101
6.5	The author’s contribution to publications . . . . .	102
<b>7</b>	<b>Future research . . . . .</b>	<b>103</b>
	<b>List of References . . . . .</b>	<b>104</b>
	<b>Original Publications . . . . .</b>	<b>113</b>

# Abbreviations

<b>1D, 2D, 3D</b>	One-, two-, three-dimensional
<b>2dFGRS</b>	Two-degree Field Galaxy Redshift Survey
<b>6dFGS</b>	Six-degree Field Galaxy Survey
<b>AAT</b>	Anglo-Australian Telescope
<b>ACS</b>	Advanced Camera for Surveys
<b>AGN</b>	Active galactic nuclei
<b>ALFOSC</b>	Alhambra Faint Object Spectrograph and Camera
<b>ALMA</b>	Atacama Large Millimeter Array
<b>BB</b>	Big Bang
<b>BH</b>	Black hole
<b>BLR</b>	Broad line region
<b>CBR</b>	Cosmic background radiation
<b>CCD</b>	Charged coupled device
<b>CDM</b>	Cold dark matter
<b>CIGALE</b>	Code Investigating GALaxy Emission
<b>CMD</b>	Color-magnitude diagram
<b>COBE</b>	Cosmic Background Explorer
<b>COSMOS</b>	Cosmic Evolution Survey
<b>CSP</b>	Composite stellar population
<b>DEC.</b>	Declination
<b>DM</b>	Dark matter (or distance modulus)
<b>DR</b>	Data release
<b>EAGLE</b>	Evolution and Assembly of Galaxies and Their Environments
<b>EFOSC2</b>	ESO Faint Object Spectrograph and Camera 2
<b>EHT</b>	Event Horizon Telescope
<b>ELT</b>	Extremely Large Telescope
<b>EMS</b>	Electromagnetic spectrum
<b>ESA</b>	European Space Agency

<b>ESO</b>	European Southern Observatory
<b>FIR</b>	Far-infrared
<b>FORS</b>	FOcal Reducer and low dispersion Spectrograph
<b>FLRW</b>	Friedmann-Lemaitre-Robertson-Walker metric
<b>FRW</b>	Friedmann-Robertson-Walker cosmology
<b>FUV</b>	Far-UV
<b>FWHM</b>	Full width at half maximum
<b>GAMA</b>	Galaxy And Mass Assembly Survey
<b>GOODS</b>	Great Observatories Origins Deep Survey (GOODS)
<b>GRB</b>	Gamma-ray burst
<b>GTC</b>	Gran Telescopio Canarias
<b>HAWK-I</b>	High Acuity Wide Field K-band Imager
<b>HDM</b>	Hot dark matter
<b>HST</b>	<i>Hubble Space Telescope</i>
<b>HUDF</b>	<i>Hubble Ultra-Deep Field</i>
<b>ID</b>	Identification
<b>IFS</b>	Integral field spectroscopy
<b>IGM</b>	Intergalactic medium
<b>IMF</b>	Initial mass function
<b>IR</b>	Infrared
<b>IRAF</b>	Image Reduction and Analysis Facility
<b>ISM</b>	Interstellar medium
<b>JWST</b>	<i>James Webb Space Telescope</i>
<b>LF</b>	Luminosity function
<b>LG</b>	Local Group
<b>LQAC</b>	Large Quasar Astrometric Catalog
<b>LINER</b>	Low-ionization nuclear emission region
<b>LIRG</b>	Luminous infrared galaxy
<b>LSS</b>	Large-scale structure
<b>LSST</b>	Legacy Survey of Space and Time
<b>KS</b>	Kolmogorov-Smirnov statistical test
<b>M87</b>	Messier 87
<b>MAGPHYS</b>	Multiwavelength Analysis of Galaxy Physical Properties

<b>MBH</b>	Massive black hole
<b>MCMC</b>	Markov Chain Monte Carlo method in statistics
<b>MIR</b>	Mid-infrared
<b>MOS</b>	Multi-object spectroscopy
<b>MS</b>	Main sequence
<b>MUSE</b>	Multi Unit Spectroscopic Explorer
<b>NASA</b>	National Aeronautics and Space Administration
<b>NIR</b>	Near-infrared
<b>NLR</b>	Narrow-line region
<b>NLS1</b>	Narrow-line Seyfert 1 galaxy
<b>NOT</b>	Nordic Optical Telescope
<b>NTT</b>	New Technology Telescope
<b>OVV</b>	Optically violent variables
<b>PSF</b>	Point spread function
<b>QSO</b>	Quasi-stellar object
<b>R.A.</b>	Right ascension
<b>RW</b>	Robertson-Walker metric
<b>SDSS</b>	Sloan Digital Sky Survey
<b>SED</b>	Spectral energy distribution
<b>SF</b>	Star formation
<b>SFG</b>	Star forming galaxy
<b>SFH</b>	Star formation history
<b>SFR</b>	Star formation rate
<b>Sgr A*</b>	Sagittarius A-star
<b>SMBH</b>	Supermassive black hole
<b>SMG</b>	Submillimeter galaxy
<b>SN</b>	Supernova (plural SNe for “Supernovae”)
<b>S/N</b>	Signal-to-noise
<b>SPS</b>	Stellar population synthesis
<b>SSFR</b>	Specific SFR
<b>SSP</b>	Simple stellar population
<b>STSCI</b>	Space Telescope Science Institute
<b>TOO</b>	Target-of-opportunity

<b>TFR</b>	Tully-Fisher relation
<b>UKIDSS</b>	United Kingdom Infrared Deep Sky Survey
<b>ULIRG</b>	Ultra-luminous infrared galaxy
<b>UV</b>	Ultra-violet
<b>VLT</b>	Very Large Telescope
<b>VLBI</b>	Very Long Baseline Interferometry
<b>WFIRST</b>	<i>Wide Field InfraRed Survey Telescope</i>
<b>WIMP</b>	Weakly interacting massive particles
<b><math>\Lambda</math>CDM</b>	Lambda cold dark matter model

# List of Symbols and Constants

a	semi-major axis of an ellipse
b	semi-minor axis of an ellipse
D	distance (also lowercase), diameter
E	energy, elliptical morphology class symbol
e	evolutionary correction
e <sup>-</sup>	electron
F	flux
G	Gravitational constant
H <sub>z</sub>	Hubble constant at redshift z
h	dimensionless constant (Hubble law)
I	intensity
K	kinetic energy, k-correction term
k	curvature parameter, parameter in Sersic power law
L	luminosity
M	mass, absolute magnitude
m	apparent magnitude, mass
N	number
n	Sersic index, number density
R	resolution, radius (also lowercase)
S	sensitivity, spiral morphology class symbol
s	distance
T	temperature
t	time
U	potential energy
V	volume
v	velocity
W <sub>eff</sub>	effective filter width
Z	metallicity
z	redshift
$\alpha$ (alpha)	Right Ascension, slope, scaling factor, angle
$\gamma$ (gamma)	photon
$\Delta$ (delta)	mathematical difference

$\epsilon$ (epsilon)	ellipticity
$\eta$ (eta)	baryon to photon ratio, accretion efficiency
$\theta$ (theta)	angle
$\Lambda$ (lambda)	cosmological constant in the $\Lambda$ Cold Dark Matter theory
$\lambda$ (lambda)	wavelength
$\mu$ (mu)	surface brightness
$\nu$ (nu)	frequency
$\pi$ (pi)	number (3.14)
$\sigma$ (sigma)	velocity dispersion, uncertainty
$\tau$ (tau)	optical depth
$\Phi$ (phi)	luminosity function
$\phi$ (phi)	luminosity function, angle
$\chi$ (chi)	comoving distance
$\Omega$ (omega)	density
$\text{\AA}$	Angstrom, $10^{-12}$ cm
a.u.	astronomical unit, $\sim 1.496 \times 10^{13}$ cm
l.y.	light year, $\sim 9.461 \times 10^{17}$ cm
pc	parsec, $3.09 \times 10^{18}$ cm
c	speed of light, $2.99 \times 10^{10}$ cm s $^{-1}$
eV	electron-Volt, $1.602 \times 10^{-12}$ erg
G	Gravitational constant, $6.67 \times 10^{-8}$ cm $^3$ g $^{-1}$ s $^{-2}$
$L_{\odot}$	Solar luminosity, $\sim 3.8 \times 10^{33}$ erg s $^{-1}$
$M_{\odot}$	Solar mass, $\sim 2 \times 10^{27}$ g



# List of Original Publications

This dissertation is based on the following original publications, which are referred to in the text by their Roman numerals:

- I *M. B. Stone*, D. Bettoni, R. Falomo, J. K. Kotilainen, K. Karhunen, S. Paiano, R. Scarpa.  
Low-redshift quasars in the SDSS Stripe82 — II. Associated companion galaxies and signature of star formation.  
Monthly Notices of the Royal Astronomical Society, 2021; 501, 1: 419.
- II D. Bettoni, R. Falomo, S. Paiano, J. Kotilainen, *M. B. Stone*.  
Low-redshift quasars in the SDSS Stripe 82 — III. MOS observations.  
Monthly Notices of the Royal Astronomical Society, 2023; 519, 2: 2929.
- III *M. B. Stone*, C. Wethers, R. de Propris, J. Kotilainen, N. Acharya, B. Holwerda, J. Loveday, S. Phillipps.  
Galaxy and Mass Assembly (GAMA): Low-redshift Quasars and Inactive Galaxies Have Similar Neighbors.  
The Astrophysical Journal, 2023; 946, 2: 116.
- IV *M. B. Stone*, R. De Propris, C. Wethers, J. K. Kotilainen, N. Acharya (GAMA collaboration).  
Galaxy and Mass Assembly (GAMA): The Properties of Quasar Host Galaxies, Star Formation Histories, and Stellar Populations.  
2024, submitted.

The original publications have been reproduced with the permission of the copyright holders.

## List of publications not included in the thesis

- I      Adebusola Alabi, A. Ferré-Mateu, A.J. Romanowsky, J. Brodie, D.A. Forbes, A. Wasserman, S. Bellstedt, I. Martín-Navarro, V. Pandya, *M.B. Stone*, N. Okabe.  
Origins of ultradiffuse galaxies in the Coma cluster — I. Constraints from velocity phase-space.  
Monthly Notices of the Royal Astronomical Society, 2018; 479, 3: 3308.
- II     Anna Ferre-Mateu, A. Alabi, D.A. Forbes, A.J. Romanowsky, J. Brodie, V. Pandya, I. Martín-Navarro, S. Bellstedt, A. Wasserman, *M.B. Stone*, N. Okabe.  
Origins of ultradiffuse galaxies in the Coma cluster — II. Constraints from their stellar populations.  
Monthly Notices of the Royal Astronomical Society, 2018; 479, 4: 4891.
- III    A. Melandri, D.B. Malesani, L. Izzo, J. Japelj, S.D. Vergani, Patricia Schady, A. Sagues Carracedo, A. de Ugarte Postigo, J.P. Anderson, C. Barbarino, J. Bolmer, A. Breeveld, P. Calissendorff, S. Campana, Z. Cano, R. Carini, S. Covino, P. D’Avanzo, V. D’Elia, M. della Valle, Show less M. De Pasquale, J.P.U. Fynbo, M. Gromadzki, F. Hammer, D.H. Hartmann, K.E Heintz, C. Inserra, P. Jakobsson, D.A. Kann, J. Kotilainen, K. Maguire, N. Masetti, M. Nicholl, F.E. Olivares, G. Pugliese, A. Rossi, R. Salvaterra, J. Sollerman, *M.B. Stone*, G. Tagliaferri, L. Tomasella, C.C. Thoene, D. Xu, D.R. Young.  
GRB 171010A / SN 2017htp: a GRB-SN at  $z=0.33$ .  
Monthly Notices of the Royal Astronomical Society, 2019; 490, 4: 5366.

# 1 Introduction

Եվ տիեզերական խորությունների  
Անճառ վայրերում հոգիս սավառնեց  
Եվ խորախորհուրդ, վեհ գաղտնիքների  
Անխոս բարբառին լուռ ունկընդդեմ:

My soul soared into the depths  
of the Cosmos mute and vast,  
Tuning carefully to the silent language  
of its noble and profound secrets.

---

Avetik Isahakyan  
translated from Armenian

The field of extragalactic astronomy was born around a century ago (1924) with Edwin Hubble’s discovery that besides the Milky Way where our planet Earth is located, there are other galaxies, thus pushing the ceiling of the sky to infinity for all of humanity. Besides galaxies, intergalactic medium (IGM), dark matter (DM) halos, galaxy clusters, as well as processes associated with those distant objects, such as gravitational lensing, are also considered. Extragalactic objects are characterized by extreme distances in space and time, rendering it impossible to perform real-life experiments in a terrestrial laboratory. We cannot create galaxies to understand their formation. Instead, astronomy relies on observations and simulations.

The history of extragalactic research<sup>1</sup> is marked by the *great debate* about the nature of the spiral nebulae in 1920, where two opposing explanations were led by Harlow Shapley from the Harvard College Observatory and Heber Curtis from the Lick Observatory (Trimble, 1995; Kutner, 2003). Harlow Shapley argued they were part of the Milky Way, while Curtis reasoned them to be separate galaxies. Prior to Hubble, other astronomers such as Shapley, Curtis, and Ernst Öpik (Tartu Observatory, Estonia) attempted to estimate the distance to the Andromeda Galaxy using various methods. On the other hand, Vesto Slipher at Lowell Observatory (Arizona, USA) studied spectra of the spiral nebulae, discovering that most were redshifted (Thompson, 2011).

---

<sup>1</sup>As with any historical text on science, two points need to be remembered. First, the records need to be considered critically, due to various biases, such as omitting credit for work by female scientists (e.g., “Matilda effect” Rossiter, 2012). Second, discovery is often a nonlinear process.

Edwin Hubble used observations collected at the Mount Wilson Observatory (California, USA) using the largest telescope at the time (100 inch) to calculate the distance to the Andromeda Galaxy employing a technique involving variable stars, which was developed earlier by Henrietta Leavitt (one of the women known as “the Harvard Computer”, Nelson 2008). Thus, it was established through Hubble’s observations that other galaxies exist, ending the debate. The field has evolved tremendously and continues to be an active research niche in astronomy today.

We observe presently that galaxies have a non-uniform distribution in the sky, with patches of sky devoid of galaxies, while on the other hand clusters are concentrations of large numbers of galaxies, together forming a web coined as the *Large-Scale Structure (LSS)*. All galaxies recede away from us in a cosmological *Hubble flow*, with the exception of the nearest galaxies within the Local Group (LG), e.g., the Andromeda Galaxy.

Observing these other distant worlds, aka other galaxies, astronomers also discovered that not all galaxies are like ours. There are elliptical galaxies in addition to spirals; galaxies exist in a variety of shapes, sizes, colors, environments. What we observe about the distant galaxies holds clues about their formation and evolution.

To perform these observations, astronomers use telescopes on the Earth and in space. The specialized instruments in observatories capture the relevant information from the messengers of light — the *photons*. Galaxies emit photons with different energies (wavelengths, frequencies) due to different processes. Plus, the Hubble flow affects the energy of the photon as well. Observers quantify the emitted amount of photons (fluxes) in large (photometric bands) and short intervals (e.g., emission lines) over the electromagnetic spectrum (EMS), as well as any absence of photons (e.g., absorption lines), from which one can deduce physical properties such as the star formation rate (SFR). Close your eyes, and imagine a path of a photon from a distant quasar — not only this photon had to travel for a long time, starting its journey long before the dinosaurs roamed the Earth, but also probably through clouds of gas between galaxies, and eventually through the Earth atmosphere to land on a detector within our instrument. Thus, the observers have to take into account these sections of the path, in order to process and isolate the signal, with corrections for instrument noise, the atmosphere, the IGM, and cosmic spacetime expansion.

Today, extragalactic astronomy uses an arsenal of cosmological simulations, usually within the framework of the *Lambda Cold Dark Matter (ΛCDM)* model. In such cosmological simulations, galaxies play an important role as the basic visible building blocks of the models. Models of the cosmos require *feedback* mechanisms (e.g., radiation, accretion disk wind, and jets from an active nucleus) to influence such processes as star formation history (SFH) and baryon recycling (Fabian, 2012). High-resolution *zoom-in* simulations focus on more specific phenomena, e.g., galaxy interactions, galaxy structure formation (disks, spiral arms). All models of the Universe must reproduce what we observe today.

Half a century ago, observers started picking out galaxies which had peculiarly bright observational signatures in their centers, such as broad emission lines in optical spectra or the puzzling high-redshift radio emitting sources which had a star-like appearance in the optical on a photographic plate (i.e., the quasi-stellar objects (QSO), e.g., Peterson & Bolton, 1973; Smith & Wright, 1980). From the spectroscopic analysis of some QSO, the identified distances were significantly beyond what was previously observed, pushing the limits of human imagination. Astronomers continued discovering *active galaxies* with very bright luminosity emanating from a surprisingly small sub-parsec central volume both in optical and in radio.

Today, the term *active galactic nuclei* or AGN<sup>2</sup> is applied to “all objects with active *supermassive black holes* (SMBHs)” (Netzer, 2013). The dominant explanation for the engine behind the observed power output is a central SMBH which accretes matter. Nowadays, we discovered quasars at very far cosmological distances, for example at redshifts of 5 and 6 (Fan et al., 2001) and even beyond, asserting their role as sort of light posts of the Universe and concurrently puzzling the theorists to explain such massive black holes (MBH) within the first gigayear of the Universe (e.g., Wang et al., 2021; Natarajan et al., 2024). Due to the bright center and overall high luminosity which often outshines the host galaxy starlight, studying AGN through observations is challenging.

The environment of SMBH is mind-boggling since humans do not encounter and do not experience such environments in the everyday life. First, within the vicinity of the SMBH, the pull of gravity is enormous. Any material that falls beyond the *event horizon* is doomed to disappear into the singularity. Before doing so, the infalling gas is heated to enormous temperatures and radiates strongly at a wide range of frequencies, placing AGN among the most luminous objects in the Universe. Around some SMBHs part of the material is able to escape the plunge to the singularity, creating jets that may affect the material beyond the host galaxy at megaparsec scales (e.g., radio-loud quasars via jets).

The conquest of the full EMS for astronomical observations opened further the prominence of AGN in the extragalactic research landscape. The activity of AGN is not limited to a single waveband, and therefore multiwavelength studies are necessary to understand their extraordinary properties.

At the time of writing this dissertation, still numerous aspects of active galaxies are not well understood. The recently launched *James Webb Space Telescope* observatory (*JWST*), the *Euclid* mission, the upcoming *Nancy Grace Roman Space Telescope*, the ground-based Extremely Large Telescope (ELT), the Rubin Observatory, and many more facilities are scheduled to aid astronomers in uncovering and building a better understanding of active galaxies near and far, in combination with the advance brought by the neutrino and gravitational wave detection campaigns.

---

<sup>2</sup>In this text, I use the terms AGN and quasars interchangeably.

The full diapason of questions pertaining to the interesting astrophysical nature of AGN and their role in the ecology of galaxy environments motivated the undertaking of the projects in this dissertation, to deepen our understanding on how these amazing objects influence the evolution of galaxies throughout the space and time of the Universe. AGN are truly cosmologically significant objects, due to their role in processes at different spatial scales, time frames, and energy levels. To appreciate their role in the evolution of galaxies, I highlight<sup>3</sup> key points as follows. In Chapter 2, I give a brief overview of how the Universe formed, the cosmological principles. Then, in Chapter 3, I review the major observational characteristics and relations pertaining to galaxies: such as morphology, kinematics, star formation (SF).

I expand on the nature of active galaxies as hosts of currently accreting SMBHs in Chapter 4, diving deeper into our current pillars of understanding regarding the AGN environments. In Chapter 5, I review the main observational techniques, surveys, as well as telescopes tapped into for this dissertation. The enclosed publications are summarized in Chapter 6. The final chapter (7) introduces future steps in this research arena. Throughout the chapters, I have included relevant images of the sky, for the reader to appreciate the observational aspect of astronomy.

---

<sup>3</sup>These chapters stress the concepts relevant to the publications enclosed in the dissertation, skipping numerous exceptional cases and alternative theories.

## 2 Overview of the formation and evolution of galaxies

J'entre dans la nuit. Je navigue... Je n'ai plus  
pour moi que les étoiles...

I enter into the night. I navigate... I only have  
the stars for me...

---

“Au centre du désert”  
Antoine de Saint-Exupéry  
Translated from French

In this chapter, I describe the big picture of how our Universe evolved and the role of galaxies in cosmological history. The currently accepted *big-bang theory* on how the Universe evolves postulates that everything we see today, including galaxies, as well as the space and time itself started from a *Big Bang* (BB), followed by a relatively brief hot and dense phase, after which the Universe continued expanding and cooling to this day.

First, I succinctly review the major steps post-BB which led to the formation of galaxies (§ 2.1). Second, I introduce the major concepts to describe the Hubble flow of matter (§ 2.2). Since galaxies are observed at large distances and our observations are affected by the expansion of the Universe, I review how to calculate distances to and between objects focusing on methods applied in this work (§ 2.3).

### 2.1 When did galaxies form?

We describe the evolution of the expanding Universe by distinct phases of temperature, age, distances, and redshift. I summarize the main eras here and pinpoint the relevance to galaxies in particular (Figure 1, Table 1). The general concepts relayed in this chapter are taken from the standard literature on the subject: Dodelson (2003); Mo (2010); Baryshev & Teerikorpi (2012); Byrd et al. (2012); Piattella (2018).

This is a vibrant area of research, since there are still many unanswered questions about the early Universe, such as the nature of *dark matter* (DM) or the way the baryons came to existence (*baryogenesis*). The various types of matter, the specific ratio of baryons to photons, and early phenomena (e.g., inflation) contribute to the formation of galaxies and large-scale structure we observe today.

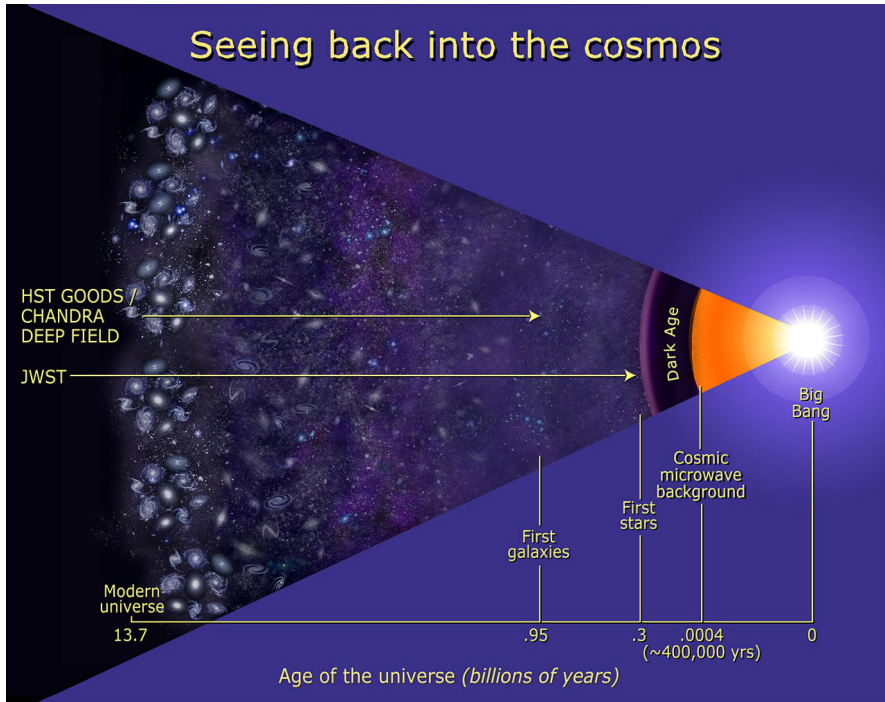


**Figure 1.** Major eras of the evolution of the Universe in the framework of the BB cosmology are schematically marked: the BB (bright star), the onset of CMB (orange section), dark ages (black band), stars and galaxies (white structures on purplish background). The *JWST* allows us to observe the period when the nascent galaxies formed. It reaches further back in time than the previously carried out Great Observatories Origins Deep Survey (GOODS) using the *Hubble* and *Chandra* space telescopes. Credit: NASA/ESA and Ann Feild (STScI), esahubble.org/images.

**Table 1.** Major phases of the history of the Universe (Schneider 2006 and e-course by Baumann (2021), “Cosmology. Part III Mathematical Tripos”). The timeline is given both in redshift and in years (or minutes). All redshifts before  $z=6$  are within the first billion years from the BB.

Phase	Time ( $t$ )	Redshift ( $z$ )	Temperature ( $T$ )
Primordial plasma	First 3 min	$>10^{15} - 4 \times 10^8$	$>100 \text{ GeV} - 100 \text{ keV}$
Recombination	260–380 kyr	1100–1400	0.26–0.33 eV (3000 K)
Photon decoupling	380 kyr	1000–1200	0.23–0.27 eV
Reionization	100 Myr – 1 Gyr	6–30	2.6–7.0 meV
Present	13.8 Gyr	0	0.24 meV



## 2.1.1 The young Universe: from the BB to the era of radiation domination

At the BB, the very fabric of spacetime was also formed. The Universe underwent a rapid expansion, an *inflation*<sup>1</sup>, by a factor of  $10^{35}$  ( $t \sim 10^{-36} - 10^{-34}$  s after the BB,  $T \sim 10^{28}$  K,  $E \sim 10^{15}$  GeV, Jones & Lambourne 2004). The first moments of the BB had extremely high energies, when processes at the particle physics level took place, resulting in the formation of baryonic matter (protons and neutrons) and when the various fundamental forces stabilized as the temperature evolved to be less hot.

During the hot and dense phase immediately after the BB, the matter and radiation are in equilibrium. The matter is in the form of ionized plasma (*primordial plasma*). The hot matter and the hot radiation fill the early Universe. Furthermore, the matter and radiation in this early phase are coupled.

The ratio ( $\eta$ ) between baryons ( $N_B$ ) and photons ( $N_\gamma$ ) is:

$$\eta = \frac{N_B}{N_\gamma}, \quad (1)$$

and is observed to be  $\sim 10^{-9}$ . This value is higher than what would have been expected if after the BB  $N_B = N_\gamma$ , and is explained by introducing *matter-antimatter asymmetry* into the initial conditions:

$$N_B - N_{\bar{B}} = \eta N_\gamma, \quad (2)$$

which also explains the fact that no antimatter ( $N_{\bar{B}}$ ) is observed today. The annihilation processes then decreased the populations of baryons and antibaryons, but because of the matter-antimatter asymmetry, most antimatter vanished, while the excess baryons remained (Roos, 2015). This one particle per billion cosmic ratio evolves to become stars and galaxies.

The interactions of a rich and diverse gamut of elementary particles dominated this hot period (e.g., cosmologically important leptons: electrons and neutrinos). Governed by the thermal equilibrium principles, as the Universe cooled, certain particles decoupled from the primordial plasma as their interaction rates slowed down faster than the expansion rate. The DM particles decoupled (*DM freeze-out*) quite early, within a minor fraction of the first second post-BB, according to the leading DM models, since their interaction with ordinary matter is very weak. This is the case within the model where DM particles are Weakly Interacting Massive Particles or WIMPs (Roos, 2015). The *neutrino decoupling* from matter took place 1 s after the BB (around 1 MeV), resulting in the *Cosmic Neutrino Background*.

---

<sup>1</sup>Inflation is not a fully developed theory yet (Longair, 1998, 2008; Roos, 2015) but resolves some of the important problems (Combes et al., 1995).

Within the first three minutes after the BB, the hot and dense conditions of the Universe allowed for the production of elements through nuclear reactions — *primordial or BB nucleosynthesis* (Jones & Lambourne, 2004; Byrd et al., 2007; Tanihata et al., 2023). Certain proportions of the light elements formed. The most abundant nuclei are Hydrogen and Helium. In fact, the origin of Hydrogen in stars around us is the Hydrogen created in these first few minutes after the BB. However, the free electrons and nuclei were in an ionized state (a hot plasma soup). The Universe was opaque to photons.

While this period was short, its importance is significant in how galaxies formed and evolved. For example, the inflation might be the period when very small inhomogeneities began in some areas. This was the foundation to the later epochs when matter started condensing and forming galaxies and galaxy clusters. Furthermore, there is an overabundance of matter (baryons) as compared to antimatter (or antibaryons), without which there would not be any matter to build galaxies from later.

## 2.1.2 From the matter domination epoch to the formation of the first stars

At  $z=3400$ , matter-radiation equality is reached, followed by the next major era, the *era of recombination*<sup>2</sup>. When the temperature of the Universe reached  $\sim 3000$  K, the temperatures were low enough for neutral atoms of Hydrogen to form. As the free electron density drops due to the formation of neutral atoms, the Thomson scattering from free electrons,  $e^- + \gamma \rightarrow e^- + \gamma$ , which coupled photons to matter becomes inefficient. The radiation (photons) and the matter are decoupled (100 000 years after BB or  $z=1000$ ), and the Universe becomes transparent. The photons begin a journey of freely traveling in the Universe in all directions. This phenomenon is observed today as the *cosmic background radiation* (CBR).

Today the vestigial CBR intensity is modeled using a blackbody with a peak at 2.7 K corresponding to the wavelength of  $\sim 1$  mm. The CBR is all around us. The *Cosmic Background Explorer Satellite* (COBE) measured the fluctuations in its intensity, also at small scales. These fine CBR anisotropies are considered to be the imprint of early small density fluctuations right before the radiation and matter decoupled and which give rise to clusters of galaxies much later. It is yet unknown why these early concentrations in the density formed.

The neutral matter engrains in itself the ratios of light elements still observable in the Universe today. Matter is the component where gravity acts as an attractive force, pulling in more matter together to form galaxies. The first galaxies are thought to have formed within the first billion years post BB. The major fraction of matter

---

<sup>2</sup>Recombination means that an electron and a proton are combined into a neutral atom. The opposite process is the ionization:  $p + e^- \rightarrow \frac{1}{2}H_{\text{neutral}} + \gamma$  (Jones & Lambourne, 2004).

is *dark*, whereas the baryonic matter (aka *visible* or *light* matter) is only  $\sim 5\%$  of the energy density of the Universe (Péroux & Howk, 2020)<sup>3</sup>. The nature of the prevalent DM is unknown, but it exerts gravitational pull aiding in formation of structure.

After the recombination phase, as the matter becomes predominantly neutral, the cosmos falls into a 100 Myr-long *dark age* phase. At around the 100 Myr mark, the matter starts getting (re-)ionized due to the first generation of quasars and stars, launching the *epoch of reionization*, which lasts about a billion years (e.g. Rees, 1999). The reionization of the IGM is considered to be the last major phase change in cosmic history. During the reionization stage, some stars are formed, however, the SFR picks up afterwards, reaching its peak around  $z=2$ , a trend followed by the accretion of SMBHs (Madau & Dickinson, 2014).

### 2.1.3 Continued structure formation till present day

As the Universe expands, it becomes less dense and cools down. Larger structures start forming: protogalaxies, galaxies, clusters. The galaxies (and also black holes, BHs) are thought to grow by accreting gas around them due to gravitational pull, and this model is employed in hydrodynamical simulations, which are tersely explained in a later subsection in this chapter, § 2.1.5.

There are two scenarios to explain how galaxies formed. According to the “top-down” galaxy formation scenario (Hot Dark Matter, HDM, models), first, the giant cluster-sized entities are formed. Then they break down to form clusters and then eventually galaxies within those volumes as they contract gravitationally.

Alternatively, according to the mainstream “bottom-up” model (*hierarchical galaxy formation theory* within the CDM models), the small mass fluctuations after the BB serve as the basis for galaxy formation. First, as the DM decouples before recombination, through gravitational pulls DM halos form a network that spans the whole universe. Later, as the universe evolves and the baryons decouple from radiation, primordial gas concentrates in the centers of DM halos, forming disks surrounded by a swarm of globular clusters from the first stars. It is assumed, thus, that stars are the first objects to form. The disk galaxy grows due to on-going SF. These spiral galaxies sometimes merge, clustering into larger elliptical galaxies. The hierarchical scenario has some unresolved areas still, for example, the problem of missing galactic satellites (Klypin et al., 1999), as there is a discrepancy between the number of observed and predicted satellites in the LG. At the same time various solutions have been reported throughout the years (Bullock & Boylan-Kolchin, 2017). In particular for the “missing satellites” problem, Sawala et al. (2016) results showed agreement with the observational data.

The first galaxies have formed within the first gigayear mark ( $z > 6$ ) of the Uni-

---

<sup>3</sup>Critical density value corresponds to the flat Universe geometry (Liddle & Loveday, 2008).

verse, after the epoch of reionization (Madau & Dickinson, 2014). The formation of the first galaxies is one of the key research areas with the *JWST* observations, which already have discovered galaxies at  $z > 12$  (Castellano et al., 2022; Yan et al., 2023). Around  $z=2$ , the epoch of galaxy assembly reached its peak. That’s when the cosmic SF was at its apogee as well. However, before the flourishing reign of galaxies, there are many unanswered questions on galaxy formation since the cosmic dark ages, including how the energy feedback from mass accretion onto SMBHs affects their environment. The galaxy formation and evolution theories try to explain the steps in the cosmic history which led to galaxies as they are observed today — their morphology, masses, energetics, composition, clustering.

### 2.1.4 Main observations defining the present-day Universe

Now that we have identified when galaxies formed within the context of the currently accepted BB cosmology, we look at what is observed about galaxies today. The dominant conclusion is that the Universe is flat and is described by several key cosmological parameters. The total energy density is the sum of matter density and of a cosmological constant, and is equal to unity,

$$\Omega_{\text{TOT}} = \Omega_{\text{M}} + \Omega_{\Lambda} = 1 , \quad (3)$$

where  $\Omega_{\text{M}} = 0.3$  and  $\Omega_{\Lambda} = 0.7$  (Planck Collaboration et al., 2020). These are the values which I adopted throughout in this thesis. The cosmological constant serves in an opposite way to the gravitational pull of the matter, enabling galaxies to move away from each other. As the Universe continues to expand, what we observe is that galaxies appear to move away from us. It has been shown that the expansion of the Universe is accelerating, based on the observations of distant supernovae (SNe, Riess et al., 1998; Perlmutter et al., 1999, Nobel Prize 2011).

The age of the Universe today ( $z=0$ ) is accepted as  $\sim 14$  Gyr. Only 20% of baryonic matter is inside stars and galaxies, the rest is scattered within the intergalactic gas in the form of ionized H. DM is believed to form sort of a filamentous backbone for galaxies in the Universe albeit *invisible* to us. Galaxies represent about 10% of the baryon fraction of the Universe. We observe two main classes of galaxies: spiral and elliptical galaxies. Generally, galaxy sizes are of the order of a kiloparsec, their masses are on the order of  $10^{10} M_{\odot}$ , and their abundance is  $10^{-2} \text{ Mpc}^{-3}$ .

The observed distribution of galaxies in the Universe is patchy. Clusters and groups contain most of the galaxies in the Universe, so galaxies typically evolve alongside other galaxies. Galaxies are not static in clusters, they are in motion. A cluster is the largest gravitationally bound structure in the Universe. Clusters themselves can group into larger entities, superclusters. Clusters and superclusters are embedded in the filaments of the LSS of the Universe, usually in the knots where filaments congregate together. For example, our own planet Earth is located in the

Milky Way, which belongs to the LG, which is located in the *Virgo cluster* of the *local supercluster*. Another example of a galaxy cluster is shown in Fig. 2.

In addition to clustering of galaxies, seemingly empty regions of space exist on large scales (*voids*). However, at scales of 200 Mpc the Universe does appear to be isotropic. It has a uniform density and is the same in each direction.

These observations elucidate the apparent importance of the environment in the life of a galaxy. Clusters are important in cosmology because they are the largest objects in the Universe held by their own gravity and are often used to test cosmological models or gain information about cosmic structure. The large-scale cluster environment is also important in understanding the evolution of galaxies (and AGN), and is touched on in the following two chapters.

Most of the phenomena are not testable in Earth’s laboratories, however, large-scale simulations have been developed to trace the evolution of the universe, and are presented in the following subsection.

## 2.1.5 Galaxy evolution simulations

Computational simulations are the testbed for different cosmological frameworks. Furthermore, the papers in this dissertation provide observational data to contrast with cosmological models of galaxy formation and evolution, such as AGN feedback assumption. Comparing simulations to observational data (for example as in publications from this thesis) is not straightforward and requires a lot of work. Observational data are collected with different selection methods and can be messy. On the other hand, the models are built using actually very different approaches and often making specific assumptions (and represent ideal patterns in a way). For example, the luminosity function (LF) of galaxies may be modeled as Schechter function, but the data points may have a scatter due to random and/or systematic errors. Thus we very briefly discuss the main concepts on how these simulations are built.

Several large simulations have been published in the last few decades. It is important to know (even as an observer) what goes into building the models<sup>4</sup>, including assumptions, in order to be able to correctly compare with the observational data (e.g., Baugh et al., 1996; Somerville & Davé, 2015; Naab & Ostriker, 2017; Vogelsberger et al., 2020; Crain & van de Voort, 2023). The cosmological simulations currently are restricted by a choice, either to provide more resolution or more statistics to the mock cosmic web output.

Starting with a few principles, the large-scale filamentary structure is built, modeling the collapse of DM, and eventually the formation of galaxies. The LSS formation leads to gas accretion into galaxies, fuelling the SF. In *DM-only simulations* the halos are considered to be DM overdensities within the growing DM cosmic back-

---

<sup>4</sup>For example, if a manual injection of BHs is employed, then comparing with observations is problematic, because observations of AGN environments currently have inconsistent results.

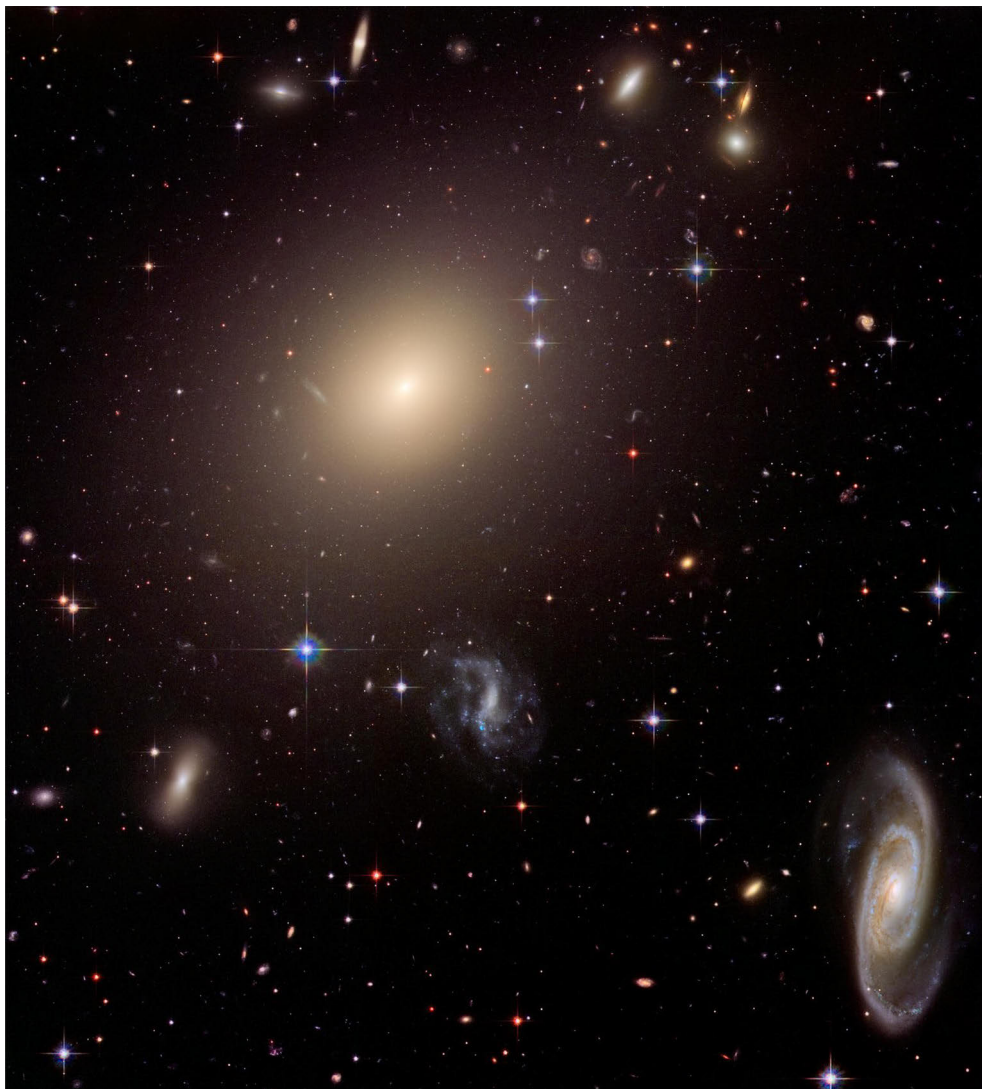


**Figure 2.** An example of a galaxy cluster hosting a variety of galaxies. Cluster Abell S0740,  $z=0.03$ , is one of the clusters in the Abell catalog of rich clusters (Abell et al., 1989). The giant elliptical galaxy, ESO 325-G004, is at the center. It exerts gravitational pull on the other member galaxies. Image Credit: NASA, ESA, and The Hubble Heritage Team (STScI/AURA), [esahubble.org/images](http://esahubble.org/images). Cluster information from the SIMBAD database (Wenger et al., 2000).

bone, and it is within their centers that galaxies are postulated to form; the visible matter is incorporated indirectly (e.g., merger tree algorithms, Jones & Lambourne, 2004; Jiang & van den Bosch, 2014; Nadler et al., 2023). For example, the Millennium Project uses the N-body simulation technique (Springel et al., 2005; Lemson & Virgo Consortium, 2006) within the cold DM ( $\Lambda$ CDM) framework.

Another approach to models of the universe is based on the *hydrodynamic method*. Here fluid dynamics concepts regulate the evolution of the gas component of the universe (baryons) coupled with DM evolution. The Illustris simulation is built in this way, Fig. 3 (Vogelsberger et al., 2014a; Nelson et al., 2015). For example, the bimodal distribution of galaxy demographics as ellipticals and spirals is reproduced reasonably well by the Illustris simulation (Fig. 4, Vogelsberger et al., 2014b).

In particular, modeling AGN feedback is crucial in the  $\Lambda$ CDM, because without it, the observed trends of the local Universe are not reproduced (e.g., the comparison between the Horizon-AGN and Horizon-noAGN simulations, Dubois et al. 2012, 2014; Kaviraj et al. 2017). This is in addition to the stellar feedback. The AGN feedback has two scenarios: radio and quasar modes, which depend on the Eddington rate (Dubois et al., 2012). *The radio mode feedback* is described by powerful jets, which release energy, momentum, and mass into the surrounding gas, while *the quasar mode's* sole input is the thermal energy via AGN-driven winds. The AGN power has high efficiency and plays a key role in regulation of evolution of high stellar mass galaxies. Various simulations, such as the Horizon-AGN simulation and the NewHorizon zoom-in simulation project (Dubois et al., 2021), attempt to refine how models approach the inclusion of AGN feedback.

## 2.2 Key concepts in cosmology

### 2.2.1 The standard cosmological model

The currently accepted cosmology paradigm of the Universe is explained by the concordance *Lambda Cold DM* ( $\Lambda$ CDM) model, a geometrically flat universe (also referred to as the “standard model”). The “lambda” constant is associated with dark energy (few key papers and reviews: Rees & Ostriker, 1977; White & Rees, 1978; Peebles, 1982; Peebles & Ratra, 2003; Bullock & Boylan-Kolchin, 2017). The small-scale early density anisotropies become more pronounced due to gravity. In some loci, the growing structure collapses into DM halos. These halos merge into bigger and bigger sizes. Baryonic matter (cold gas) is attracted to the DM halos, eventually condensing in the center of the halo and forming stars and galaxies.

The three components of the Universe are: visible matter (baryons), DM, and dark energy. The baryonic component is only about 5% of the total energy density of the Universe. The baryons are the smallest component, however, they represent what we can see or observe. In fact the dark energy comprises the largest component

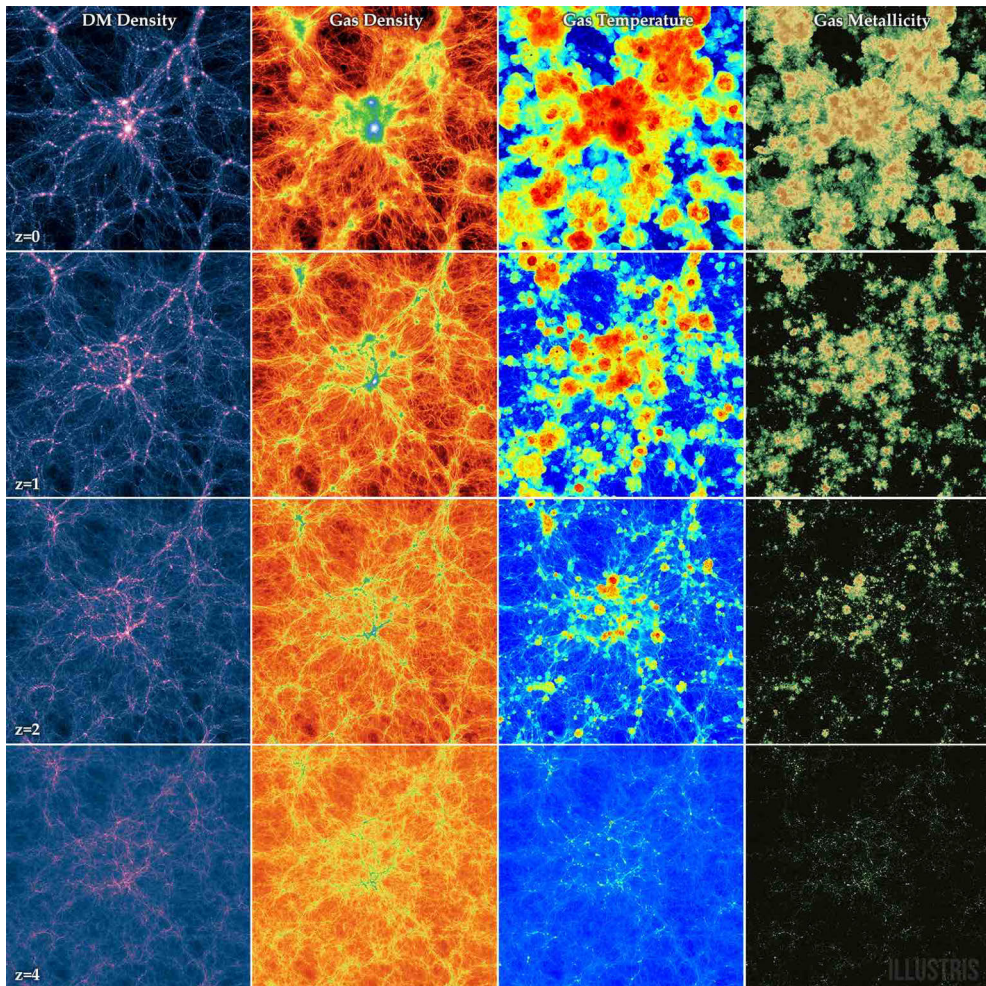


**Figure 3.** The time evolution of a box, showing DM and visible matter properties from Illustris simulation (top row with the most recent snapshots). The DM-based simulations do not provide a ready insight into the galaxies, while the advantage of simulations such as Illustris is that besides DM, baryonic component evolution is also carried out, making it easier to bridge the modeling results with observations of galaxies. Credit: Illustris collaboration / Illustris simulation, [illustris-project.org](http://illustris-project.org).

today, and is of unknown nature so far. It is responsible for the accelerated expansion of the Universe. The DM interacts gravitationally, and its nature is also unknown.

## 2.2.2 Laws of physics

When studying the Universe at extragalactic scales, few global concepts guide our work and need to be redefined, especially when factoring in the cosmic expansion to which all the galaxies are subject to. The first principle is that the fundamental



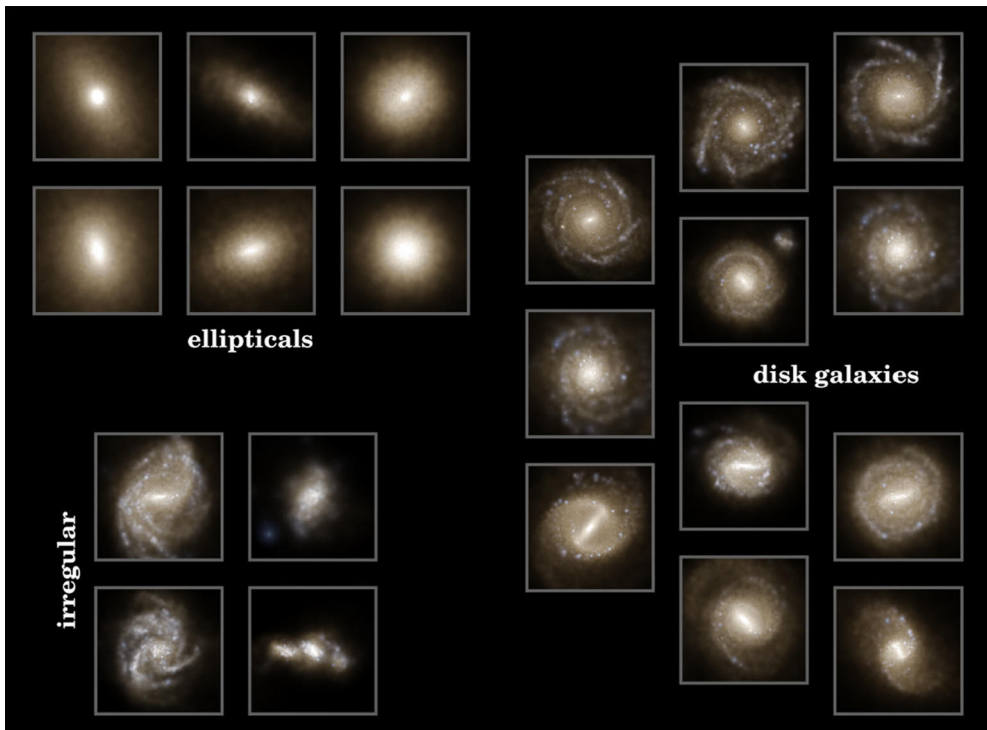


**Figure 4.** Mock galaxies from Illustris simulation at  $z=0$ , illustrating how Illustris cosmological simulation results can be contrasted to real observations of galaxies. In this case, the morphology classes may be compared to observed categories (see the following chapter). Credit: Illustris collaboration / Illustris simulation, [illustris-project.org](http://illustris-project.org).

physical laws that describe nature (e.g., laws of motion, electromagnetic interaction) are the same today as they were yesterday. They are also the same everywhere. Thus, we can apply our knowledge of physics from the laboratory to distant galaxies. For example, that's why we assume that since the early Universe had temperatures higher than stellar interiors, nuclear fusion could have taken place to form nuclei of Hydrogen and other light elements. Furthermore, light has a finite speed and it is the fastest speed in nature,  $c = 29\,979\,245\,800 \text{ cm s}^{-1}$  (in vacuum). The photons of electromagnetic radiation, be it in radio-frequency or at very high energies (gamma rays), travel at the speed of light.

### 2.2.3 Cosmological principle

According to the *cosmological principle*<sup>5</sup>, at larger scales, the Universe is homogeneous and isotropic, i.e., invariant in translation and in rotation respectively. In his

<sup>5</sup>It is also called the Copernican principle, after the Polish astronomer Copernicus (proponent of a heliocentric model of the Universe).

textbook ‘First Principles of Cosmology’, Linder (1997) elegantly defines these two concepts: “*homogeneity* says that all points in space have the same physical conditions, e.g., density and temperature” and “*isotropy* signifies that all directions have the same physical appearance.”

This principle is very important in studying galaxies because it is difficult to study the whole sky in great detail, although large-sky-coverage surveys are more common nowadays. Instead, smaller areas of the sky are observed in detail and then the observations are extrapolated to galaxies in general. In this work, in Paper III, I studied quasars within the equatorial regions of the sky. However, we assume that properties of quasars observed in this patch of the sky can be reasonably extrapolated to quasars at any other Right Ascension (R.A.) and Declination (Decl.) celestial coordinates (for the same quasar type and redshift range).

At this point in the discussion, it is appropriate to evoke the concept of *cosmic variance*, with respect to its effects on observational results in surveying smaller patches of sky. At large enough scales, the Universe is close to the ideal model corresponding to the cosmological invariance in translation and rotation, however, at smaller scales it might not, because at smaller scales “not all patches of sky are equal” — some patches are in voids, some in clusters, for example (Driver & Robotham, 2010). It is an important aspect in understanding surveys. In practical terms, cosmic variance is the “field-to-field variation due to large-scale structure” (Somerville et al., 2004; Moster et al., 2011). It introduces uncertainty into the observed quantity (e.g. number density of quasars) beyond the Poisson shot noise.

## 2.2.4 Hubble’s law

Observations should take into account that a galaxy may emit at one wavelength, but due to the expansion of the Universe, the light that we receive at the telescopes arrives at a different wavelength. This difference depends on the distance and time traveled, and is quantified as a cosmological redshift,  $z$ :

$$z = \frac{\lambda_{\text{observed}} - \lambda_{\text{emitted}}}{\lambda_{\text{emitted}}} . \quad (4)$$

The *red* part of the term *redshift* signifies the fact that all photons from the galaxies are shifted towards the *redder* (and therefore longer) wavelengths. In this case of cosmological redshift, the spacetime fabric of the Universe itself expands, lengthening the wavelength of the observed photons, which were emitted originally at a shorter *rest* wavelengths by the galaxy.

Actually, this fundamental observation about galaxies which supported the idea of an expanding Universe was made by Edwin Hubble, who may be considered as the founder of extragalactic astronomy. The velocity of a given galaxy is described by the *Hubble’s law* :

$$v_r = H \times D , \quad (5)$$

where  $v_r$  is the galaxy's recessional velocity ( $v_r=cz$ ) and has a radial or line of sight direction,  $D$  is the distance away from the Earth, and  $H$  is the Hubble Constant (Hubble, 1929). The Hubble Constant is the same in every point in space, but changes with time. Currently, at  $z=0$ ,

$$H_0 \sim 100 \text{ km s}^{-1} \text{ Mpc}^{-1} \times h , \quad (6)$$

where  $h$  is a dimensionless parameter. For example, in Papers I of this dissertation, the value  $h \sim 0.7$  is used. The relationship in Equation 6 describes that a galaxy that is further away from us (greater  $D$ ) has a greater recessional speed (larger  $v$ ). That means that we have to be careful how we define and measure distances, one of the crucial observables in astronomy (discussed in the next section).

The linear relation in Equation 5 holds up to redshifts of  $z \sim 0.2$  (Jones & Lambourne, 2004). It is only applicable to those galaxies which are far enough away so that their recessional velocities are dominated by the cosmic expansion. If we rearrange Equation 5, we can express it with the cosmological redshift ( $z$ ) on one side as:

$$z = H \frac{D}{c} , \quad (7)$$

for non-relativistic velocities, i.e.,  $v_r \ll c$ . Thus, if we measure the redshift from Equation 4, we can also get the distance to the galaxy.

The recessional velocity representing the expansion of the universe might not be the only velocity component to describe the full picture between the observer and the galaxy observed along the line of sight (or radial) direction. Any additional (relative) motion beyond the Hubble flow is termed as the *peculiar velocity* (Linder, 1997). Here I use, without derivation, Equation (2.19) from Mo (2010), showing that in the FRW (Friedmann-Robertson-Walker) cosmology, there is an additional component for calculating redshift due to peculiar velocity ( $v_r^{(\text{pec})}$ ):

$$v_r = cz + v_r^{(\text{pec})} , \quad (8)$$

where the subscript  $r$  under the peculiar velocity term signifies the radial direction (since peculiar velocity may also have a non-zero transverse component), see Fig. 12. Peculiar velocities are usually non-negligible in the Local Universe. On the other hand, for much more distant galaxies, gravitational force between the observer and the high-redshift galaxy is not a concern when calculating the cosmological expansion (Linder, 1997).

## 2.3 Cosmological distances

As in this work I deal with galaxies and quasars at large distances, it is important to note how astronomers calculate distances and separations at cosmological scales.

This is especially important for the work in this thesis, since I am trying to identify neighbors of quasars, e.g., in Paper III, within a comoving volume of few megaparsecs. We know that on a 2D image, nearby galaxies might in actuality be far away, due to projection effects. It could be a background galaxy or a foreground galaxy projected into the same field. In Fig. 5, in the top diagram, we show the imaginary comoving volume around a quasar. The neighboring galaxies are identified within a fixed comoving volume of radius,  $R$ , around each quasar in Paper III based on the GAMA survey data. Now in 2D representation, the central quasar is marked as a filled star (Fig. 5, bottom plot). All galaxies (gray dots) here have R.A. and Decl. coordinates similar to those of the quasar neighbors (filled circle and pentagon). However, actually, only two galaxies have a comoving separation below 2 Mpc. This diagram illustrates how the 2D visualization does not obviously reveal the physically close galaxies, necessitating careful cosmic separation calculations.

### 2.3.1 Comoving and proper distances

So, how can we find the actual distances? First, through spectroscopy, we can obtain the redshift of the galaxy, which is then used to calculate the distance. The fundamental distance measure in cosmography is the *comoving* (line of sight) distance,  $\chi$ , between two objects in the Universe with the expansion effect factored out. It is because in a comoving coordinate system, the system itself expands with the Universe.

Note that on small scales when the universe breaks from the ideal isotropy, such as in a cluster of galaxies, the motion of galaxies within that cluster may contribute to the final distance calculation as a local effect. For example, between an observer on the Earth and a galaxy outside of the Milky Way, peculiar velocities of several hundred  $\text{km s}^{-1}$  scale are significant — up to a few megaparsecs (Linder, 1997). Additionally, we are under the gravitational influence of the Virgo cluster, within about 20 Mpc radius (Linder, 1997). A bit further from the Earth, that of 40 Mpc ( $z < 0.01$ ), distance is not measured reliably by the linear Hubble’s law equation (Jones & Lambourne, 2004). Our Galaxy has a peculiar velocity with respect to the Virgo Cluster, and is called the “Virgo infall” (Combes et al., 1995). The velocity dispersion of Virgo cluster members is  $> 500 \text{ km s}^{-1}$  (Combes et al., 1995). So, it is important to account for any contamination stemming from local gravitational effects, when assessing the redshifts (distances). However, in all of the publications in this thesis, the lowest redshift boundary ( $z=0.1$ ) was at least 10 orders of magnitude higher than this limit and consequently outside of the influence of the Virgo Cluster pull.

Furthermore, overdensities, such as clusters of galaxies, can have hundreds of members and can be very massive. Thus, gravity plays a significant role in these overdense regions of the Universe. Galaxy members are attracted to each other and interact gravitationally. This influences their proper velocities, which in turn contaminate the Hubble flow.

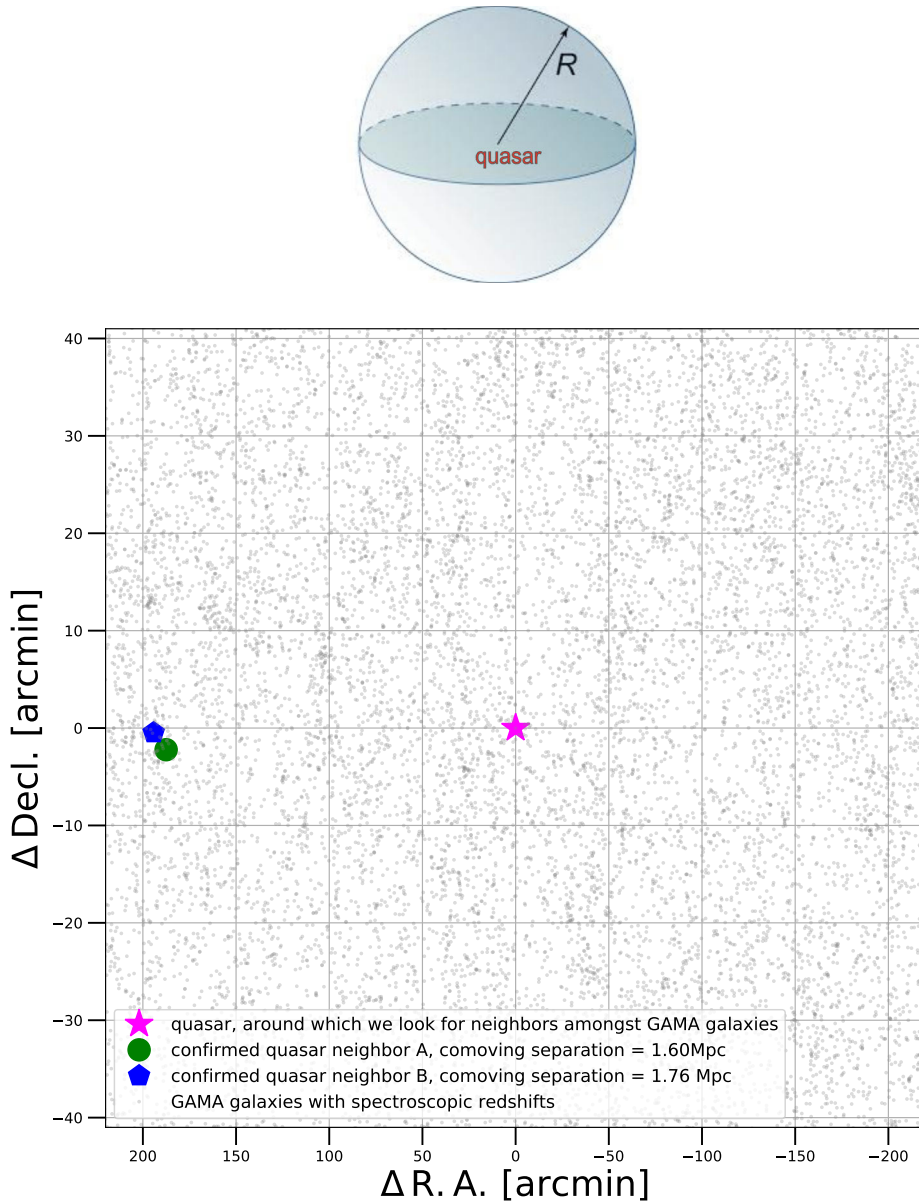


**Figure 5.** Illustration of differences between apparent angular and comoving separations. *Top.* A comoving volume (of radius  $R$ ) around a quasar, investigated in Paper III, where the aim was to identify all of the galaxies within that comoving volume ( $R = 2$  Mpc). However, typical catalogs usually only provide the R.A. and Decl. coordinates of galaxies. *Bottom.* GAMA survey galaxies (gray dots) around one of the quasars (pink star) plotted in R.A./Decl. space. In Paper III, we estimated the comoving separations for these galaxies, showing that only two neighbors (green circle and blue pentagon) were within the 2 Mpc limit.

Closely related to the comoving distance is the *proper distance* (or physical distance), which is defined to be the distance to the object at a specific moment in cosmological time, and thus by definition can change over time due to the expansion of the Universe. Only at present time ( $z=0$ ) the comoving distance and the proper distance are equal for a given galaxy.

Thus, at other epochs, a *scaling factor*,  $a(t)$ , needs to be used to account for the expanding Universe. According to the *Friedmann-Lemaitre-Robertson-Walker metric* (FLRW), the time-dependent scaling factor is:

$$a(t) = \frac{1}{z + 1} . \quad (9)$$

The scale factor is unity at present and zero at the instance of the BB.

GAMA spectroscopic survey provides redshifts for quasars and galaxies in Paper III. Assuming the standard cosmology (Planck Collaboration et al., 2020), I was able to determine the comoving distance corresponding to the redshift of the object. It is important to remember that the measured redshift differs from the cosmological redshift (due to the cosmic expansion) through the peculiar velocity term.

Currently various online calculators and software packages are available to perform this calculation. I compared the NASA Extragalactic Database calculator (Wright, 2006) results with Astropy-ecosystem based results (Astropy Collaboration et al., 2018), and they were consistent with each other. In the end, due to using python numerical codes, I chose the Astropy cosmology package results for the published calculations, which is based on Hogg (1999) methodology for various cosmologies (Linder, 2003).

At the core, the redshift-to-distance conversion is based on the chosen cosmology model, cited individually for each paper, where a specific definition to the spacetime metric is given. For the FRW models, the Robertson-Walker (RW) metric is used. In the comoving form, it is:

$$ds^2 = -dt^2 + a^2(t)[dr^2 + \chi^2(d\theta^2 + \sin^2\theta d\phi^2)] , \quad (10)$$

where  $ds$  is the line element,  $a$  is the scale factor,  $r$  is the radial coordinate,  $\chi$  is the comoving coordinate,  $t$  is the time coordinate,  $\theta$  is the polar angle, and  $\phi$  is the azimuthal angle (Linder, 1997; Liske, 2000). For the case when the curvature parameter is zero ( $k=0$ ), the comoving and the radial ( $r$ ) coordinates are equal.

In Paper III, as an example, we assumed that the Universe is described by the flat  $\Lambda$  CDM cosmology. It is a special case of the FLRW cosmology model family, where the cosmos is isotropic and homogeneous. Additionally, this special case has a non-zero cosmological constant and is curvature-free ( $k=0$ ). The exact calculations are based on numerical integration methods.

### 2.3.2 Comoving separation between galaxies

In Paper III we have the problem to calculate the comoving separation between two galaxies based on their spectroscopic data from GAMA. This question is put clearly by Liske (2000) publication at the turn of this millennium: “How to calculate the distance between two cosmological objects given their redshifts and angular separation on sky?” If the two objects move consistently with the cosmological expansion of the Universe (or Hubble flow), the comoving distance between them remains constant with epoch, i.e., does not change in time (Hogg, 1999; Liske, 2000),

$$\chi = D_H \int_0^z \frac{dz'}{E(z')}, \quad (11)$$

where  $z$  represents the redshift,  $D_H \equiv \frac{c}{H_0}$  is the Hubble distance, and  $E(z)$  function (Peebles, 1993) is defined using the three density parameters as:

$$E(z) \equiv \sqrt{\Omega_M(1+z)^3 + \Omega_k(1+z)^2 + \Omega_\Lambda}. \quad (12)$$

$\Omega_k$  is the density of a parameter which measures the "curvature of space" and is equal to zero for a flat Universe. Using the `astropy.cosmology` subpackage, one can calculate the comoving distance (as well as other common cosmological quantities) from redshift within a specified cosmological model (Astropy Collaboration et al., 2013, 2018; Hogg, 1999).

As the next step, to identify neighbors around quasars, based on the comoving distances, I identified the comoving separation between the seed object and the candidate neighboring galaxy. In a flat Universe ( $k=0$ ), the comoving separation reduces to a cosine rule:

$$r = (\chi_1^2 + \chi_2^2 - 2\chi_1\chi_2 \cos \theta)^{\frac{1}{2}}, \quad (13)$$

where  $\theta$  is the angular separation between two objects, calculated based on the R.A. and Decl. coordinates (J2000 epoch for GAMA database). Thus, I robustly identify all of the neighbors using spectroscopic redshifts, weeding out the background and foreground galaxies projected by chance in the same field. For a more general treatment of the problem, see Liske 2000 and examples of papers with similar calculations are Lindsay et al. 2014; Truebenbach & Darling 2018; de Carvalho et al. 2018.

### 2.3.3 Angular diameter distance and luminosity distance

Two additional distances from cosmology are used in this thesis, the luminosity distance and the angular distance (Hogg, 1999; Binney & Merrifield, 1998; Mo, 2010). The *angular distance*,  $D_A$ , is the distance to the object with intrinsic diameter  $d$ , which subtends an angle  $\theta$  (Fig. 6):

$$\delta\theta = \frac{d}{D_A}, \text{ for } D_A \gg d. \quad (14)$$

Qualitatively, the angular distance describes galaxies where they were at the time they emitted the light observed in space and time, meaning that the galaxies were younger and closer to the observer. As Linder (1997) puts it, “we pretend that there is no spacetime curvature so the angular diameter distance only corresponds to a physical distance”, Fig. 6.

The *luminosity distance*,  $D_L$ , describes how distant galaxies appear dimmer, since the photons are stretched out. Here it is the bolometric luminosity, i.e. luminosity from all bands. The canonical definition states that the luminosity distance is “the distance to an object of intrinsic luminosity  $L$  is the quantity  $D$  such that the observed flux from the source is  $F = L/(4\pi D^2)$ ” (Binney & Merrifield, 1998). Rearranging to put the luminosity distance  $D_L$  on one side (Hogg, 1999), we get:

$$D_L \equiv \sqrt{\frac{L}{4\pi F}} . \quad (15)$$

In the publications included in this thesis in particular, the luminosity distance was used when calculating the absolute magnitude values for galaxies (see § 5). The luminosity distance is correlated to the angular diameter distance (Hogg, 1999):

$$D_L = (1 + z)^2 \times D_A . \quad (16)$$

If instead of bolometric luminosities, one uses the specific luminosity,  $L_\lambda$ , restricted to a certain wavelength range,  $\Delta\lambda$ , then a correction needs to be applied to Equation 15, as discussed in § 5.



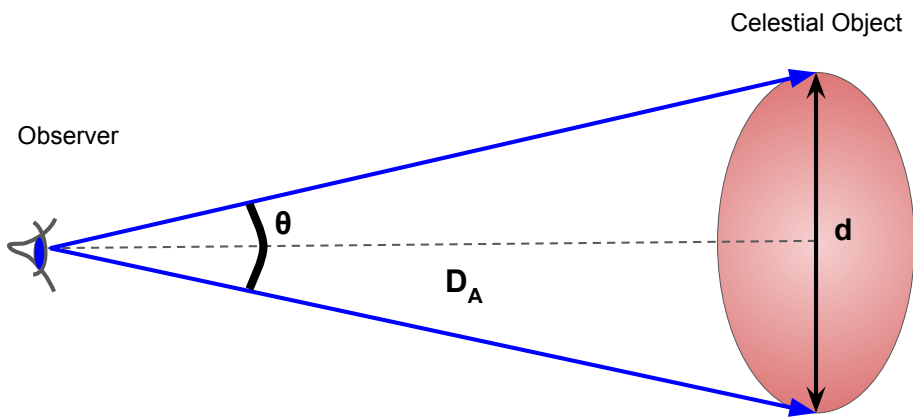


**Figure 6.** Angular diameter distance (Equation 14).

# 3 Observed properties of galaxies

Երկինքը վառեց ոսկե բուրվառներ...

The sky is lit with golden burning cinders...

---

Vahan Teryan  
translated from Armenian

As the particles, radiation, and forces performed their cosmic dance since the BB, the resultant picture of the Universe is what we observe today with telescopes — a spacetime fabric sparsely populated with matter and voids, where galaxies hold the title of *building blocks of the Universe*. In this chapter I relay major observational results generally described as the *bimodality* of galaxy populations. Here the bimodality refers to the qualitative description of the distribution of various galaxy properties, such as color-magnitude (Baldry et al., 2004a), stellar mass (Kauffmann et al., 2003b), and surface brightness (Blanton et al., 2003).

In order to understand as much as possible about the intricate tapestry of galaxy formation and evolution, we take advantage of both the observations of the Milky Way and of other galaxies across cosmic distances and times. On one hand, studying our own Galaxy helps us to apply more detailed knowledge to other galaxies. On the other hand, beyond the LG, we rely on interpreting observed fluxes from the whole galaxy to assess gas content, stellar populations, ages. This is because while there are some observations of extragalactic SNe, generally it is impossible to resolve individual stars in galaxies with distances beyond the LG.

In this chapter, first, we review the main morphological classes of galaxies (§ 3.1). The observed shapes of galaxies engrain a general bimodal trend in the galaxy properties. Galaxies in the different morphological classes exhibit different properties, for example in colors, SF, ages. Then we discuss the galaxy dynamics (§ 3.2), the distribution of light of galaxies (§ 3.3) and the main scaling relations (§ 3.4). In the last section, we consider the formation of stars (§ 3.5). Here, it is important to remember, that the visible structures of galaxies are considered to be the lower fraction of overall matter; the dominant component is the DM.

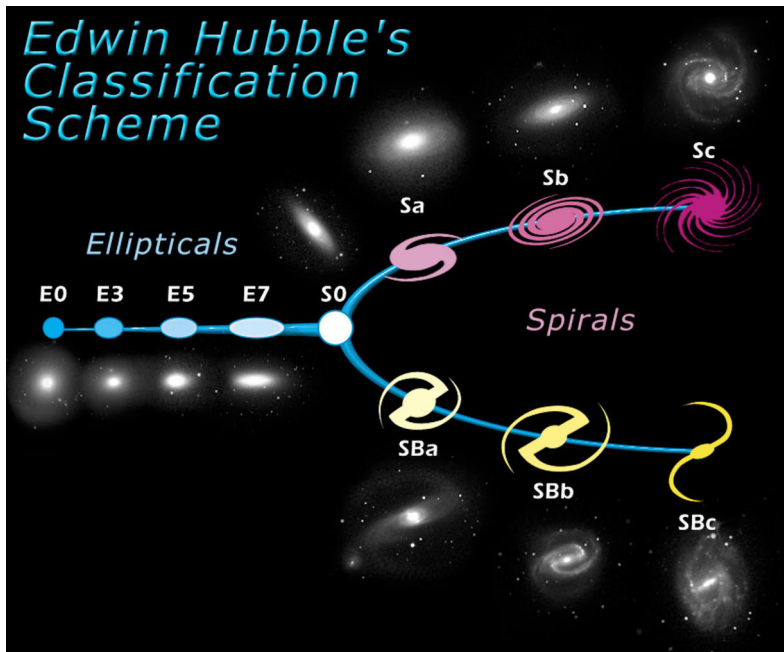


**Figure 7.** Hubble's "tuning fork" (Hubble, 1936) is a morphological classification of bright galaxies in the Local Universe. The ellipticals are grouped on the left, starting with the more circular shaped ones. The spirals are further bifurcated into two groups based on the presence of a bar. In the middle is the S0 category, which is described by the presence of bulge and disk, but no spiral pattern (Phillipps, 2005). Credit: NASA & ESA, ESA *Hubble* images.

### 3.1 Galaxy morphology

One of the first observational properties noted by Hubble (1926) when studying galaxies was their diverse morphology. In his seminal book, *The Realm of the Nebulae*, Hubble (1936) organized a *tuning fork diagram* classification scheme of galaxies, as presented in Fig. 7. The *Hubble diagram* of galaxies is based on the observations in the optical regime of the EMS and its basics are still used today.

On one side of the diagram, Hubble grouped the *elliptical galaxies*, starting from the most round ellipticals. On the opposite side are located the *spiral galaxies*, which are divided into two groups based on the presence or absence of a *bar* in the center (barred spirals). The spirals are subclassified based on the prominence of the central bulge and how tightly the spiral arms are wrapped around. The galaxies at the root of the prongs of the fork-diagram have large central bulges (Sa/SBa spirals) which are less and less pronounced as one travels down to the tip of the prongs, reaching at the end magnificent spirals with widespread spiral arms and relatively smaller bulges (Sc/SBc types). In the middle of the diagram are the *lenticular galaxies* (S0), which have a disk, but no spiral arms — named so due to their lens-like shape (Phillipps, 2005). Spirals are furthermore a flat structure, while the ellipticals are ellipsoidal.

For example, our own Milky Way is a spiral galaxy, as is the nearby Andromeda Galaxy (M31). On the other hand, the giant galaxies in the middle of the Coma Cluster are ellipticals, as generally are the central galaxies in clusters. In the nearby universe, most bright galaxies are spirals, while about a third of galaxies are either elliptical or lenticular.

The *bimodality* in morphology is correlated to the bimodality in color (e.g. Chester & Roberts, 1964; Roberts & Haynes, 1994; Baldry et al., 2004b; Cattaneo et al., 2009). In color-magnitude space, the ellipticals and spirals generally fall into different loci (Fig. 8). For example, in the same Coma Cluster, the bright galaxy members with larger (redder) color values lay in a narrow band (*red sequence*), while the members with smaller (bluer) color values are scattered in a different area (*blue cloud*) (Yamanoi et al., 2012; Stone, 2017). Generally, spirals are blue and ellipticals are red in the optical.

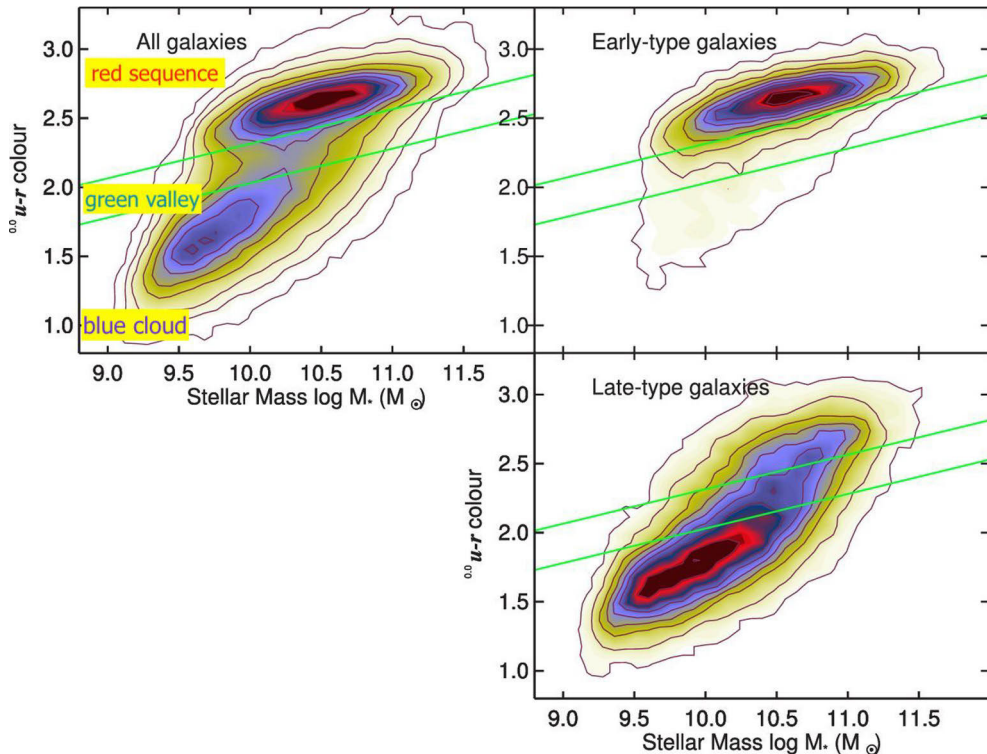


**Figure 8.** An example of a color- $M_*$  plot showing the color bimodality of low-redshift galaxies (density contours) (Fig. 2 from Schawinski et al., 2014). The x-axis represents the  $M_*$  — a proxy for luminosity. The y-axis holds the optical SDSS  $u - r$  color from bluer to redder (smaller to larger) values (DR7, York et al., 2000; Abazajian et al., 2009). Galaxies congregate into three loci in color- $M_*$  space: red sequence, green valley (green lines), and blue cloud. The subplots on the right show early-type (top) and late-type galaxies only (bottom) — early-types congregate strongly in the red sequence area, while the late-type galaxies are more prevalent in the blue cloud region.

Hubble proposed that the morphological classification was also an evolutionary sequence — the elliptical and lenticular galaxies were formed early on (*early type* galaxies), and then they morphed with time into more complex spiral structures (*late type* galaxies). The spiral galaxies evolved from Sa (early type spirals) to Sc shape spirals (late type spirals). According to the accepted standard theory, the opposite is the case — spiral galaxies merge to form elliptical galaxies. One piece of evidence to refute the original scenario is that only spirals also have ample numbers of young stars in addition to older stellar populations (Bell & de Jong, 2000), while the stellar populations of elliptical galaxies are predominantly old. However, the nomenclature is still used in literature.

Numerous refinements to this classification have been introduced throughout the years, but the main classes remain. This classification is relevant mostly to the present time, as at higher redshifts, especially in the Early Universe, the morphologies of galaxies were more irregular, such as cigar shaped galaxies. Any evolutionary model of the Universe must reproduce this observation of apparent galaxy shapes. In the following subsections we describe in more detail these major classes of galaxies.

### 3.1.1 Elliptical galaxies

On the left of the Hubble fork diagram are galaxies which have an elliptical morphology in the optical images (Fig. 9). The *E-number* ( $E_n$ ) refers to the formula:

$$E_n = 10 \times (1 - \epsilon) , \quad (17)$$

where the *apparent ellipticity*,  $\epsilon$ , is defined as a ratio of the semi-minor ( $b$ ) and semi-major ( $a$ ) axes of the ellipse:

$$\epsilon \equiv \frac{b}{a} . \quad (18)$$

The ellipticity describes the shape of the galaxy (Hubble, 1926; Schneider, 2006). Hence, the E0 galaxies are circular (have circular isophotes<sup>1</sup>). With a larger value of the E-number, the elliptical form of the galaxy becomes increasingly flatter. The elliptical galaxies are 3D objects, and this classification is based on their apparent 2D shape, thus dependent on the viewing angle. Using different techniques it is possible to understand better the possible 3D shapes as well (e.g., 2D to 3D deprojection method, Chen et al., 2016).

To quantify the size of a galaxy it is common to use the *effective radius*<sup>2</sup>,  $R_e$ , within which half of the light of the galaxy is contained (Schneider, 2006). While typical elliptical galaxies have effective radii of a few kiloparsecs, the sizes range from dwarf to giant ellipticals (Table 2). The largest elliptical galaxies, *cD galaxies*,

<sup>1</sup>An isophote is defined as a “contour of constant surface brightness” (Sparke & Gallagher, 2007).

<sup>2</sup>The term effective radius is synonymous with *half-light radius* label.

are found in the centers of clusters. On the other hand, the dimensions of the dwarf ellipticals may be similar to that of a globular cluster.

The elliptical galaxies span a large range in luminosity as well (Kutner, 2003). The elliptical galaxies have less gas and dust compared to spiral galaxies, and their SFRs are low. The spectrum of an elliptical galaxy is dominated by old stellar populations (of stars with low masses), resulting in reddish appearance in the optical. For that reason, the elliptical galaxies are often described as “red and dead”.

Ellipticals are pretty uniform blobs which lack large-scale distinctive features of spiral galaxies (spiral arms). Their starlight distribution is more concentrated in the centers and gradually falls off with increasing distance from the center (e.g., Kormendy & Djorgovski, 1989). Ellipticals have smooth color profiles and are featureless. Their stellar motions are random. Furthermore, the elliptical galaxies are characterized by high metal abundances. Additionally, it is observed that ellipticals often have globular cluster systems around them. Massive ellipticals are surrounded by X-ray emitting gas ( $T > 10^5$  K). Galaxy mergers are postulated to result in the for-



**Figure 9.** IC 2066, an elliptical galaxy (Constellation Eridanus). Credit: ESA/Hubble & NASA; Judy Schmidt and J. Blakeslee (Dominion Astrophysical Observatory), ESA *Hubble* images.

**Table 2.** Measurements of spiral and elliptical galaxies (Kutner, 2003; Sparke & Gallagher, 2007). Here the effective radius is used as a proxy for galaxy size.

Type	$R_e$ kpc	Mass $M_\odot$	Luminosities $L_\odot$
Spiral	5–100	$10^9$ – $10^{12}$	$10^8$ – $10^{11}$
Elliptical	0.3–100s	$10^7$ – $10^{13}$	$10^5$ – $10^{13}$

mation of giant ellipticals, which are often found in the centers of clusters. Actually, even though we start thinking about elliptical galaxies by considering them “red and dead spherical cows”, as my Master’s thesis supervisor Aaron Romanowsky jokingly used to put it, in recent decades research showed new discoveries on kinematics of elliptical galaxies shaking our previous assumptions (e.g., Cappellari, 2016).

### 3.1.2 Spiral galaxies

The morphology of spiral galaxies is described by the presence of spiral arm(s) which emanate from the center of the galaxy, e.g., Fig. 10. The spiral galaxies may have a bar in their central regions (*barred spirals*). The rotational speeds of spirals are also faster, leading the overall galaxy shape to the flattened disk structure. In fact, it is by observing the dynamics of the spiral galaxies that astronomers came to a model where the visible structure of the spiral galaxy is embedded in a large halo dominated by DM. The spiral galaxies are observed at higher frequencies outside of clusters, compared to the ellipticals (Dressler, 1980).

Spirals are richer in gas and dust than ellipticals. The spirals are characterized by an on-going SF. The center of the spiral galaxies is dominated by old stellar populations. The disk region away from the center is abundant in gas and dust. There are hotspots of SF speckled in the spiral arms. The stellar population has a larger abundance of young stars (O and B class). The young stars in the spiral arms give the disk a bluish appearance in the optical (and the more recently formed stars are



**Figure 10.** NGC 1300, a majestic barred spiral galaxy. Credit: NASA, ESA, and The Hubble Heritage Team (STScI/AURA), ESA *Hubble* images.

more metal rich). The Sc spirals have a larger fraction of gas and dust involved in SF compared to Sa. Young stars and significant ISM are evidence for recent SF.

For spiral galaxies, the overall metallicity of the stellar population increases with the mass of the galaxy (Henry & Worthey, 1999). A similar trend is observed for ellipticals. The metallicity does not stay consistent throughout the volume occupied by the galaxy — instead, the central parts are more metal-rich than the outskirts. The metallicity varies within the disk as well. At the stellar metallicity level, the stars which formed in the past are metal poor compared to the stars birthed by the recent ISM due to the local metal enrichment processes. Actually, observing metallicities and correlating them to other galactic properties sheds light into the galactic evolution history. This is an active research area — with higher resolution instruments paving way to gain more insights.

Most nearby galaxies are easily determined to be spirals or ellipticals from their images. However, images are 2D projections of the three-dimensional galaxies, and especially with further distance, the angle of observation may have a large effect. The spiral galaxies exhibit various orientations towards the observer, ranging from face-on to edge-on; the ellipticals also may exhibit projection effects in the images. Furthermore, additional substructures may be present in galaxies, such as rings, and the appearance of galaxies changes also with the band (e.g., IR versus UV).

### 3.1.3 Other morphological types

#### Lenticular galaxies

A third type of common morphology is observed in the nearby universe, with features from both elliptical and spiral galaxies, called *lenticular galaxies* (S0). They have a disk structure, but lack spiral arms, as gas seems to be required for a spiral (Sparke & Gallagher, 2007). They harbor old stars. Their bulges are similar to ellipticals. S0 galaxies may have a bar. Some lenticular galaxies also have gas and dust (usually at low amounts) but the presence of gas is not typical for S0 galaxies (Kutner, 2003).

#### Dwarf and irregular galaxies

Besides these main groups, there are irregular and dwarf galaxies. The first dwarf galaxy was discovered in the constellation Sculptor by Shapley (1938). Local examples of dwarfs are the Large and Small Magellanic Clouds visible in the Southern Hemisphere. They are satellite galaxies of the Milky Way. The numerous dwarf galaxies are subdivided into their own categories. In the Local Universe, the dwarf spheroidal galaxy type is the most abundant, however massive galaxies account for the most mass.

Other types of galaxies exist: such as irregular galaxies, numerous dwarf galax-



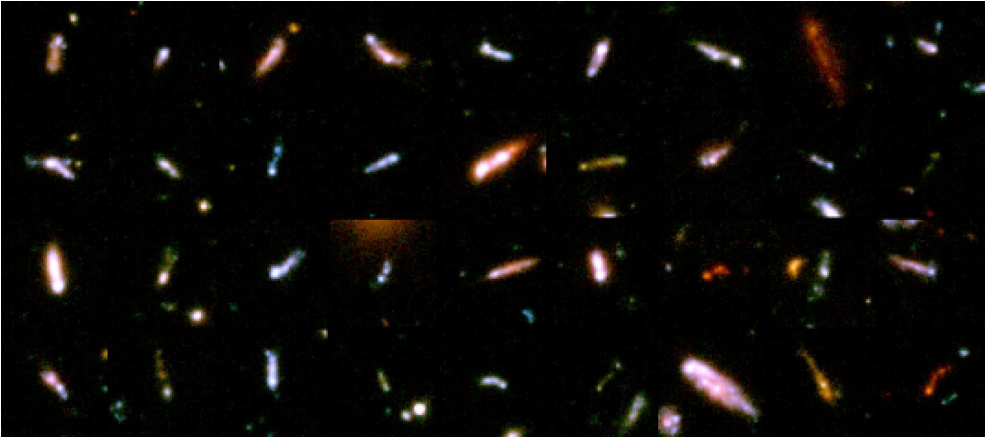


**Figure 11.** The Hubble tuning fork diagram for galaxy classification is not applicable to galaxies at higher redshifts, as they exhibit other types of shapes. For example, this image shows the distant galaxies of “tadpole”-type. These tadpole galaxies exhibit a knot-shaped end and a tail-shaped end, differing from both spirals and ellipsoidal galaxies in morphology. All 36 tadpole galaxies here are postulated to be young galaxies going through a merger (Straughn et al., 2004, 2005). Credit: NASA, A. Straughn, S. Cohen, and R. Windhorst (Arizona State University), and the HUDF team (Space Telescope Science Institute). ESA *Hubble* images.

ies, low surface brightness galaxies (e.g., ultra-diffuse galaxies). For example, the “Green Pea” galaxies (Cardamone et al., 2009) have been discovered through the Galaxy Zoo project (Lintott et al., 2008). Some irregular galaxies appear distorted or interacting and represent a sizable fraction of all galaxies. The foundational classification method, however, focuses on the bright galaxies, excluding other types, such as most of the dwarf galaxies which are nevertheless numerous in the Universe.

### 3.1.4 Morphologies of very distant galaxies (high redshift)

At high redshift, the morphological patterns of the Hubble diagram break down, Fig. 11. The high redshift observations are challenging due to the significant distances and interpretations are sometimes debated. Historically, the observations through the *Hubble Space Telescope (HST)* at  $z > 1.5$  revealed significant fractions of galaxies with unusual shapes (van den Bergh et al., 1996), e.g., “tadpole” galaxies (Straughn et al., 2004), chain galaxies (Cowie et al., 1995).

The discoveries of high- $z$  galaxies continued further. At  $z > 2.5$ , the appearance of galaxies is even more irregular (Giavalisco et al., 1996). For example, the classification by Elmegreen et al. (2005) of  $\sim 1000$  galaxies in the Hubble Ultra-Deep Field (HUDF) revealed that merely  $\sim 35\%$  of galaxies were either elliptical or spiral, as most ( $\sim 65\%$ ) of the galaxies had non-standard structures. The fraction of interacting galaxies is also higher than in nearby galaxies (Abraham et al., 1996).

The HUDF is a deep optical image of a small area in the constellation Fornax

obtained by the *HST* Advanced Camera for Surveys (ACS). This deep image constituted one of the first glimpses into the richness of the very distant Universe. While it has a historical significance, when reading literature it is important to keep the perspective that these early studies did not have yet spectroscopy of the distant objects nor ready photometry-based redshifts — these assessments were done a bit later. For example, the sample of galaxies in (Elmegreen et al., 2005) was selected from the *i* band filter image, which was the deepest at that time. The galaxies were identified by eye, following the restriction that the major axis is larger than 0.3 arcsec.

Furthermore, Elmegreen et al. (2005) study was not based on spectroscopic (nor photometric) redshift range, but rather the galaxies were determined to be qualitatively at a higher redshift due to the fact that the deep imaging “brings to light” more distant galaxies. The galaxies in the sample had a range of redshifts. Nevertheless, the color-color distributions modeled with stellar evolution models indicated (inferred) redshifts up to  $z \sim 4.5$  (see paper’s Fig. 4). The high-redshift galaxies in and beyond the HUDF continued to be studied, e.g., Elmegreen et al. (2007a,b); Sheth et al. (2008); Bournaud et al. (2009); Elmegreen & Elmegreen (2010).

Understanding this distant cosmic epoch morphologies as well as exactly when proto-spiral and proto-elliptical structures formed is an area of currently ongoing research with *HST*, ALMA and *JWST* data (e.g., Conselice et al., 2004; Kartaltepe et al., 2023). Often advanced computational algorithms are employed, such as machine learning techniques (e.g., Tohill et al., 2021). For example, while earlier studies were able to use the human eye to perform morphological classification, advanced data science techniques allow processing large data sets from large surveys.

## 3.2 Dynamical features in galaxies

Unlike the ancient belief that stars are frozen in space, in reality stars do move in galaxies, along with other constituent components (e.g., gas). When considering dynamical features, disks rotate, while the elliptical galaxies are described by the random motion of their stars (Phillipps, 2005) and rotate slowly or not at all. Several parameters describe these observed dynamical patterns from the collective motions of stars in galaxies.

### 3.2.1 Velocity dispersion

To describe the random motion of stars in an elliptical galaxy, the velocity dispersion ( $\sigma^2$ ) quantity is used, defined as “the mean square velocity” (Phillipps, 2005)<sup>3</sup>. This statistical description of motion shows how the data spreads around a central value.

Let’s now consider an elliptical galaxy with  $N$  stars. Given the velocity of each

---

<sup>3</sup>Jeans equations include the treatment of the velocity dispersion tensor. Dynamically hot systems have larger values of stellar velocity dispersion than dynamically cold systems.

star,  $v_i$ , the average velocity of all stars is:

$$\langle v \rangle = \frac{1}{N} \sum_{i=1}^N v_i . \quad (19)$$

Here, we use angled brackets to represent the average of the term they enclose. Each individual star deviates from the average by:

$$\Delta v_i = v_i - \langle v \rangle . \quad (20)$$

Then mathematically, the velocity dispersion is defined as follows (Liddle & Loveday, 2008):

$$\sigma \equiv \sqrt{\frac{1}{N} \sum_{i=1}^N (\Delta v_i)^2} . \quad (21)$$

This is basically from the statistical definition of the standard definition. Sparke & Gallagher (2007) provide a formula (their Equation 2.9) which is an alternative way of writing Equation 21, as we show in the inset “Derivation”.

*Derivation.* To transform, first we substitute Equation 20 into Equation 21. Then the left side of Equation 21 can be expanded:

$$\frac{1}{N} \sum_{i=1}^N (v_i - \langle v \rangle)^2 = \frac{1}{N} \sum_{i=1}^N (v_i^2 - 2v_i \langle v \rangle + \langle v \rangle^2) . \quad (22)$$

From the three terms inside the parenthesis, we take advantage of the fact that the values without subscript  $i$  do not depend on  $i$  and can come out of the summation. Then, the middle term is just the average velocity definition from Equation 19. Hence, we can rewrite this as,

$$\begin{aligned} \frac{1}{N} \sum_{i=1}^N (v_i^2) - 2 \langle v \rangle \frac{1}{N} \sum_{i=1}^N (v_i) + \langle v \rangle^2 &= \frac{1}{N} \sum_{i=1}^N (v_i^2) - 2 \langle v \rangle \langle v \rangle + \langle v \rangle^2 = \\ &= \frac{1}{N} \sum_{i=1}^N (v_i^2 - \langle v \rangle^2) = \langle v_i^2 - \langle v \rangle^2 \rangle , \quad (23) \end{aligned}$$

where in the last two steps we used a standard summation rule and again the definition of the average.

Observations allow the measurement of the 3D velocity vector in the line of sight (radial) direction for elliptical galaxies (Sparke & Gallagher, 2007; Liddle & Loveday, 2008), however this measured radial velocity,  $v_r$ , is for one direction only

(Fig. 12). To get the projection components of the velocity vector then, the standard vector operations apply in the desired geometry system. Consequently, the velocity dispersion is also estimated along the line of sight,  $\sigma_r^2$ . Plus, it is limited to the central region of the galaxy (Phillipps, 2005; Combes et al., 1995). For example, for the cases where a spherical symmetry is assumed, then the total velocity dispersion is simply calculated as three times the measured component (Bowers & Deeming, 1984a):

$$\sigma^2 = 3\sigma_r^2. \quad (24)$$

The typical velocity dispersion for giant ellipticals is  $\sim 250 \text{ km s}^{-1}$  or more.

In most cases, the source is not resolved into individual stars. Instead the actual measurement is from the observed width of the spectral lines because the *Doppler broadening* of the line is related to the velocity dispersion (Phillipps, 2005; Liddle & Loveday, 2008). In Fig. 13, the illustration shows how the combined effect of many stars smears the spectral line signature. The full width at half maximum (FWHM) measurement of the broadened spectral line can be carried out, and then used to calculate the standard deviation ( $\text{FWHM} \sim 2.355\sigma$ ).

### 3.2.2 Rotational velocity and $v_{\text{rot}}/\sigma$

The spectacular disks of spiral galaxies rotate (Phillipps, 2005). This dynamical feature is characterized by the rotational velocity,  $v_{\text{rot}}$  (Phillipps, 2005). Binney & Tremaine (1987) textbook puts it as “circular-speed”. With the advance of integral field spectroscopy (IFS), instruments such as MUSE<sup>4</sup> can be used to study in detail the mesmerizing kinematics of the disks (e.g., Kolcu et al., 2023).

The rotation parameter (Davies et al., 1983) is the ratio between the rotational velocity and the velocity dispersion ( $v_{\text{rot}}/\sigma$ ). This ratio provides a quantitative difference between the ordered motion and the random motion in the galaxy (Mo, 2010). For disks, it has high values, on the other hand for elliptical galaxies it roughly ranges between 0 and 1.

In contrast, bulges in spiral galaxies are dynamically similar to the lower luminosity elliptical galaxies. The velocity dispersion of the Galactic bulge is  $\simeq 110 \text{ km s}^{-1}$ , and the  $v_{\text{rot}}/\sigma \simeq 1$ . This signifies that the bulge structure is supported by random motion against the forces of gravity (Mo, 2010).

Furthermore, for ellipticals, since the rotational velocities are low, usually, their rotational parameter  $v_{\text{rot}}/\sigma \sim 0.2$  (Phillipps, 2005), considering the maximum rotational velocity. The low value for giant ellipticals means that the chaotic motion is relatively more important. This observation suggests that compared to spiral galaxies, the formation of elliptical galaxies with low rotational measure has violent en-

---

<sup>4</sup>The second-generation integral-field spectrograph Multi Unit Spectroscopic Explorer (MUSE) operates at the VLT/ESO (Bacon et al., 2010).

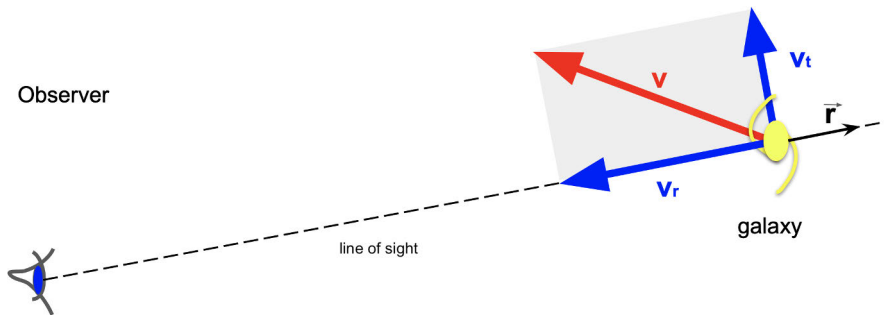


**Figure 12.** The space velocity ( $v$ ) is a vector. We observe the radial velocity,  $v_r$ , component. However, other velocity components might be non-zero (e.g., transverse component,  $v_t$ ).

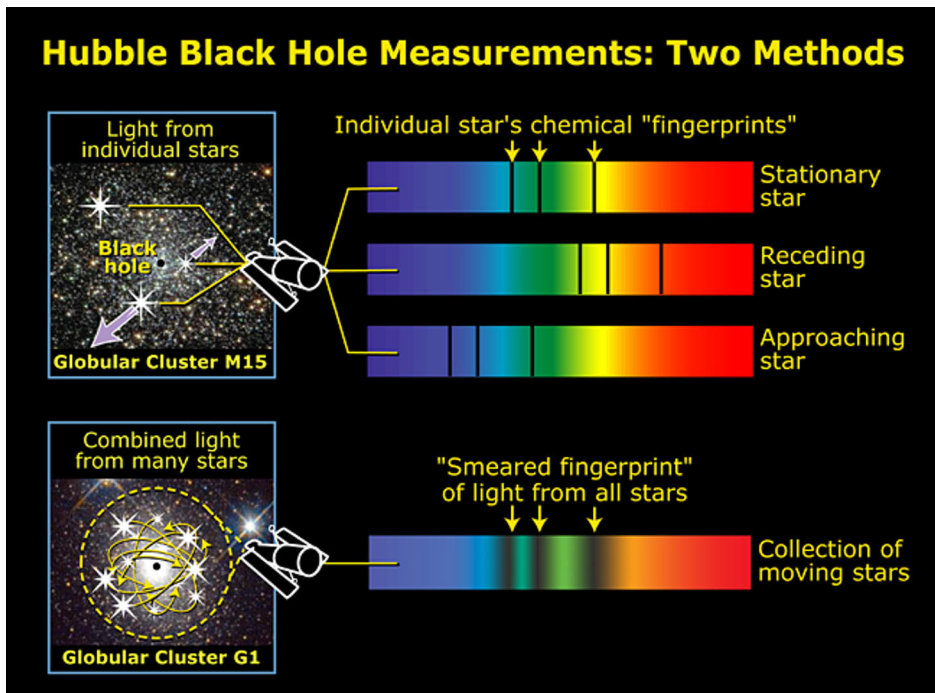


**Figure 13.** Velocity dispersion effect on a spectral line. Here the spectroscopy is used to measure velocity dispersion for two globular clusters to study BHs. The spectral line from an individual star has a clear signature at a particular wavelength. The approaching or receding of a single star just shifts the spectral line. The combined effect of many stars smears the spectral signature and is called *line broadening*. Credit: *Hubble* image, NASA, A. Feild, and R. Van Der Marel (STScI).

counters with other galaxies (Mo, 2010). Moreover, the flattened look observed in some elliptical galaxies is explained as due to the larger value of average velocity in one direction — anisotropy in velocity space (Schneider, 2006).

Within the early-type galaxies themselves, the rotation parameter is correlated to the ellipticity, and in more contemporary classifications, they are divided into kinematically distinct groups of *slow rotators* and *fast rotators* (e.g., Cappellari et al., 2011). The internal kinematics of giant ellipticals are described by slow rotation, while normal ellipticals are fast rotators (Cappellari, 2016). The ratio between the random velocities and rotational velocities is higher for slow-rotating ellipticals, compared to the spiral galaxies (Kutner, 2003).

### 3.3 Surface brightness profiles

The density of the stars drops with the radial distance. A major body of literature based on galaxy observations describes how the surface brightness of the galaxy decreases as we go from the center to larger and larger radii. The functional form that describes this fall is modeled by the *Sérsic power law*<sup>5</sup>:

$$\ln I(R) = \ln I_0 - kR^{1/n} , \quad (25)$$

where  $R$  is the radius,  $I_0$  is the intensity at the center ( $R=0$ ),  $n$  is the Sérsic index, and the value of  $k$  depends on the scale length which describes how quickly the light drops off with radius  $R$  (Phillipps, 2005). A larger Sérsic index means that the light is strongly concentrated in the center and that the “wings” of the galaxy are spread to larger radii, Fig. 14. In particular, the *de Vaucouleurs profile* ( $n=4$ ) is common for spheroidal systems (elliptical galaxies and bulges). For disks, the luminosity decreases sharply with radius and is well-described by an *exponential profile* ( $n=1$ ). The disk model is usually used for disks of spiral galaxies, dwarf elliptical galaxies, and S0 systems. Some galaxies have a very bright nucleus and are discussed in more detail in the next chapter.

### 3.4 Scaling relations

We observe interesting correlations between physical properties of galaxies. These scaling relations reflect internal physics of galaxies and are a product of evolution histories. Like a conductor keeps different instruments in a symphony in sync to produce harmonious melodies, the scaling relations are the conducting sticks of Nature (physical laws) which orchestrate the majestic evolutionary paths of the galaxies.

---

<sup>5</sup>We use nomenclature as in Peng et al. (2010), so the exponential disk and de Vaucouleurs profiles, for example, are special cases, as explained in the text.

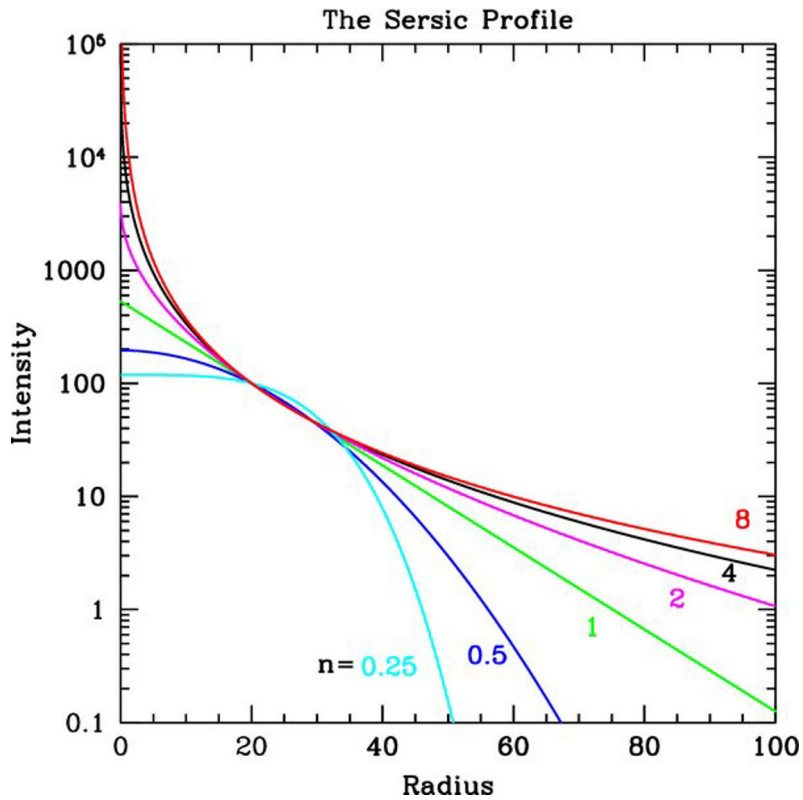


**Figure 14.** Sérsic profiles with different indices (Peng et al., 2010, Fig. 3). The Sérsic profile shows how the intensity changes with increasing radius for any given galaxy. The exponential profile ( $n=1$ ) is typical to describe disks, while the model profile for an elliptical galaxy is described by Sérsic index  $n=4$  value. The smaller the Sérsic index value, the faster the wing is truncated, and the flatter is its core. In the opposite way, the higher the Sérsic index value,  $n$ , the steeper is the core profile and the wings of the light profile spread to larger radii at the same time.

### 3.4.1 Color-magnitude relation

There is a tight relation between the color and magnitude quantities for the elliptical galaxies, the *color-magnitude relation* (Renzini, 2006). Galaxy colors retain information about stellar population properties. The color also reflects the metallicity of the galaxy. According to this relation, the larger galaxies retain their metals better. For example, Stone (2017) reports that in the Coma Cluster, the color-magnitude relation for the galaxies closer to the cluster’s center is  $g - i = -0.06 \times r + 2.06$ , (Fig. 15) based on the SDSS magnitudes  $g$ ,  $r$ , and  $i$ .

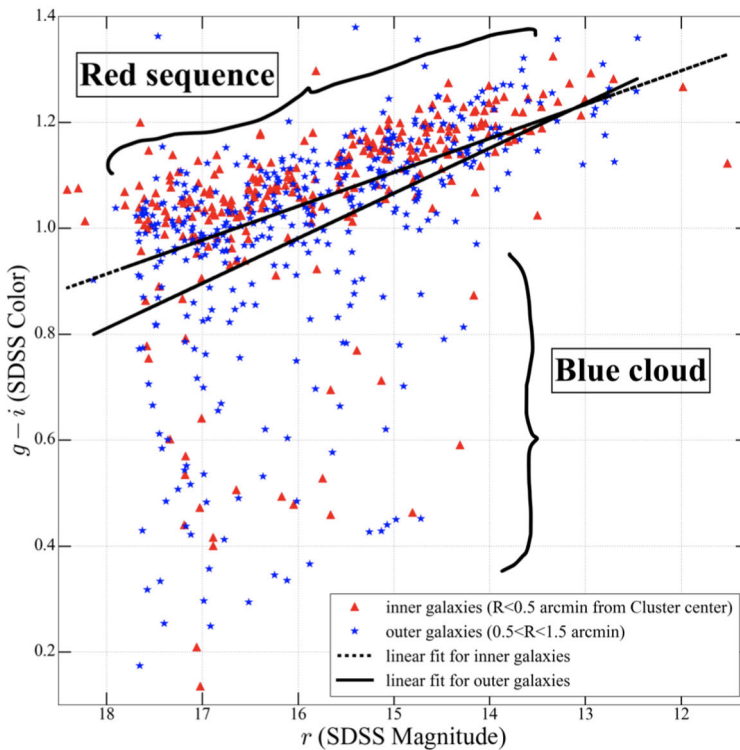


**Figure 15.** This is an example of color-magnitude diagram (CMD), based on SDSS (DR13) photometric data for the Coma Cluster member galaxies (Stone, 2017, Fig. 4.22). The galaxies near the cluster center are represented by triangles (inner galaxies) and galaxies with larger apparent separation from the cluster center by stars (outer galaxies). This CMD illustrates how “redder” (larger color values) galaxies congregate in a tight red sequence, while the “bluer” (smaller color values) galaxies spread into a cloud. The lines represent “red sequence” trends of inner (dashed line) and outer (solid line) galaxies.



### 3.4.2 Luminosity function

Furthermore, the galaxy *luminosity function* (LF),  $\phi$ , is a quantity used to show what is the number density of galaxies in a volume of space and in each luminosity bin. The more luminous galaxies are rare. This distribution is described by *Schechter function*, where  $L_*$  is the characteristic luminosity, the  $\phi_*$  is a normalization factor, and  $\alpha$  is the slope, Fig. 16:

$$\frac{dn}{dL} = \phi(L) = \frac{\phi_*}{L_*} \exp(-L/L_*) \left( \frac{L}{L_*} \right)^\alpha. \quad (26)$$

### 3.4.3 Tully-Fisher relation for spiral galaxies

For spiral galaxies, there is a fundamental relation between the luminosity and the width of emission lines, called the *Tully-Fisher relation* (TFR, Tully & Fisher, 1977). It is useful in estimating cosmic distances. The width of an emission line is related to the rotational velocity,  $v_{\text{rot}}$ . The emission line is broadened due to the Doppler broadening and due to the rotation of the disk. Along the line of sight, some stars

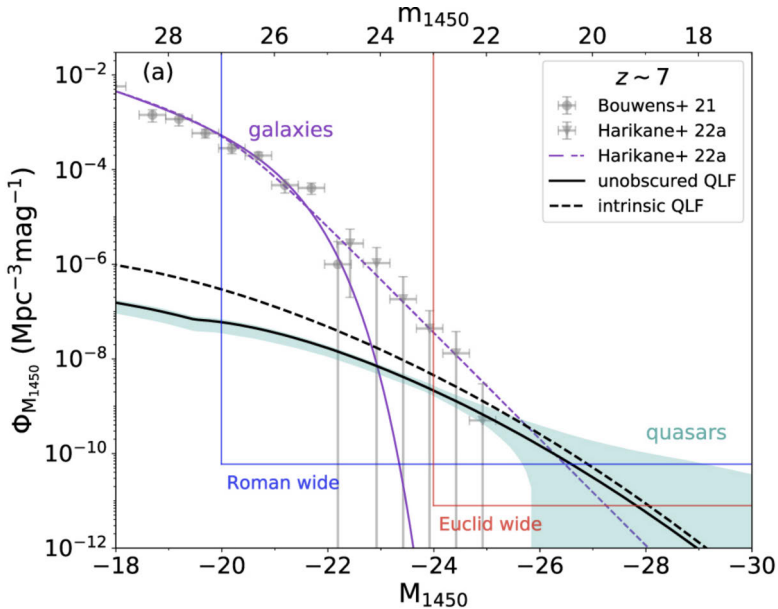


**Figure 16.** Quasar LF at high redshift of  $z=7$  (Li et al., 2023, Fig. 7). The purple solid line represents the Schechter function, and the dashed purple line is a fit with an alternative function for galaxies (represented by gray dots). The quasar LF is a prediction, with a shaded area representing the uncertainty. The redshift evolution of the LF is a key area of exploration. The luminosity is represented by the absolute magnitude at 1450 Å (rest-frame UV).

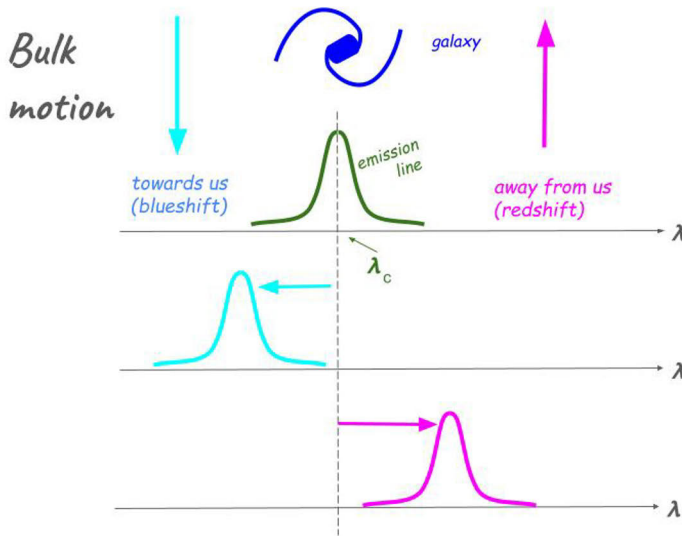


**Figure 17.** The kinematics of a rotating disk is described by motion towards the observer (blueshift) and away from the observer (redshift). This effect is registered in the spectrum as a deviation of the emission line from the central wavelength to shorter and/or longer wavelengths. The observer registers larger apparent rotation for the edge-on spirals due to their large inclination, compared to negligible observed rotation in face-on spirals. The emission line is also affected by the instrument resolution and by Doppler broadening due to random motion (§ 3.2).

have Doppler shifts towards us (blueshifted), while the others away from us (redshifted), broadening the emission line (Fig. 17). The observed effect in emission lines due to the ordered motion of stars and gas also depends on inclination with respect to the observer. The TFR has a form of a power-law (Mo, 2010):

$$L \propto v_{\text{rot}}^{\alpha}, \quad (27)$$

where the exponent  $\alpha$  is band-dependent — it is larger for redder wavebands.

Within the standard CDM cosmogony framework, galaxy population simulations early-on failed to reproduce the TFR, but this obstacle was corrected recently after introducing AGN feedback into the models amongst other improvements (Crain & van de Voort, 2023). The TFR is one way to study the evolution of disk galaxies over cosmic time. For example, Böhm & Ziegler (2016) studied intermediate redshift disk galaxies, and found that compared to the local relation, there is an offset (Fig. 18). The more distant galaxies are roughly brighter by half of a magnitude. The authors suggest that this luminosity evolution is explained primarily by the fact that more distant galaxies have younger stellar populations.

### 3.4.4 The fundamental plane for elliptical galaxies

#### Virial theorem

The key concept of the elliptical galaxy dynamics is the virial theorem. The glorious virial theorem statement is one of the fundamental equations as it ties the microscopic phenomena to the macroscopic properties of the gravitational system (Binney & Tremaine, 1987). For a system with kinetic energy,  $K$ , and potential energy,  $U$ , the *scalar virial theorem* is given as:

$$2K + U = 0 , \quad (28)$$

when the system is in equilibrium (Phillipps, 2005; Binney & Tremaine, 1987). In this case, the other requirement is that the particles of the gravitational system have on average nonrelativistic energies (Bowers & Deeming, 1984b). The corollaries of the virial theorem permeate many areas of astrophysics (stars, dark matter halos, galaxies, clusters) and beyond (orbital mechanics, thermodynamics, statistical mechanics, Hamill 2010). However, as Dr. Thayer Watkins, a physics professor from the San Jose State University, warned in his classes, it must be applied with aware-

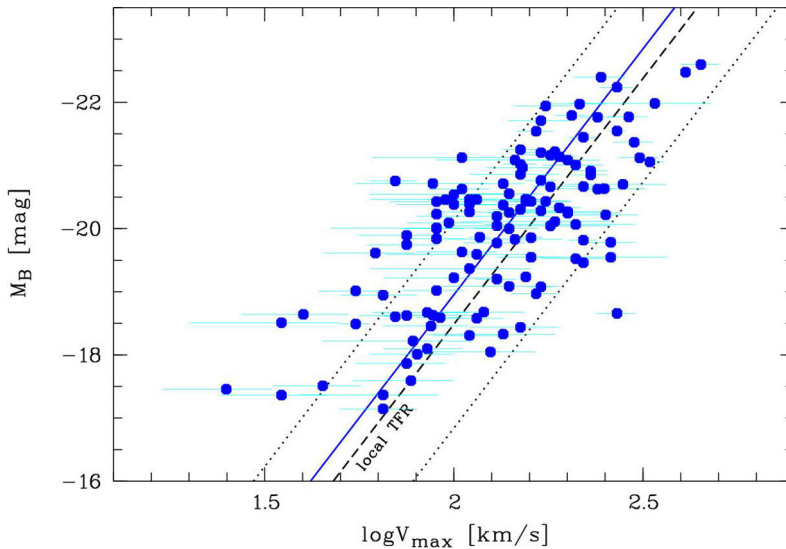


**Figure 18.** An example of TFR,  $0.05 < z < 0.95$ , B band (Böhm & Ziegler, 2016, Fig. 2). The luminosity is represented by the B band absolute magnitude. The maximum rotation velocity,  $V_{\max}$ , is based on spectroscopy with FORS instrument (ESO/VLT). The sample of 124 galaxies (blue circles) for which  $V_{\max}$  was measured in this work consists of field disk galaxies, selected from the FORS Deep Field and *William Herschel* Deep Field. The TFR fit to this sample of galaxies is shown with the solid blue line. The local TFR (black dashed line) is from Tully et al. (1998) and its  $3\sigma$  scatter is represented by small-dashed black lines. The luminosity evolution is deduced from the systematic offset from the local TFR, and is explained by the presence of younger stellar populations at this earlier epoch.

ness about its limitations. For example, wrong results will be derived if the virial theorem is applied to a gravitationally unbound system<sup>6</sup>, e.g., actively collapsing or interacting systems (Sparke & Gallagher, 2007).

In astrophysics, often we can assume an (at least approximate) virial equilibrium for star clusters, elliptical galaxies, clusters, and general overdensities (Phillipps, 2005). The most massive virialized objects in the Universe are clusters (Mo, 2010). For example, as the cluster forms, in the stage of the proto-cluster, the gravitational pull collapses the system, but the motions of galaxies act in the opposite way (*virialization*). When the system reaches steady-state equilibrium, it is *virialized* (Liddle & Loveday, 2008). Estimates of physical properties such as mass and size can then be derived based on the virial theorem, in particular for elliptical galaxies.

### Faber-Jackson relation

Thus, the random motions of stars within elliptical galaxies allow us to apply the virial theorem to describe the state of the equilibrium (like in a hot gas cloud). Taking also into account the dependence of the luminosity on the radius from the center of the elliptical, we can roughly assess how now for ellipticals, luminosity (or mass) is correlated to the central stellar velocity dispersion,  $\sigma$ . This relation is called the *Faber-Jackson Relation* (Faber & Jackson, 1976; Phillipps, 2005):

$$L \propto \sigma^n , \tag{29}$$

where generally  $n \sim 4$ , but is larger for more massive ellipticals.

The velocity dispersion can be measured from the spectrum of the elliptical galaxy. The more luminous elliptical galaxies have much larger dispersion values for their constituent star velocities. The velocity dispersion values can also provide clues about the mass (even “hidden” mass), because mass and velocities are correlated stemming from an application of the virial theorem. This power-law relation is important in determining distances, since from the luminosity the absolute magnitude can be calculated.

### Kormendy relation

The *Kormendy relation* describes the relation between the surface brightness of a galaxy and its effective radius (Kormendy, 1977). It is used because it is difficult to pinpoint exactly where the galaxies end. This relation holds for ellipticals and for bulges of spiral galaxies. This relation suggests that larger galaxies are less dense and less bright than less massive galaxies. The massive elliptical galaxies are observed to have “missing light” in their cores — it is attributed to “binary scouring”, a

---

<sup>6</sup>Web article “The Virial Theorem: Its Explanation, Proof, Application and Limitations”.

process where after a merger two central SMBHs eject nuclear stars by gravitational interactions (e.g., Begelman et al., 1980; Thomas et al., 2014; Rantala et al., 2019). The consequent mergers deepen the mass deficit (reviewed in context of SMBH-host galaxy coevolution in Kormendy & Ho, 2013).

### Fundamental plane

Actually, for elliptical galaxies, astronomers discovered that galaxy size, surface brightness, and velocity dispersion are not random, but form the 3D *fundamental plane* (Dressler et al., 1987). From Phillipps (2005), its functional form may be given as:

$$R_e \propto \sigma^{5/4} I_e^{-5/6} . \quad (30)$$

The particular relations are simply projections of the fundamental plane (Sparke & Gallagher, 2007). The fundamental plane is evidence for important underlying processes common to all elliptical galaxies and is a rich source of research in extragalactic astronomy at all redshifts (Renzini, 2006). Furthermore, the fundamental plane is a pattern against which the galaxy evolution and cosmology models can be compared. Plus, for the studies of quasar hosts, the fundamental plane location has been used to identify AGN host galaxy properties (e.g., Dasyra et al., 2007, Fig. 19).

## 3.5 Star formation

Galaxies are hubs where stars congregate in the Universe, where the SF is present. One of the measurements of activity levels in a galaxy is its SFR ( $M_\odot \text{yr}^{-1}$ ). Ellipticals usually are considered to have no or very low current SF along with a large time interval since the last SF activity. SFR in spirals is  $0.1\text{--}20 M_\odot \text{yr}^{-1}$  (Phillipps, 2005). In the Galaxy the SFR is  $\sim 3\text{--}5 M_\odot \text{yr}^{-1}$ . However, this is a modest SFR. Star forming galaxies (SFGs) can have SFR values of  $10\text{--}20 M_\odot \text{yr}^{-1}$ , for example Sc-type spirals, while *starburst* galaxies reach SFR of  $10^2 M_\odot \text{yr}^{-1}$  or more. For example, the hyperluminous IR galaxies are reported to have  $\text{SFR} > 10^3 M_\odot \text{yr}^{-1}$  (e.g., Rowan-Robinson, 2000). The SFGs have a characteristic tight relation between their SFRs and stellar masses, called the *main sequence* (MS), e.g., Fig. 20 (Silk et al., 2014).

The SF indicators can be found in galaxy spectra. Examples of starburst, spiral, and elliptical spectra are shown in Fig. 21. The prominent emission lines of  $\text{H}\alpha$  and  $[\text{O II}]$  are indicators of SF. The spiral galaxy spectrum also has absorption lines due to the older stellar populations, alongside the emission features. The elliptical galaxy is devoid of emission lines, and is dominated by absorption troughs.

Stellar birth, evolution, and death are the ever-so burgeoning fields, capturing the imaginations of astronomers and amateurs alike. The stellar birth takes place in *molecular clouds* where the temperature and density conditions are optimum. SF

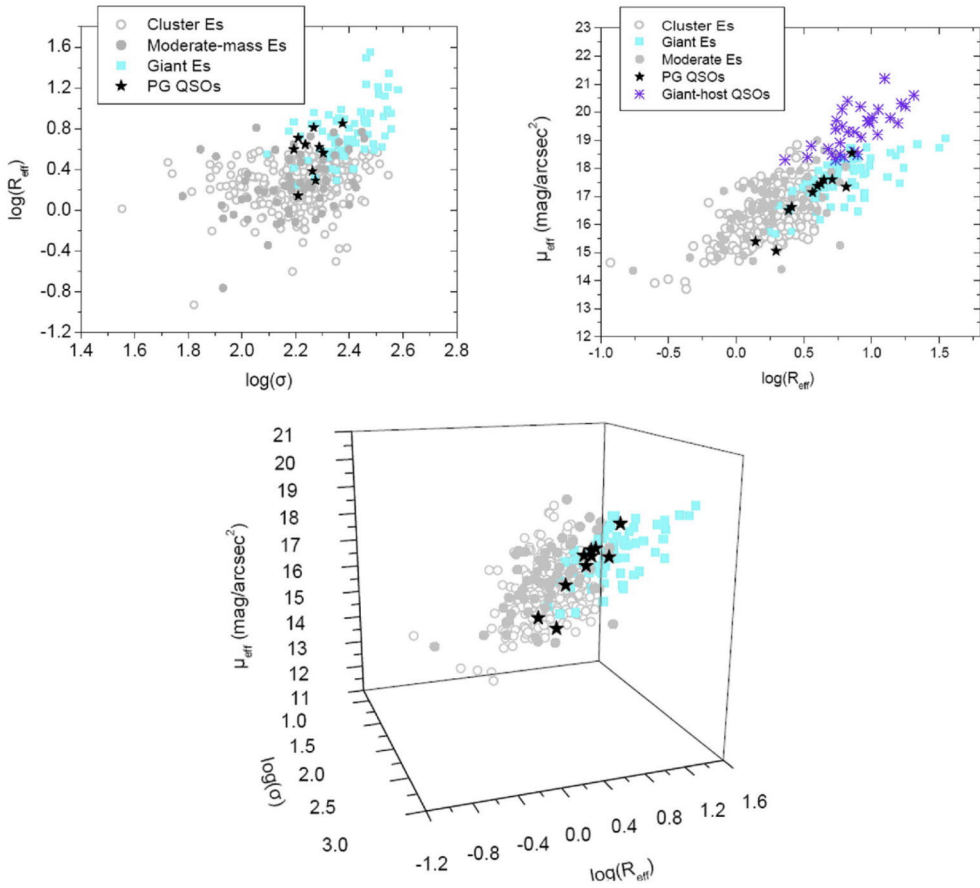


**Figure 19.** Fundamental plane (K band) of early-type galaxies and its various projections (Dasyra et al., 2007, Fig. 6). The local quasar hosts in this study are depicted as asterisks and stars, while inactive elliptical galaxies as circles and squares.

requires relatively cooler temperatures (a cold neutral medium prerequisite), that's why in the cluster centers, where the gas is ionized, the SF is not possible (Mo, 2010). Stars are formed from gas, thus additionally an abundant ISM is needed (density requirement). The 10–30 K temperatures and  $300 \text{ cm}^{-3}$  densities allow atoms to combine together to form molecules, mostly molecular hydrogen ( $\text{H}_2$ ).

Unfortunately, observers do not use molecular hydrogen to trace SF.  $\text{H}_2$  is a very inefficient radiator since it has no electric dipole due to the symmetry of the molecule — not true for the deuterium-substituted molecule HD (Dyson, 1997; Schneider, 2006). It radiates very weakly by quadrupole radiation. Instead, other molecules are used to trace the star forming regions, such as carbon monoxide (CO).

It is known that stars are born typically in large groups. Within a spiral galaxy, the spiral arms have a high abundance of star forming regions (e.g., Knapen et al., 1993). As a spiral galaxy evolves, generations of stars are born and others die off, sometimes through violent SN explosions which output into the surrounding ISM various atoms, thus enriching it especially in heavier elements (Dyson, 1997).

The SF in galaxies is typically studied at a population-level. Within singular

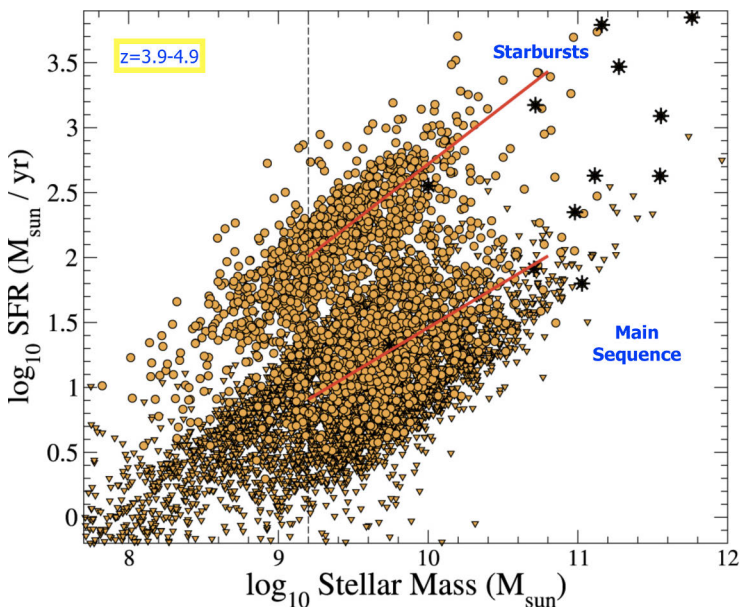


**Figure 20.** An example of the MS of SFGs,  $3.9 < z < 4.9$  (Caputi et al., 2017, Fig. 2). The SFR-stellar mass plane of around 6000 galaxies (various markers) illustrates how the two clouds of galaxies congregate in distinct areas and have separate trends — these clouds are occupied by the starbursts and MS galaxies, located in the COSMOS field (Scoville et al., 2007). Caputi et al. (2017) identified  $\text{H}\alpha$ -excess galaxies (circles) using broadband  $3.6 \mu\text{m}$  MIR (mid-infrared, mid-IR) filter, considering the  $\text{H}\alpha$  ( $\lambda = 6563 \text{ \AA}$ ) emission line as the SFR tracer. Triangles represent galaxies without  $\text{H}\alpha$  excess. Asterisks are galaxies which may have an active SMBH. The vertical line shows the limit in mass from which the linear fits (red solid lines) were estimated.

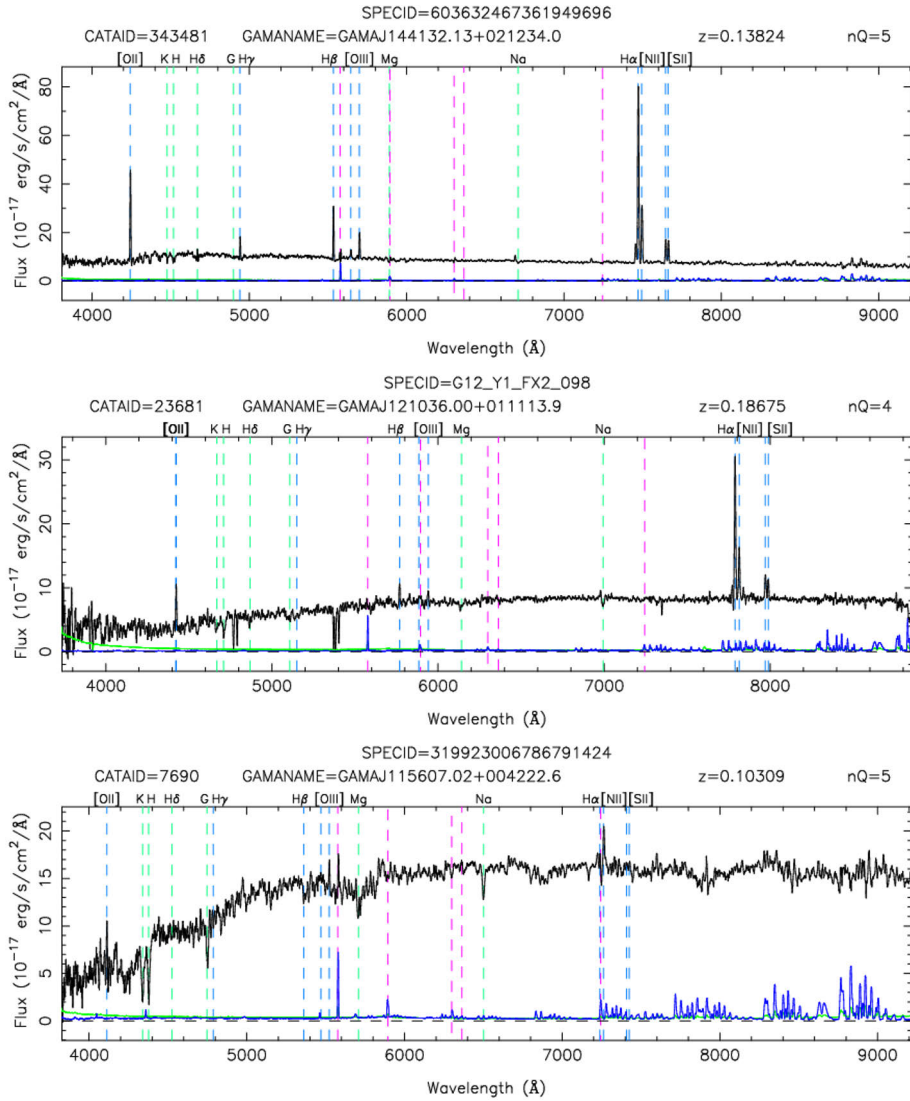


**Figure 21.** Optical spectra (black) of a starburst (top), a spiral (center), and an elliptical galaxy (bottom) which are located less than 2 Mpc (comoving) away from a quasar (Paper III). Their SFRs are  $\sim 30$ ,  $\sim 6$ , and  $0 M_{\odot} \text{yr}^{-1}$ , respectively. The eminent H $\alpha$  emission line is in the spectrum of the starburst galaxies, while the elliptical's spectrum has prominent absorption lines. Credit: GAMA Survey (Hopkins et al., 2013; Liske et al., 2015; Driver et al., 2022). The sky emission spectrum is in blue and the  $1\sigma$  error spectrum in green (Baldry et al., 2014; Liske et al., 2015).



galaxies, the stellar birth rate evolves differently through cosmic time. The *star formation history* (SFH) is fundamental to the evolution of galaxies, which advanced based on the work of talented astronomers, e.g., Salpeter (1955) and Tinsley (1980).

The ellipticals are thought to have had a brief but intense SF burst at earlier stages of the galaxy's lifetime. On the other hand, the spiral galaxies begin to form stars but use their gas (SF fuel) slower, holding their SFR consistent over billions of years (e.g., Kennicutt, 1983). The SF is regulated in galaxies, possibly by SNe and AGN activity (Mo, 2010). The peak of cosmic SFH coincides with the peak of the quasar activity in the universe at  $z=2-3$  when the Universe was about 2-3 billion years old. This period is known as the "cosmic noon" (Madau & Dickinson, 2014).

# 4 Active Galactic Nuclei

Double, double toil and trouble;  
fire burn and kettle bubble.

---

Witches chant from *Macbeth*  
Shakespeare

A small fraction of galaxies (*active galaxies*) are observed to have a compact region in their center from which ample non-stellar emission is observed. This region of activity is called an *active galactic nucleus* (AGN). The radiation from AGN spans across all regimes in the EMS: high energy (gamma-ray, x-ray), ultraviolet (UV), optical, infrared (IR), and radio wavelengths. Active galaxies are the galaxy hosts to AGN, modeled by the presence of a central SMBH which is actively accreting matter (Lynden-Bell, 1969). The AGN fraction is small in the general population of galaxies in the Universe. For redshifts below 0.1,  $\sim 2\%$  of galaxies have a fast-accreting SMBH activity (Netzer, 2013).

Actually, SMBHs (above a million solar masses) reside in the centers of most massive ( $\geq 10^{10.3} M_{\odot}$ ) normal galaxies, but are predominantly dormant (inactive). They are thought to be important in the evolution of the host galaxy, because tight correlations have been observed between the BH mass and the properties of the host. For example, the more massive SMBHs are found in more massive bulges.

The Milky Way is not an active galaxy, however, a dormant SMBH does lie in its center (Morris & Serabyn, 1996). It is called Sagittarius A\* (Sgr A\*), and its mass is  $\sim 4 \times 10^6 M_{\odot}$ . However, astronomers think that the Milky Way has undergone periods of quasar activity in the past, suggested by the discovery of colossal *Fermi* bubbles<sup>1</sup> (Su et al., 2010; Sarkar, 2024).

Astronomers within the last century began observing quasars using different regimes of the EMS. The observed objects seemed unusual and interesting, but were only later determined to be "faces" of the same astronomical phenomenon and

---

<sup>1</sup>*Fermi* bubbles extend to Galactic scales, are diffuse, and have a very large high-energy emission perpendicular to the plane of the Galaxy discovered by the *Fermi Gamma-ray Space Telescope* ([fermi.gsfc.nasa.gov](http://fermi.gsfc.nasa.gov)). They are thought to be remnants of SMBH output after ingesting stellar material (e.g., Yang et al., 2022a; Mou et al., 2023; Fujita, 2023). Even more titanic in size and energetic bubble structures have been discovered in X-ray with *eROSITA* satellite (Predehl et al., 2020, 2021). As an alternative energy source to the past AGN activity, the origin of Galactic bubbles in the CGM of the Milky Way is attributed to stellar winds from SF at the Galactic Center and SNe explosions both as a stand-alone and hybrid model (e.g., Gupta et al., 2023).

some erroneous interpretations were weeded out (e.g., astronomers even misclassified AGNs as stars). Moreover, the resulting “AGN zoo” from discoveries by happenstance in radio and optical wavebands brought about an eclectic slew of esoteric terms for these new objects, which are often used today. Nevertheless, according to the currently accepted unification paradigm, all AGN have an accreting SMBH at their cores. The different observational signatures are actually the result of the point-of-view (observational angle).

In this chapter, I first go through the observational particularities of AGN (§ 4.1). I present the AGN types within the mainstream *Unified Model* to explain the “AGN zoo”. Then, I dive into the standard model of the AGN structure and review a few key astrophysical concepts related to the central engine, such as the accretion rate and Eddington luminosity (§ 4.2). Further follows a discussion of the role of environments for AGN at different scales (§ 4.3) and AGN triggering (§ 4.4). In the last chapter, the role of AGN through cosmic history is highlighted (§ 4.5).

The general textbook information is from classical sources Robson (1996); Peterson (1997); Krolik (1999); Netzer (2013). As the topic is vast, I highlight the aspects of the background relevant to the dissertation publications. Every major aspect of SMBH phenomenon has competing theories, special cases, and outstanding questions (e.g., Chapter 10, Netzer, 2013).

## 4.1 Observational signatures of AGN

AGN hold the title of the most luminous non-transient objects in the Universe. The luminosity of active galaxies is usually larger than for normal galaxies by several orders of magnitude and may exceed  $10^{12} L_{\odot}$ . Due to the bright luminosities quasars can be observed at very high redshifts.

Their nuclei also shine very brightly, unlike the nuclei of normal galaxies. The normal galaxies are luminous due to their stellar (thermal) emission, however, the nuclear emission from AGN activity is non-stellar. Plus, the nuclear emission of AGN may actually outshine the starlight of its host galaxy.

In radio, some quasars are observed to have *jets* (Böttcher et al., 2012). For example, the closest active galaxy to the Earth is the Centaurus A galaxy, which has giant radio jets protruding from its nucleus. Jet structures can be observed in other wavelengths as well and at very large scales from the galaxy (Blandford et al., 2019).

Some AGN show great *variability* in luminosity which comes from a very small central volume within a galaxy. Since we can observe from the Earth that the light from AGN changes within short timescales for humans, then the size of the emission region must be very small (light hours or light days). This size is comparable to the size of our Solar System. This is one evidence for AGN explanation as an active SMBH in the center of a galaxy, where the emission comes from the radiation output of gas infall.

Why does the gas radiate? The classical textbook explanation is as follows (Schneider, 2006; Beckmann & Shrader, 2013). The general principle of the accretion process is that the gas falling onto an SMBH (a compact object) loses its gravitational potential energy by viscous forces. Few historical papers include works by Zeldovich in the 1960s (Shakura, 2014) as well as works such as Salpeter (1964); Lynden-Bell (1969); Shakura & Sunyaev (1973).

Based on the angular momentum conservation, the gravitational energy is first converted into kinetic energy — this is the rotating motion of gas in an accretion disk around the SMBH. The internal friction heats and decelerates the gas clouds as they collide with each other while drifting inward towards the SMBH. The generated heat from the viscous disk radiates away as blackbody radiation. It is efficient and localized to the inner region around the SMBH. Thus viscosity in the disk is responsible both for angular momentum transport and for converting angular momentum to heat. The observational signature is the UV-bump of AGN SED, for example. The astrophysics concepts of SMBH accretion are detailed a bit more in § 4.2. Let’s now see how these “beasts” show up in observations.

### 4.1.1 AGN types

All galaxies with active SMBHs are now considered as AGN (Netzer, 2013). There are two basic types of AGN (within the commonly accepted unification model presented in § 4.1.2). Type I AGN have unobscured lines of sight to their central emission, while Type II AGNs have a heavy obscuration along the line of sight resulting in extinction of the optical-UV radiation from the central parsec (Netzer, 2013). However, historically, different terms have been used to describe certain subclasses, although those categories did not have precise definitions accepted by all astronomers. Nevertheless, let’s review a few of them.

*Seyfert galaxies*, named after an Ohioan astronomer who discovered them, are spiral galaxies with very bright nuclei in the optical (Seyfert, 1943). Less than 5% of spirals have this appearance. These relatively nearby active galaxies possess strong emission lines, which are broader than in normal galaxies. There are two categories of Seyfert galaxies based on their spectra: some Seyferts (Type I) have both very broad ( $>1000 \text{ km s}^{-1}$ ) and narrow lines in their spectra ( $<1000 \text{ km s}^{-1}$ ). Others only exhibit the narrow lines (Type II Seyferts), although they are still wider than in the case of inactive galaxies.

*Quasars* are another type of AGN. The word “quasar” comes from the name quasi-stellar object (or QSO), because the first images of these objects revealed star-like point sources, but their redshifts placed them into the extragalactic domain. Quasars were some of the first objects to be observed at very high redshifts. Their luminosity places them as the most luminous AGN. Due to their high luminosity, we can observe Type I quasars at large distances, even at  $z > 5$ . In Fig. 22, optical spectra

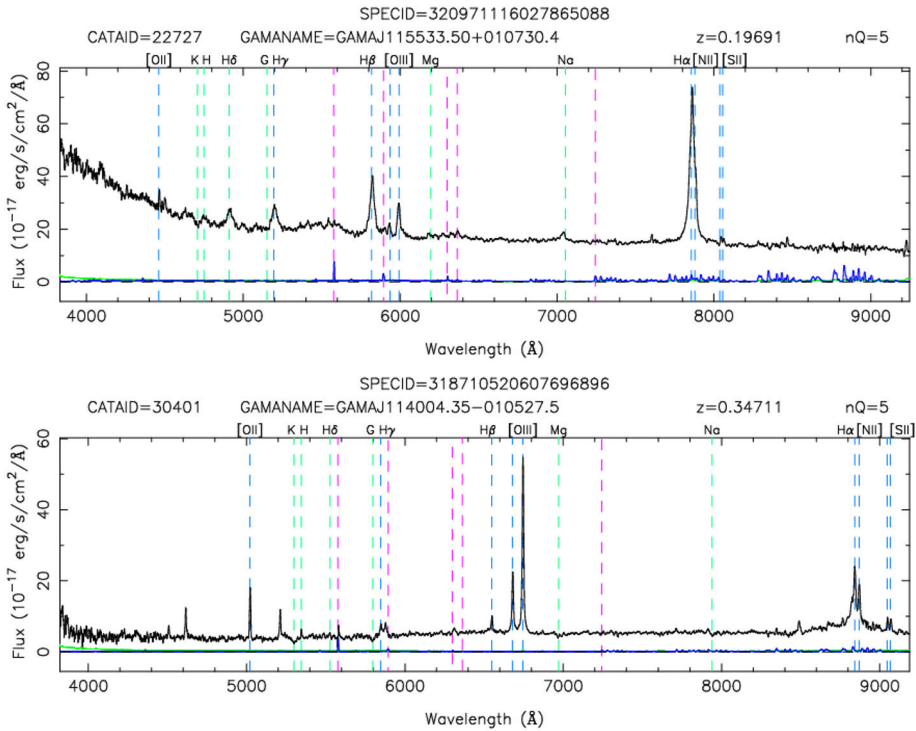


**Figure 22.** Type I quasar spectra examples from the GAMA survey, retrieved via the Single Object Viewing Tool (Liske et al., 2015; Driver et al., 2022). The top quasar has a spiral host and the bottom one is an elliptical galaxy (Paper IV). The top quasar is identified by SDSS DR16 as a starburst (Ahumada et al., 2020).

of Type I quasars are shown (see § 5 for details about spectral lines). The broad Balmer lines (H $\alpha$ , H $\beta$ ) are clearly visible. Other prominent lines are [O III] and [O II] in the optical. However, in this work and in the enclosed papers, I use the terms quasar and AGN interchangeably.

*Radio galaxies* are elliptical galaxies which exhibit radio emission thought to be due to synchrotron emission from electrons. Usually, in radio, the galaxy has a compact radio core and one or two lobes. The radio lobes are powered by AGN in host galaxy (Jones & Lambourne, 2004) and are classified into two groups: Fanaroff and Riley type I (low luminosity, compact emission) and type II (high luminosity, extended emission) (Robson, 1996; Beckmann & Shrader, 2013). These lobes may be Mpc-sized and may be connected to the nuclear region by narrow radio jets. They are called radio galaxies because the radiation power in radio is above that of the visual interval. However, their host galaxy starlight is still visible.

*Blazars* have a strong emission in radio as well as in gamma-rays. Blazars are extremely variable (e.g., Nilsson et al., 2018). It is thought that their extreme luminosity is due to the orientation of the jet axis towards the observer (e.g., Hovatta &

Lindfors, 2019). A subclass of blazars, BL Lac objects<sup>2</sup>, were incorrectly considered to be a variable star BL Lacertae at the time of their discovery. BL Lac objects' spectra lack any emission lines. Another type of a blazar is the flat spectrum radio quasar (FSRQ).

There are other AGN types (Padovani et al., 2017). For example, the Low Ionisation Nuclear Emission-line Region galaxies (*LINERs*) have low ionization lines in their spectra. Another example is the esoteric Narrow-line Seyfert 1 (NLS1) galaxy category, which groups AGN with comparatively narrow emission features. In the radio domain, more specialized terminology is also employed to classify AGN.

### 4.1.2 Unification theory

The Standard Model of the central kiloparsec describes the structure of AGN from the SMBH to the narrow line region (NLR). It is illustrated in Fig. 23. In the center lies the black hole (Shakura & Sunyaev, 1973), surrounded by an accretion disk (size of a few light days). At about 100 light days of distance, broad line region (BLR) gas clouds are moving at high speeds. Further on, at  $\sim 10$  pc, a thick *torus* of cold molecular gas surrounds the accretion disk. This optically thick doughnut blocks from the observer the SMBH accretion disk.

At about  $\sim 10^2$  pc NLR clouds reside. They are smaller and lower in density. The speeds are lower than in BLR. This is the assumed region responsible for the narrow emission lines in AGN spectra. The widening<sup>3</sup> of the emission lines in quasar spectra is due to the Doppler shifts of gas clouds traveling at high speeds  $v = 10^4$  km s<sup>-1</sup>.

The radio jets emanate from the core of AGN. They are perpendicular to the accretion disk plane. The AGN jets can propagate for several Mpc in distance from the galaxy cores.

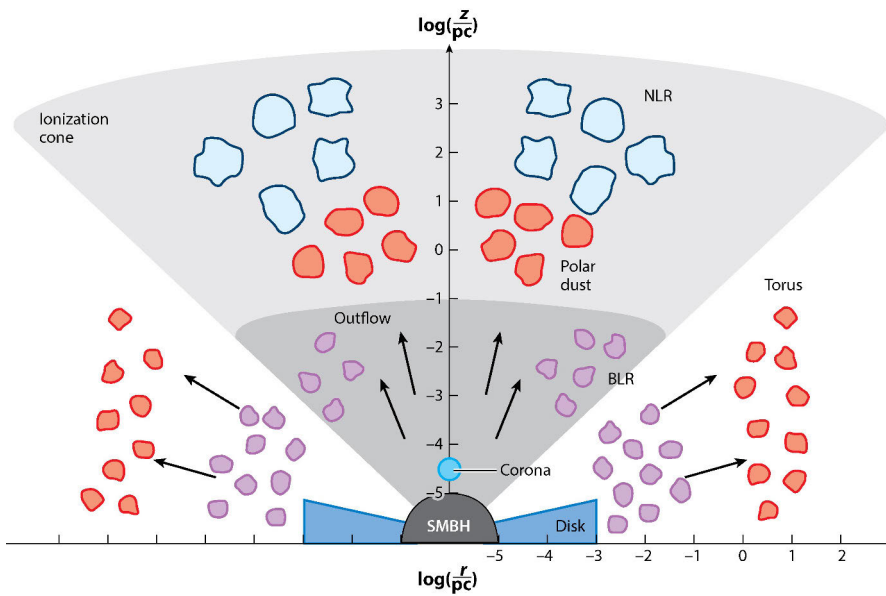
According to the unification theory, blazars (or BL Lac objects), Seyferts, quasars, they are all AGN, just observed from a different angle, Fig. 24 (Antonucci, 1993; Urry & Padovani, 1995). The same is true for radio-loud and radio-quiet sources (Cirasuolo et al., 2003). Due to the thick molecular torus, if the line of sight is intersected by the toroidal structure, then the BH, the accretion disk, and the BLR are hidden. Nevertheless, the torus may have gaps in it, e.g., the clumpy torus model (Hopkins, 2012; Hönig, 2019; Combes, 2021).

Due to the presence of the nuclear obscuration, in Type II AGN, only narrow emission lines are present, as well as some IR emission from the dusty torus (Seyfert II, narrow line radio galaxies, obscured quasars), Fig. 25. If one looks at a 45 degree angle towards the SMBH center, the torus no longer blocks the whole structure. Such cases are observed as Seyfert I, broad line radio galaxies, and unobscured quasars.

---

<sup>2</sup>A famous BL Lac object example is OJ 287 which was monitored also with the Tuorla Observatory and which shows evidence of a BH binary (e.g., Valtonen et al., 2008).

<sup>3</sup>This actually provides one of the ways to derive BH masses.



 Hickox RC, Alexander DM. 2018.  
*Annu. Rev. Astron. Astrophys.* 56:625–71

**Figure 23.** The physical model of the central kiloparsec around an SMBH (distance is in pc). SMBH, the accretion disk, and BLR are located within the first parsec from the center. The torus and the NLR clouds follow. The colors match the SED components, § 4.2. Credit: Figure 2 from Hickox & Alexander (2018); Ramos Almeida & Ricci (2017).

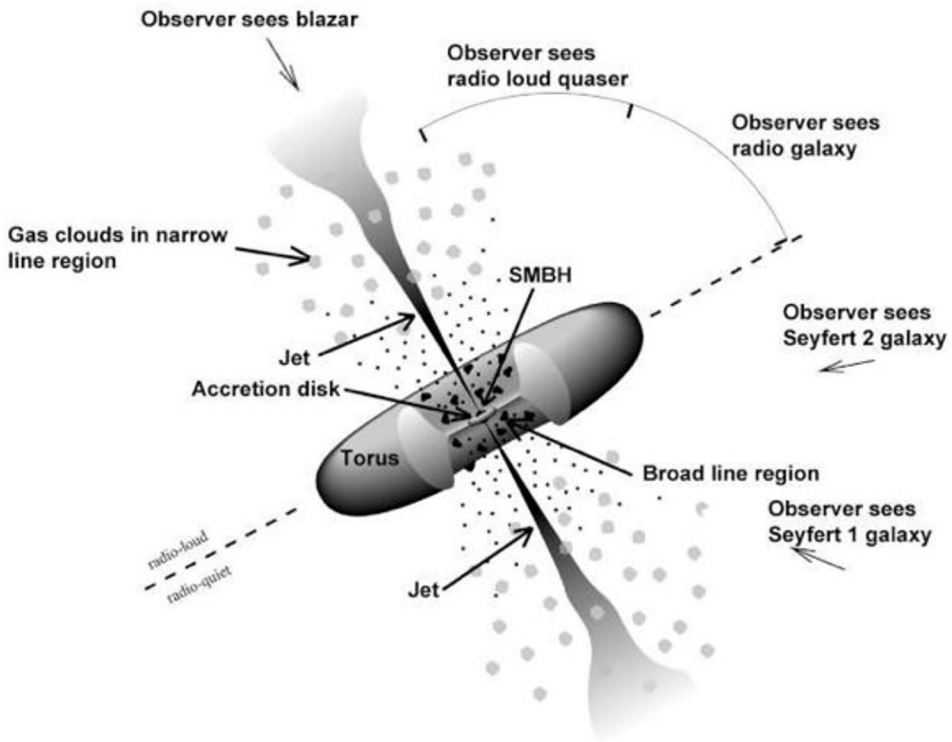


**Figure 24.** Unified Model of AGN. The unification paradigm explains the existence of AGN zoo as the same phenomenon of an accreting central SMBH in a host galaxy, but viewed at different angles. The torus model of the immediate area around SMBH is not spherically symmetric, but instead has a donut-shaped structure, which blocks the accretion disk and BLRs at certain angles. For example, if the observer line of sight coincides with the direction of the jet axis, a bright blazar is observed (Type I AGN). On the other hand, if the viewing angle is in line with the toroidal structure, then the BLR is obscured, and the object is observed as a Seyfert 2 type galaxy (Type II AGN). (Credit: NASA, *Fermi* images).



Looking directly into the center of the AGN, the observer actually faces the nucleus and probably also the jets. The radiation from the jets is beamed and highly variable. The radio spectra appear featureless, since AGN emission is so strong. The blazars, BL Lac objects, and optically violent variables (OVV) are examples of such observations.

In summary, now with the unified system, the classification is simplified, so that depending on the viewing angle, the galaxy can appear as Type I or Type II AGN. If we are viewing directly into the disk, then it is Type I (unobscured). If we view along the plane of the accretion disk, our line of sight is intercepted by obscuring material close to the SMBH, then it is Type II (obscured) (Hickox & Alexander, 2018). Their spectra look different. The observational characteristics of AGN of Type I category are the broad emission lines with widths  $>1000 \text{ km s}^{-1}$ .

Both the BH mass and its accretion rate have a role in what the observer sees. Radio-quiet QSO and Seyfert galaxies don't have a jet. Seyferts are thought to not have such a massive central BH in their center, as compared to quasars. Nevertheless, the highly luminous quasars and moderately luminous Seyferts have the same central engine structure. In the following section, we dive into the inner workings of AGN power house.

## 4.2 AGN astrophysics

We now dive into the major thoughts to explain the physical processes of the active nucleus phenomenon, namely that the active nucleus is actually an accreting BH, which means a BH unto which gas is falling. The theoretical physics of SMBHs is within the framework of general relativity, which describes how spacetime is altered in the presence of a massive object due to its gravity. A “black hole” is a region in space where the extreme conditions of gravity result in such a curved spacetime that the electromagnetic radiation is not able to escape, thus containing all emissions inside that volume, rendering this object “black”. BHs have mass (gravitational influence), spin, and charge. This model explains well the observed luminosity of AGNs due to potential energy conversion to light photons, and the variability of distant AGN in association with a compact region in space (keep in mind, though, that some illustrations of the immediate volume around the BH are artistic representations).

### 4.2.1 Where is the SMBH boundary?

The BH is described by the *Schwarzschild radius* or event horizon (Robson, 1996). Past this radius and going further into the BH, any matter will not be able to escape and remains trapped in the BH. Recently the apparent image of the SMBH horizon has been taken using the Event Horizon Telescope (EHT), Fig. 26. In a simplified Newtonian framework (as an approximation), by equating the potential energy due to

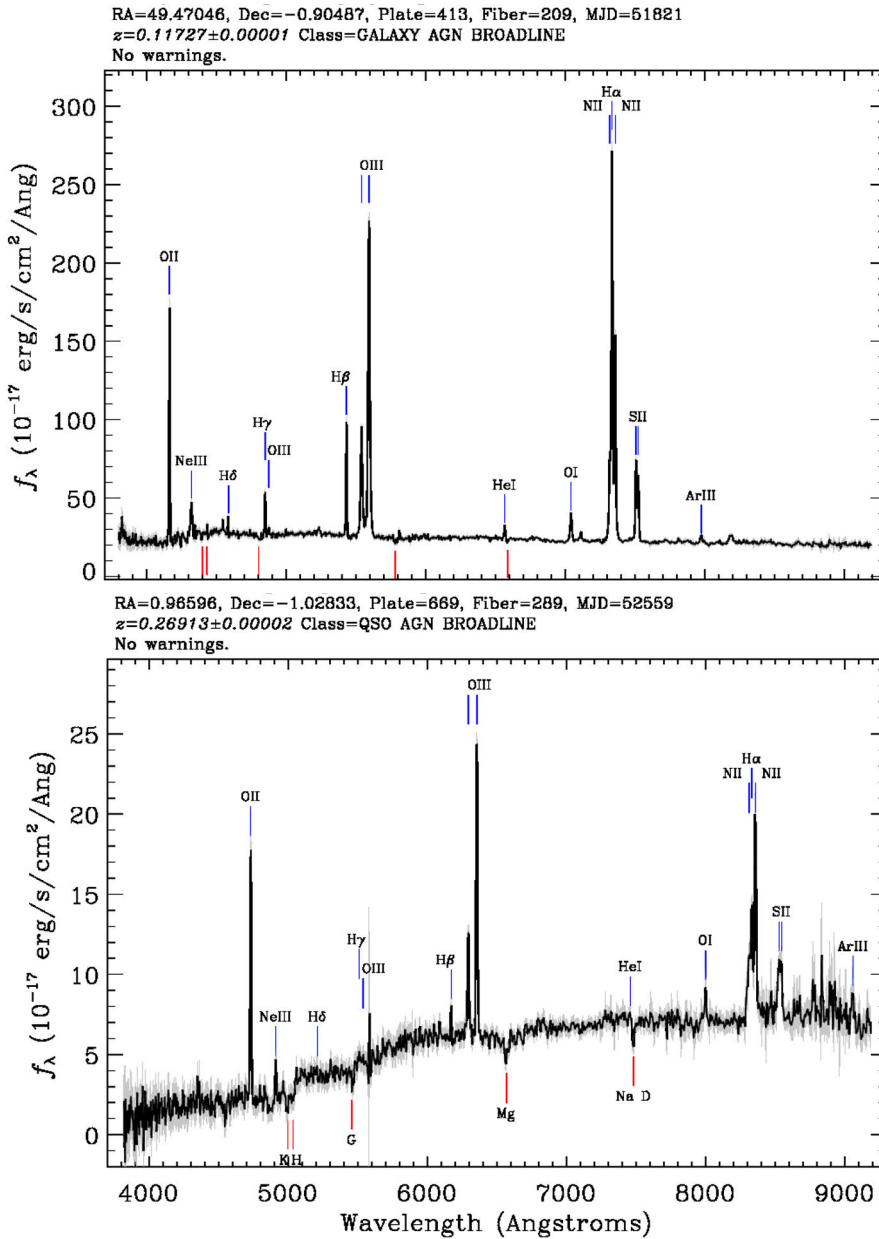


**Figure 25.** Type II quasar spectra examples from Reyes et al. (2008) catalog, retrieved from SDSS DR17 (Abdurro'uf et al., 2022). Top quasar host is visually identified to have a spiral morphology based on SDSS images. The bottom AGN is an elliptical (identified by the Hyper Suprime Cam Map, Aihara et al. 2022).

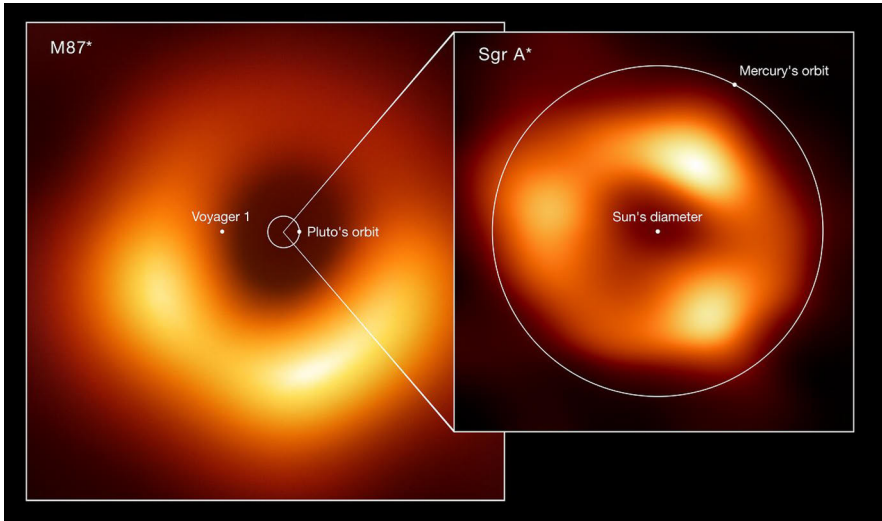


**Figure 26.** Images of the closeup area around two SMBHs. The BH is not seen in the center, but the glowing halo is from the material falling into the BH, the darker central hole of the donut-like image is BH *shadow*. The M87 SMBH is  $>1000$  times more massive than Sgr A\*. For comparison, the Sun's diameter, Mercury's orbit, Pluto's orbit, and Voyager 1 space probe location are overlaid. Credit: EHT collaboration (acknowledgment: Lia Medeiros, xkcd), ESO.

the BH to the escape kinetic energy, and using the fact that the escape velocity equals the speed of light, we can derive the formula for the Schwarzschild radius ( $R_S$ ):

$$R_S = \frac{2 \times GM_{\text{BH}}}{c^2}, \quad (31)$$

where  $G$  is the gravitational constant,  $M_{\text{BH}}$  is the mass of the BH within the  $R_S$  (Netzer, 2013). For an SMBH with a mass  $M_{\text{BH}} = 10^8 M_{\odot}$ ,  $R_S = 3 \times 10^{13} \text{ cm}$  ( $\sim 2 \text{ AU}$ ), rendering the SMBH to fit within the Solar System (Netzer, 2013). Furthermore, the closest stable orbit radius is  $3 R_S$  for a non-rotating BH.

#### 4.2.2 Accretion of infalling gas

During accretion, the infalling gas is arranged into a flat structure, called the *accretion disk*, due to the angular momentum conservation. In disk accretion, the orbiting gas that falls onto the central SMBH has to lose angular momentum, which then needs to be balanced with angular momentum gain (Shakura & Sunyaev, 1973; Beckmann & Shrader, 2013). Typically, the accretion disk area is below parsec scale, which is very small compared to the host galaxy sizes at the kiloparsec scale.

Actually, the gas flow is often modeled as gas clouds (gas particles) which also collide with each other in the SMBH vicinity (Robson, 1996) as they rotate in their respective orbits. This frictional interaction is how the kinetic energy is transformed

into frictional heating. The gas that spirals in a disk configuration slowly loses momentum due to the internal *viscosity* of the disk and hence the radius of the gas orbit continually shrinks (e.g., Pringle, 1981) — at the same time the viscosity continually increases. In this way, the viscosity in the disk is used to explain the *angular momentum transfer* from BH vicinity to outer regions (King, 2008; Netzer, 2013).

Eventually gas flow spirals past the last stable orbit and falls into the BH, the whole time radiating away its gravitational potential energy. This process releases up to 42% of rest energy<sup>4</sup>, which is a lot more efficient when compared to 0.7% of the nuclear burning in the stars. The accretion disk radiation is modeled by black-body radiation (Peterson, 1997), thus the peak wavelength is determined with Wien's displacement law:

$$\lambda_{\text{peak}} = b/T , \quad (32)$$

where T is the temperature and b is a constant. The total energy radiated (luminosity) is proportional to temperature:

$$L \sim T^4 , \quad (33)$$

per Stefan's law. There is a gradient in temperature in the accretion disk, increasing from outer edge towards the inner edge. Accretion disks are encountered beyond AGN and are actively studied (e.g., Krolik, 1999; Abramowicz & Fragile, 2013).

### 4.2.3 Eddington luminosity

How the gravitational potential energy from accretion flow is converted to photons is described by the mass accretion rate:

$$\dot{M} = L/\eta c^2 , \quad (34)$$

where  $\eta$  is the mass-to-luminosity accretion efficiency Netzer (2013). The accretion rate increases with time as more gas is consumed by the BH, but only up to a critical point, called the *Eddington limit*, when the gravitational forces are in equilibrium with the radiation pressure. The *Eddington luminosity* ( $L_{\text{Edd}}$ ) is:

$$L_{\text{Edd}} = 1.3 \times 10^{38} \frac{M_{\text{BH}}}{M_{\odot}} \text{ erg s}^{-1} . \quad (35)$$

Thus, if we substitute into the previous equation the Eddington luminosity, the resultant mass accretion rate is the Eddington accretion rate,  $\dot{M}_{\text{Edd}}$ . If we calculate what mass the BH needs to be in order to produce these exiguous luminosities, then we can see that it is very large, about  $10^7 M_{\odot}$ , aka *supermassive*. The total BH mass is usually up to  $10^{8-10} M_{\odot}$ .

---

<sup>4</sup>The rest energy of the material with mass m is given by  $E=mc^2$ .

#### 4.2.4 BLR and NLR gas cloud velocities

The accretion disk is surrounded by an optically thick toroidal structure (Netzer, 2013). The BLR and NLR gas clouds near the accretion disk are heavily ionized by the central engine emission. The BLR velocities range is 1000–10000 km s<sup>-1</sup>. The NLR gas clouds move at lower velocities compared to the BLR clouds, ranging from 100–1000 km s<sup>-1</sup> and are located further away from the central BH than BLR, as previously described (Krolik, 1999).

As a rough but close estimate, the characteristic velocities ( $v_{\text{rot}}$ ) describing gas kinematics in the emitting region are related to the distance ( $r$ ) from the “nuclear cinder”:

$$v_{\text{rot}} \sim \sqrt{\frac{GM_{\bullet}}{r}} = \frac{c}{\sqrt{2}} \left( \frac{r}{r_{\text{S}}} \right)^{-1/2}, \quad (36)$$

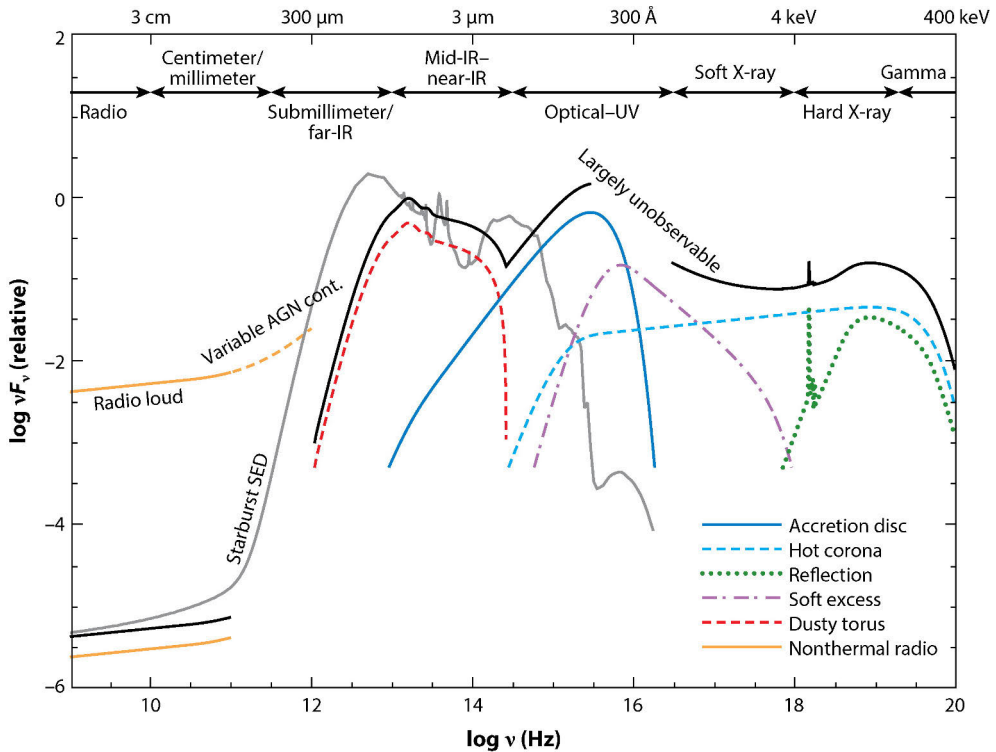
where  $r_{\text{S}}$  is the Schwartzchild radius defined earlier (Schneider, 2006). Thus, from this inverse relation, it is possible to explain that the further the gas clouds are from the SMBH, the lower is their velocity.

#### 4.2.5 SED signatures echo AGN structure

The SMBH accretion disk and torus models can explain the SED and spectral features at different regions of the EMS as emission that comes from different structures of the SMBH model (Elvis et al., 1994; Elvis, 2009; Harrison, 2014). In Fig. 27, for example the emission in the optical-UV is due to the accretion disk, while the hot corona contributes to the X-ray energies. The AGN SED research continues to improve modeling SEDs for various quasar populations, as an example, for  $z > 5$  quasars (Leipski et al., 2014) or blazars (Hovatta & Lindfors, 2019).

### 4.3 AGN environment

The environment of galaxies is important within its neighborhood and at larger scales (Peterson, 2012). As we saw in the previous chapter, the large-scale environment can influence the evolutionary path of a galaxy. On the other hand, zooming in closer to look at the host galaxy properties, such as gas abundance, may provide clues to how the AGN is powered. In particular with AGN, both the influence of the environment on the active galaxy and the influence of the AGN activity on its environment are to be considered. The observing programs reported in the literature often describe contradictory results at every scale as this topic is still subject of on-going research. I review the major lines of reasoning below.



Hickox RC, Alexander DM. 2018. *Annu. Rev. Astron. Astrophys.* 56:625–71

**Figure 27.** The SED of unobscured (Type I) AGN (black curve) and its main physical components (colored curves) (Harrison, 2014; Hickox & Alexander, 2018, Fig. 1). This diagram shows that the AGN emission may span a long range of wavelengths from radio (radio-loud AGN) to X-rays. For comparison, in gray color, the curve of a typical starburst SED is shown — starburst galaxies have a significant emission only in a portion of the electromagnetic regime. Different models are investigated to explain the observed emission at different wavelengths, such as what causes the emission and which physics laws govern it. As an example, the component due to thermal emission from the accretion disk is thought to be responsible for building up the AGN SED in the optical/UV region (blue curve).

### 4.3.1 AGN host galaxies

Host galaxies are the closest environment around the AGN. We would like to compare the various properties of AGN host galaxies with inactive galaxies to see if there is anything special about AGN host galaxies. Since the host galaxy is the immediate environment of the SMBH activity, studying the properties of the host might reveal clues about the AGN activity itself — What causes the onset of the SMBH activity in the center of a galaxy (*AGN triggering*)? What mechanisms support maintaining the accretion onto the SMBH (*maintenance*)? How do the timeframes associated with SMBH accretion correlate to the host galaxy evolution timescales? How frequently a galaxy may turn into an AGN? How long does the AGN phase last? How does the AGN timing correlate to the timing of SF in a host galaxy?

Host galaxy studies are challenging. First, the study of AGN host morphology even at lower redshifts is complicated by the bright nucleus which often outshines the whole galaxy. It is difficult to separate the nuclear light from the host galaxy's starlight. Second, astronomers early on realized that there are major selection effects, such as selection effects on galaxy luminosity (e.g., Yee, 1992).

Images of nearby quasars allow us to identify the Hubble classification of the quasar host visually. From morphological analysis, low luminosity Seyfert galaxies are spirals (Adams, 1977). The high luminosity quasars are hosted by ellipticals (e.g., Floyd et al., 2004, also based on *HST* images,). For low- $z$  quasars, sometimes it is still possible to detect the host galaxy in the image using 2D image decomposition software such as GALFIT (Peng et al., 2002, 2010). The nuclear source is modeled by a 2D *point spread function* (PSF). If we subtract the scaled PSF from the quasar image, then the host galaxy is the remaining nebulosity, which is modeled using a Sérsic model (see previous chapter). For low- $z$  quasars in Paper I, Falomo et al. (2014) reported that the host galaxies had various morphologies.

As the redshift gets higher, it is harder to pick up the light of the host. For the very high redshift quasars, the host galaxy is typically not visible even in the spectrum. The high- $z$  quasar study arena has a surge now due to observations supported by the *JWST* and ALMA observatories (Decarli et al., 2023).

Another way of characterizing the quasars is by the presence of the radio emission. Typically, the radio-loud galaxies are ellipticals (Wolf & Sheinis, 2008), while spirals are usually radio quiet. An additional point to consider is the luminosity of AGN. The more luminous AGN are hosted by more luminous galaxies.

### 4.3.2 AGN co-evolution

For inactive galaxies, the SMBH and their host galaxy evolutionary paths are entwined as indicated by a series of correlations discovered between SMBH mass ( $M_{\bullet}$ ) and host properties (Kormendy & Ho, 2013). However, astronomers are still debat-

ing regarding the origin of the tight relations and their evolution through time. One of the problems is that it is difficult to measure the SMBH masses accurately<sup>5</sup>, nor is it trivial to identify reliable values for host galaxy parameters.

The *HST* observations revealed that a tight correlation exists between the SMBH mass and the velocity dispersion  $\sigma$  of the host galaxy bulge (e.g., Ferrarese & Merritt, 2000; Gebhardt et al., 2000). This is surprising given the fact that the SMBH occupies a very small volume of the host galaxy. However, more correlations have been found between other properties of the SMBH host galaxy and SMBH mass: e.g., host mass (Håring & Rix, 2004), bulge luminosity (Kormendy & Richstone, 1995), light concentration (Graham et al., 2001), and halo circular velocity (Ferrarese, 2002).

These correlations lead to the interpretation that co-evolutionary processes take place between the central SMBH and the bulge of the galaxy throughout the host galaxy’s life, coined as *BH-galaxy co-evolution* (Kormendy & Ho, 2013). Thus, according to the trends, more massive normal galaxies host on average more massive BHs (Kormendy & Ho, 2013). This holds true for massive galaxies. The case of less massive galaxies is under investigation. These correlations also hold true regardless of the morphology or shape of the massive galaxy.

Galaxies of lower luminosities harbor instead compact stellar nuclei, which also follow the  $M_{BH}-M_{host, virial}$  relations (Ferrarese et al., 2006). The demonstrated continuum between the central compact and massive object’s (CMO) mass and the host’s properties implies that there the growth of the CMO and the evolution of the galaxy are tightly linked. This result suggests that perhaps the CMO fails to collapse into a BH in less massive galaxies, while in the more luminous galaxies the stellar nuclei existed alongside the growing SMBH but later on collapsed into the SMBH increasing its mass even more.

Correlations for presently active galaxies also exist. More recently, a large ( $N = 11500$ ) number of quasars at  $z < 0.35$  has been studied, concluding that the early-type and late-type AGNs follow the same relation for  $M_{BH}-M_{\star}$  (Zhuang & Ho, 2023). Higher redshifts have also been investigated. For galaxies with low mass BHs, Sanghvi et al. (2014) showed that at  $z=0.5-1$  the relation is consistent with the local function, if solely the bulge component is considered for the disk galaxies.

The energy and radiation from the SMBH activity is accepted to impact the host galaxy by interacting with the host gas via *AGN feedback* processes (Alexander & Hickox, 2012; Harrison, 2017). The observational evidence suggested in some papers is controversial and it is a hot topic of research impacting the astronomy community beyond AGN (e.g., a recent workshop on the topic, Husemann & Harrison, 2018). Jets are proposed to be one way of influencing their environments (Blandford et al., 2019), and may influence both the host and nearby galaxies. AGN-driven

---

<sup>5</sup>BH mass measurements can be done in various ways, mostly indirectly, and more robustly for local galaxies, for example, the megamaser-based method (e.g., Gao et al., 2017) and the reverberation mapping method (Grier et al., 2012).



outflows also are suggested as a mechanism for regulating the quenching of the SF (Förster Schreiber & Wuyts, 2020).

SFR is one of the major properties assessed for host galaxies. Ellison et al. (2016) found that SFRs are enhanced in certain classes of AGN, and attributed this difference to triggering mechanism differences, such that triggering by galaxy mergers in powerful Type II AGN is correlated with higher SFRs. They argue that the SFR enhancement is an additional product of the merging event.

### 4.3.3 AGN neighborhoods

Observational studies have been carried out to survey the immediate surroundings around the quasars at the scale of several megaparsecs distance from the host (co-moving), or for low-redshift quasars up to 1000 kpc of projected distance. These immediate environments are harder to observe at higher redshifts. The studies are usually limited to the brighter neighbors. Theoretically, both normal galaxies and active galaxies may be present or the quasar may be isolated in that immediate volume.

Checking for the presence of close neighbors is important because a nearby galaxy is a potential candidate for merger. The population statistics of close neighbors may be compared against the simulation results where AGN are triggered via galaxy interactions. Furthermore, the properties of neighboring galaxies may give information on whether there is any effect on them from a nearby AGN. Plus, at a cosmic level, the abundance of quasars and quasar pairs at various redshifts provide a check for hierarchical models (Djorgovski, 1991; Eftekharzadeh et al., 2017).

It is also crucial to understand the techniques used in such studies. Photometry-based studies, where images are analyzed for the presence of companions, may suffer from projection effects. Spectroscopic studies are more robust as a redshift can be used to determine if there is a physical association or not between a galaxy and a neighbor, however, it is resource and time intensive to get spectroscopic data.

One set of studies analyzes galaxy pairs. The studies based on 2D images of galaxies mainly use the following two parameters to identify true close companions in the real (3D) space: the projected separations and relative velocities (e.g., Paper I). A series of papers based on the SDSS data investigated galaxy pairs and their connections to various observational indices, such as their surrounding environments (Ellison et al., 2010), nuclear activity (Ellison et al., 2011), SF (Scudder et al., 2012; Ellison et al., 2013), which were used in part to evaluate how these observations can be interpreted in terms of various AGN triggering scenarios. When considering the nuclear activity, an *AGN fraction* is often computed, which shows the fraction of close companions which are also AGN (e.g., Silverman et al., 2011). In all cases (and extending to all studies of AGN environments), it is crucial to have a properly constructed control sample.

This line of study extends to the rare quasar pairs (and even higher multiplets) as well (e.g., Djorgovski, 1991; Hennawi et al., 2010; Farina et al., 2011). However, care should be taken not to confound binary quasars with gravitational lenses (Mortlock et al., 1999). For higher redshifts, high resolution IR imaging studies are usually one avenue to observe close quasar pairs (e.g., Decarli et al., 2009). For the low-redshift quasar pairs, according to one research study, it is suggested that the host galaxies and galaxy overdensities near the quasars are similar to isolated quasar cases, suggesting that triggering two quasars close to each other is possible without any different properties in the environment (Sandrinelli et al., 2014). Other studies show that at closer distances, the galaxy density is a bit enhanced around quasar pairs (Hennawi et al., 2006; Sandrinelli et al., 2018). More studies on the subject had divergent interpretations. Quasar pairs, for example, are proposed to be good tracers of high density environments, such as clusters (Boris et al., 2007), however, a multiwavelength study of binary quasars suggests that quasar pair environments are similar to those of isolated quasars (Green et al., 2011).

Another line of investigation assessed galaxies within a certain nearby volume or within a certain distance from the quasar. Care must be taken when reading literature whether the distance selection criteria are based on projected distance, physical distance, or comoving distance. For example, Fig. 28 shows a compilation of several studies of quasar companions. Even though Paper I investigated seemingly close companions ( $\sim 100$  kpc projected separation), when converted to comoving separations they are much further, especially compared to Paper III. Thus, care must be taken when comparing and interpreting the results.

Note that while comoving distances are equal to physical distances (or proper distance) at present time, for higher redshifts the comoving distances remain constant while the physical distances change due to the expanding universe. To produce the plot in Fig. 28, I had to take care of converting all the distances to one type. I transformed the physical distances ( $d$ ) of Fogasy et al. (2017) data to comoving distances ( $\chi$ ) using the scale factor ( $a$ ):  $d(t) = a(t) \times \chi(t)$ . For the data points from Paper I and Paper III, we used *astropy* cosmology packages (Hogg, 1999) followed by the application of Equation 8 (§ 2.3) to calculate the comoving separation between objects, which is possible with the spectroscopic redshift data. Standard cosmology parameters are assumed and are detailed in respective papers.

#### 4.3.4 AGN environments at larger scales

Clusters of galaxies are environments with high galaxy density. Usually there is a central giant galaxy. For example, the *Coma* cluster has two large ellipticals in the center. The local motion of the galaxy within a particular cluster is separate from the general *Hubble flow*. The dynamics of galaxies within a cluster is affected by the processes of dynamical friction, which causes mass density inhomogeneity (Schnei-

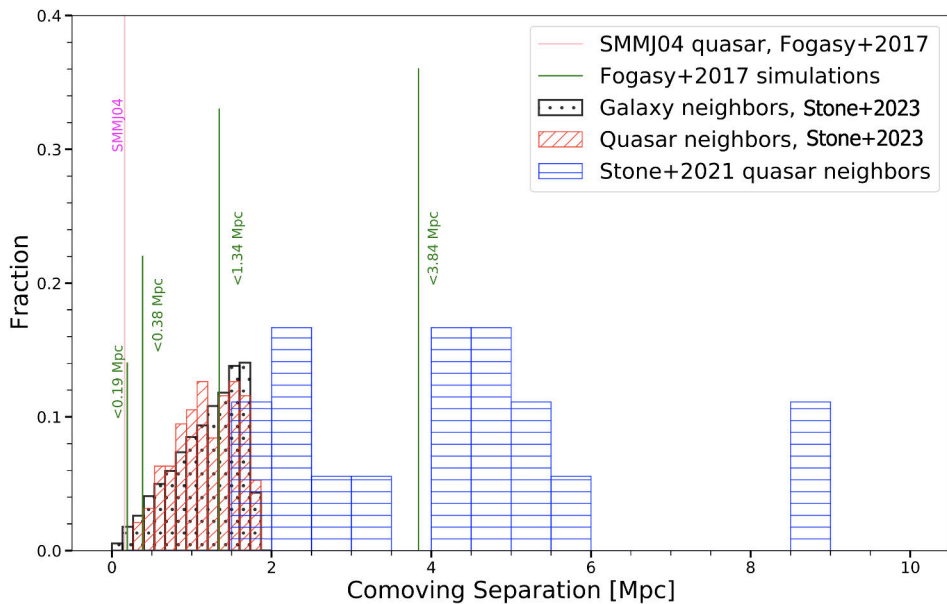


**Figure 28.** Comoving distance separation distributions of neighboring galaxies from this dissertation and from literature. Paper I and III quasar sample is at redshifts  $z < 0.5$ , while Fogasy et al. 2017 data are from higher redshift ( $z \sim 3$ ). Paper I data points were converted to comoving distances from projected separations whereas Fogasy et al. (2017) data points from physical distances. The green lines from that study indicate the fraction of quasars which have a companion within that distance mark, e.g., 36% of quasars have a companion galaxy within 3.84 Mpc comoving separation. This figure also illustrates how the GAMA-based study focused on a very close volume around quasars (red histogram, Paper III).

der, 2006). Dynamical friction effect is stronger for objects with larger mass and is one way to explain how the enormous massive galaxies are formed in cluster centers (cD galaxies and galactic cannibalism, Schneider, 2006). To explain qualitatively this effect, basically as the galaxy enters a cluster, the dynamical friction causes the galaxy to decelerate as it orbits around the central galaxy, eventually getting engulfed by the central giant.

Some galaxies may collide and merge. Since the cluster galaxy density is higher, interactions between galaxies could happen due to gravitational pull. However, interacting galaxies are found in all galaxy environments. In fact, major mergers, where two galaxies of equal mass collide, occur in environments of lower density (outskirts of galaxy clusters, compact groups) and not in cluster centers — for example, the Milky Way and Andromeda galaxies. In groups, the full-on collisions are also possible due to the low relative velocities of group members. For this exact reason, in Paper III, we considered bright neighbors of quasars whose masses are similar in order to explore the major merger possibility. The cluster member galaxies in the cluster core have higher relative velocities and are instead subject to *galaxy harassment* as the weak impacts of numerous interactions strip away stars. Due to this cumulative effect, it is postulated that spiral galaxies in cluster core environments gradually shrink and deform into ellipticals (e.g., Moore et al., 1996, 1999).

Interestingly, not all clusters have such extreme relative velocities. Some clusters actually have moderate relative velocities. Also various groups, including small groups, may fall into the cluster and remain as a substructure within that cluster. These considerations among others suggest that actually direct collisions are quite possible in cluster environments as well and should not be ignored (e.g., Mihos, 2003; Benavides et al., 2020).

Cluster members are predominantly early-type galaxies (ellipticals and S0 galaxies) especially in the central volume while spirals dominate the population of intracluster spaces. Another aspect of clusters is that the intergalactic gas within the clusters is quite hot, which has consequences for SF processes. The temperature is around  $10^7$  K, visible in the X-ray regime.

Let's consider now where AGN reside at these larger scales. At a global scale, with the completion of sky-wide astronomical surveys, it was possible to assess the quasar environments with respect to large-scale density enhancements. In early 2000s, Söchting et al. (2001) presented the analysis of quasar environments at  $z < 0.4$ , showing that quasars trace the LSS and that they lie on the peripheries of clusters. Further studies confirmed that quasars populate less dense areas of these LSS filaments (e.g., Söchting et al., 2004; Lietzen et al., 2009).

The cluster mergers were proposed as a route to quasar formation, suggesting that while galaxy-galaxy interactions may be one avenue for quasar formation, the interaction of cluster gas with galaxies<sup>6</sup> during a cluster merger could be another way since several quasars were observed at the common periphery between two clusters

(Söchting et al., 2001, 2002, 2004) and because of the fact that hot gas is one of the components in a cluster of galaxies (intracluster gas, Schindler, 1999). At higher redshift, a similar geometrical pattern was observed for quasar positions (Haines et al., 2001; Tanaka et al., 2000), suggesting that cluster mergers could be responsible for quasar phenomenon where it was noted that some quasars have an adjacent line of star-forming galaxies.

One way to measure environment density is by calculating the number density (e.g., a study from the University of Turku of environments around nearby SDSS quasars, Lietzen et al., 2009). The number counts are also important from the cosmological perspective. Given a certain cosmological model, it is possible to check the evolutionary models by comparing the predicted number counts with the observed number counts (e.g., Singh et al., 2023).

However, such earlier studies had a limited number of quasars and relied on analysis of images and statistics to identify clusters, which may not be precise methods. In general, for environment studies at large and small scales, a small number of quasars in studied samples might introduce the problem of the sample not being representative of the whole population. Images of the sky are contaminated with background and foreground galaxies projected by chance in the same field and nearby galaxies on an image could actually not be close to each other in 3D space. Another problem was that many studies lacked control samples to compare the active galaxies to inactive (normal) galaxies. The reader should compare the results in studies keeping these points in mind.

## 4.4 AGN triggering

What leads to the ignition of this formidable activity is debated today. I further explain the two main theories: the merger scenario and the secular scenario, Fig. 29. There are still various (sometimes contradictory) explanations for AGN triggering and it is one of the unanswered questions to date (Alexander & Hickox, 2012). This dissertation focused on Type I (unobscured) AGN, addressing the low-redshift regime. Obscured AGN, highly luminous quasars, or AGN at higher redshifts may have a different dominant triggering mechanism (e.g., Satyapal et al., 2014). Each mechanism discussed here provides solutions to several obstacles cool gas has to overcome in order to feed the SMBH accretion in the center of the host galaxy: 1) crossing host-galaxy scales to subparsec volume of the SMBH accretion disk, 2) angular momentum, and 3) forming stars instead (Alexander & Hickox, 2012).

---

<sup>6</sup>In this early study, the authors argued that in a cluster besides galaxies there is also cluster gas in between the galaxies. So this cluster gas plays a role when two clusters merge, as a galaxy might be influenced by this cluster gas and nuclear activity may be triggered.

### 4.4.1 Galaxy interactions

In the merger scenario, the interactions of galaxies lead to inflows of gas which feed the SMBH in the center of its host galaxy and turn on the accretion. Merger signatures in galaxy images have been observed since 1970s, such as tidal tails, protrusions, bridges, giving insight to astronomers that galaxies interact with each other gravitationally and that material may flow from one galaxy to another (e.g., Toomre & Toomre, 1972). In fact, mergers cause major changes in a galaxy. For example, some galaxies are observed to be distorted from disk shapes. Other galaxies appear irregular in morphology. These cases are thought to be a product of a violent merger. The merging galaxies may deform and even lose their symmetrically spiral structure, their morphology may change, and the spiral arms may be stretched. The gas and stars in merging galaxies are affected by the interaction. For example, gas clouds in the colliding galaxies may bump into each other resulting in starbursts and stars may be stripped or ejected out of their parent galaxy.

One approach to quantify the close encounters is by measuring the merger fraction. The galaxy images are inspected to see if there are any disturbed morphologies, as disturbed morphologies can be considered as relics of close encounters. Using this approach, Hong et al. (2015) concluded that luminous AGN activity is associated with galaxy merging for a sample of low-redshift active galaxies (early-type).

Merger simulations also show that gas can be driven from outer radii to the nuclear regions, triggering starbursts in the nuclear regions (e.g., ultraluminous IR galaxies or ULIRGS). Furthermore, some simulations result in inflow of gas that can feed the SMBHs. SF activity can also be boosted in the host (Di Matteo et al., 2005).

However, major merger simulations still have aspects which are not completely resolved (Naab & Ostriker, 2017). For example, often merger simulations ignore the bigger picture of the cosmological context. Also, the low rate of the major mergers may not be able to explain the existence of all of the massive galaxies. In the case of

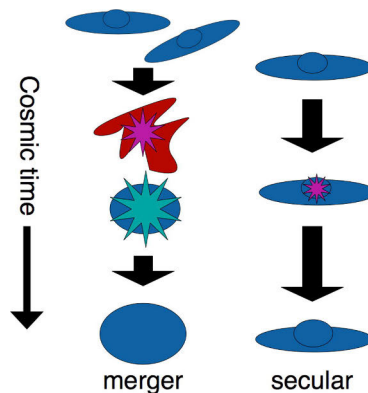


**Figure 29.** AGN triggering scenarios (Alexander & Hickox, 2012, Fig. 2).

AGN, it is observed that AGN-host galaxies are disk-like and not predominantly in the merger systems. Even for obscured AGN, some research shows that mergers are not responsible for BH triggering (e.g., Lambrides et al., 2021).

The SFR has a tight correlation with galaxy mass, termed the *SF main sequence*. The main type of galaxies to form stars are spirals. Since mergers deform spirals and result in loss of the disk and spiral arms due to the interaction, it is clear that most of the SF is not due to the merger-driven starbursts. It is known that equal-mass mergers do not happen frequently enough to contribute significantly to the SF budget of the Universe (Naab & Ostriker, 2017). On the other hand, mergers play an important role in the formation of massive early-type galaxies.

Moreover, some observational studies show that there is no evidence of galaxy mergers and interactions in triggering AGN, especially at lower redshifts (Cisternas & Jahnke, 2015; Smethurst et al., 2024). Another set of studies shows that the major mergers may be one mechanism but it is not enough to account for the whole AGN population (Orban de Xivry et al., 2011; Draper & Ballantyne, 2012). Yang et al. (2019) showed that low luminosity AGN at low redshifts may be triggered by minor mergers, via high resolution hydrodynamical simulations. For example, Cisternas et al. (2011) analyzed AGN at  $z < 1$ , and found that most host galaxies do not have merger signatures such as distorted morphology. And the distortion fractions between active and inactive samples are statistically similar. Thus, their study suggests that instead of major mergers, at this redshift, the internal secular mechanisms and minor interactions are responsible for SMBH growth.

#### 4.4.2 Secular mechanisms

In the secular scenario, no external triggering is necessary. The instabilities within the host galaxy itself drive gas into the center to fuel the SMBH activity. Furthermore, secular processes may be responsible not only for triggering but also for resolving the angular momentum problem (Combes, 2001).

Instability-driven inflows have been shown to feed high-redshift galaxy BHs (Bournaud et al., 2011; Bournaud, 2016). Cold gas accretion onto high- $z$  disk galaxies trigger gravitational instability in these simulations when accompanied by high gas fractions in the host (Bournaud et al., 2011). Observations by Bournaud et al. (2012) confirm these simulation results, using emission line diagnostics method. SNE may also induce accretion in the centers of galaxies (Kumar & Johnson, 2010).

The triggering mechanism may depend on the quasar luminosity, as indicated by simulations. Menci et al. (2014) investigated SMBH accretion triggered by disk instabilities in isolated galaxies. They tested their simulation results against cosmological models, and found that the disk instabilities may be one of the main drivers in the cosmological evolution of AGN population of low and intermediate luminosities at redshifts  $z < 4.5$ . On the other hand, the quasar LF is in good agreement between

the observed data up to  $z \sim 6$  and the galaxy interaction mechanism predictions. This is the case even for the high-luminosity quasars.

Another body of research considers the role of bars in fueling AGN in isolated disk galaxies. For example, Cisternas et al. (2015) concluded that the presence or absence of bars does not influence the AGN strength, suggesting that the LSS of a galaxy does not influence the triggering and efficiency of the SMBH activity. The bars may be an avenue, however, to funnel the gas into the host’s center (Du et al., 2017), using, for example, gravitational torques (Alexander & Hickox, 2012). Furthermore, at higher redshifts, their study showed that more than half of the active disk galaxies did not have a bar, further confirmed by Cheung et al. (2015).

## 4.5 Quasars through time

SMBHs are involved as key role players in many epochs of the cosmogony theories. One aspect of quasars is that they are extremely luminous. They can be thus observed at very high redshift, although high- $z$  quasars are rare, already in the early stages of luminous structure formation (by 1 Gyr mark after the BB), when the Universe was less than 10% of its present age (cosmic dawn) (e.g., Bañados et al., 2018). At this cosmic time, the largest scale structures may not have yet condensed. Very high redshift ( $z > 6$ ) quasars have been found (e.g., Maiolino et al., 2024). Then, based on SDSS data, quasars at redshifts  $z \sim 6$  have been discovered, with SMBHs above  $10^9 M_{\odot}$ , i.e., at the end of the epoch of reionization (Fan et al., 2006). Current cosmological models are attempting to explain how such MBHs already existed by 1 Gyr since the BB, perhaps by several formation mechanisms (Volonteri et al., 2021). For example, Silk & Rees (1998) argue that primordial baryonic clouds could have MBHs as first objects, even before stars. It is thought that the early MBHs started out as seeds more modest in mass, which later grew larger (Inayoshi et al., 2020) by gas accretion and through mergers (Volonteri et al., 2021). Nowadays, most massive galaxies harbor an SMBH in their center, rendering their existence ubiquitous throughout the cosmos now and in the distant past.

The quasar density through time peaks slightly earlier ( $z > 2$ ) than the peak of galaxy formation ( $z \sim 1.5$ ) — in the literature these refer to the “quasar comoving density peak” and “SFH of luminous galaxies” (Silk & Rees, 1998; Madau et al., 1996). Thus, the quasars were much more numerous in earlier epochs of the galaxy assembly timeline.

Decarli et al. (2017) reports 4 out of 25 quasars at  $z > 6$  with close companions with high SFR ( $> 100 M_{\odot} \text{ yr}^{-1}$ ). This is important, because massive elliptical galaxies in early cosmic epochs require high SFRs at high redshift galaxies to build up enough stellar mass in time. The massive quasar-like objects through quasar winds may halt the SF in their own galaxy host by removing the necessary gas supply. However, the ejected gas may cool down and eventually fragment into dwarf galax-



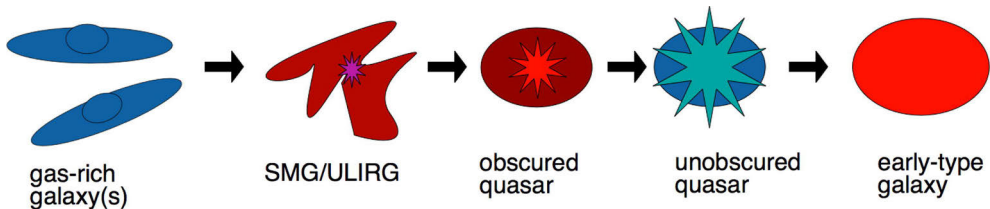


**Figure 30.** The stages of galaxy evolution after a major merger (Alexander & Hickox, 2012, Fig. 6).

ies without DM halos in the vicinity of the proto-AGN. Furthermore, the expulsion of gas also starves the accretion flow and the MBH in the center ceases to grow in mass.

The antihierarchical trend is known as “the downsizing of AGN” since the most luminous and massive AGN were also the most abundant at cosmic noon (Netzer, 2013). The less luminous AGN density peaked later, with the least luminous AGN peak being at  $z=1$  (e.g., Babić et al., 2007; Kalfountzou et al., 2014). This pattern contradicted the hierarchical CDM, according to which more massive objects form after less massive objects. The explanation for this phenomenon is that the quenching of quasar activity is due to AGN feedback processes (e.g., Scannapieco et al., 2005; Antonuccio-Delogu & Silk, 2010; Hirschmann et al., 2014), however, other aspects can play a role as well, such as obscuration (Fanidakis et al., 2012).

One important aspect of AGN activity is its relation to the SFR of the galaxy. AGN activity is thought to affect the SF in the host galaxy, for example, in simulations by Di Matteo et al. (2005). The cosmic SFR density peaks at redshift  $z\sim 2$ , and so does the quasar activity (Madau & Dickinson, 2014). This supports the co-evolution of BHs with their host galaxies. For example, due to quasar activity, a major-merger evolutionary scenario takes a gas-rich galaxy through several stages culminating in a low SFR early-type galaxy, Fig. 30 (Alexander & Hickox, 2012). The SFR estimation might be overestimated, though, for AGN in SED-model based studies (e.g., Florez et al., 2020). State-of-the-art instruments and telescopes are often employed both to study cosmic noon epoch’s AGN host morphology and kinematics, e.g., the SUPER survey (Circosta et al., 2018).

The future observations of AGN continue, at all redshifts. Besides insight into the quasar itself, other aspects of the universe can be studied through them. For example, the high-redshift quasar spectra have a characteristic feature called the *Lyman- $\alpha$*  forest, which is a multitude of Lyman- $\alpha$  absorption lines due to the intergalactic gas at different redshifts that the light passes through. At very high redshifts the absorption lines are so frequent due to a high density of the neutral Hydrogen, that the spectrum is greatly reduced beyond the Lyman- $\alpha$  line and this feature is called the *Gunn-Peterson trough* (Gunn & Peterson, 1965). Studying these observational features can shed light on the reionization epoch timing and on the intergalactic gas properties at

different redshifts (Fan et al., 2023). Furthermore, beyond the optical and near-IR (NIR), high energy and radio observations, gravitational lensing, neutrino observations, and gravitational wave detections from SMBHs continue to expand the arena of quasar research in future years.

## 5 Observational methods

Moi aussi je regarderai les étoiles.

Me too, I will be watching the stars.

---

Le Petit Prince  
Antoine de Saint-Exupéry  
Translated from French

Before the advent of telescopes, humans relied on the *naked eye* observations (e.g., the Danish astronomer Tycho Brahe). The objects were classified into six groups based on brightness order, where the first category had the brightest objects and the subsequent categories held less bright objects — an approach still used in the current magnitude systems. Nowadays, the general task of observational astronomy is to collect information about objects by examining them through telescopes. The information type used is typically the *electromagnetic radiation* — photons which carry energy. The optical imaging and spectroscopy are presented in the first two sections (§5.1 and §5.2), the particularities of the IR regime are described in §5.3, followed by a brief review of the major sky surveys (§5.4), the spectral energy distribution technique (§5.5), and the telescopes used in this body of research (§5.6).

### 5.1 Optical imaging

The *optical regime* spans a relatively short interval of wavelengths (or frequencies) in the EMS, from shorter more energetic blue wavelengths to longer reddish wavelengths ( $\lambda \sim 300\text{--}900\text{ nm}$ ). It is mostly visible to human eye<sup>1</sup>. For example, while an elliptical galaxy emits at other wavelengths as well, most of its stars are old and cool, so that the peak intensity is in the redder wavelengths. On the other hand, the spiral arms of galaxies are full of patches with hot blue stars which are young and shine brightest at the shorter wavelengths in the optical/UV — the more energetic bands.

One of the most common ways that astronomers observe the sky since the advent of telescopes is by producing images of sections of the sky. For example, the great Galileo Galilei published hand drawings of the Moon, the Pleiades, and other constellations several centuries ago (Galilei, 1655). Today we use technology instead of

---

<sup>1</sup>The *visible light* covers about one octave of wavelengths 3700–6700 Å (Roth, 1975).

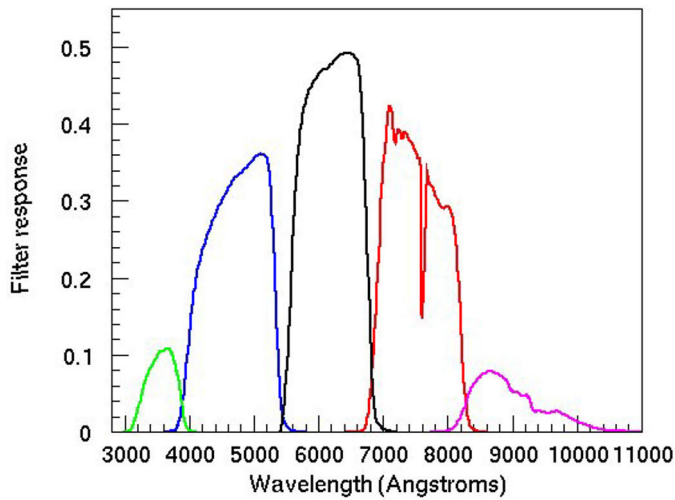


**Figure 31.** Filter response curves (*ugriz* from left to right). Image Credit: Sloan Digital Sky Survey.

our eyes and translate the observed information into digital 2D images. An image is a projection of a 3D volume onto a 2D plane. Images can be used to perform astrometric, morphological, and photometric studies. For example, in Paper IV, I used measurements from images to construct the SED diagrams for the quasars in our sample. Images can be used to study galaxy morphologies.

The imaging process uses the telescope to focus and collect the light over an interval of time, to be able to obtain the desired detection. Different filters are used. For example, in the SDSS, the filters are *ugriz*:  $\lambda_{\text{center}} = 3551, 4686, 6166, 7480, 8932 \text{ \AA}$  respectively, with width of about  $100 \text{ \AA}$  (Doi et al., 2010, Fig. 31).

The optical imaging instruments use charge coupled devices (CCD) to measure photons. The CCDs release electrons as light photons hit their pixels, which are then counted by the device. The images are processed for calibration in order to separate the pure source signal from the noise as much as possible. The raw images are corrected for instrumental effects (bias, readout noise, dark noise), for interpixel variation (flat fielding). Plus, the sky background subtraction is performed.

When reporting the number of photons measured, i.e., the signal ( $S$ ), it is also important to calculate the noise ( $N$ ). The signal-to-noise ratio ( $S/N$ ) then gives an idea of how good the observation quality is. One source of noise is the photon counting noise. For  $N$  photons, the photon noise is simply  $\sqrt{N}$ . That's why, to double the  $S/N$ , one needs to quadruple the exposure time.

Point sources appear differently at different seeing conditions. For each image, the PSF shows what the 2D shape of a point source looks like. As an example, a point source is a star or a distant quasar.

### 5.1.1 Measuring galaxy brightness

The amount of energy that crosses an area of one square meter per second is termed *flux*,  $F$  ( $\text{erg s}^{-1} \text{cm}^{-2}$ ). The photons emitted from a luminary can be expressed as that object's *luminosity*,  $L$ , which is the total amount of energy emitted by the whole object per second. Flux and luminosity are correlated via the luminosity distance between an observer and an astronomical object. The Solar luminosity is  $L_{\odot} = 3.8 \times 10^{33} \text{ erg s}^{-1}$ . The *bolometric* luminosity is used to account for the photons from all bands of the EMS. In other cases, astronomers need to only consider the energy from a certain interval of the spectrum, e.g., IR or optical luminosity.

#### Apparent magnitudes

Astronomers also have a comparative way of expressing the flux of an object, which was developed some 2000 years ago and is still used today in an updated form — *the system of magnitudes*. The transformation between a flux,  $F$ , of a celestial object (as received at the Earth) and its apparent magnitude,  $m$ , is defined relative to the reference flux density  $F_0$  as:

$$F = F_0 \times 10^{-0.4m}, \quad (37)$$

where reference flux is specified by the magnitude system used. In the Vega magnitude system, the star Vega is used as a reference and  $F_0$  depends on filter, while in the AB magnitude system,  $F_0$  is constant and is equal to 3631 mJy for all filters (Bessell, 1990, 2005). Brighter stars have numerically smaller magnitude values. The concept of magnitudes is employed many times throughout the papers, for example to correct for instrumental magnitudes, to correct for extinction loss, to introduce the  $k$ -correction, to convert between SDSS  $r$  and  $i$  magnitudes.

The Johnson-Cousins standard broadband photometric system divides the visible and part of the IR region of the sky into 5 bands (U, B, V, R, and I) which can be observed by broad filters (Table 3). Filters are designed in a way to restrict the light to a particular interval of wavelengths (Romanishin, 2002). The spectral resolution for each passband can be calculated using:

$$R = \frac{\lambda_{\text{eff}}}{\Delta\lambda}, \quad (38)$$

where,  $\lambda_{\text{eff}}$  is the central wavelength and  $\Delta\lambda$  the FWHM measurements of the passband; these quantities also generally specify the bandpass function (Sutton, 2011).

#### Surface brightness

At low redshifts, unlike stars which are point sources, galaxies generally appear as *extended* objects in the sky. Flux coming from an angular area in the sky image is

termed *intensity*,  $I$  ( $\text{erg s}^{-1} \text{arcsec}^{-2}$ ) =  $F / \alpha^2$ , where  $\alpha$  is the angle subtended. In this case, the *surface brightness* of two (extended) astronomical objects, spread out over the same angular area on the image, is:

$$\mu_1 - \mu_2 = -2.5 \times \log_{10} \left( \frac{I_1}{I_2} \right) . \quad (39)$$

### Galaxy luminosity

Galaxy luminosity is important in luminosity-mass and other relations of galaxy properties. Optical images can provide an apparent magnitude ( $m$ ), from which an *absolute magnitude* ( $M$ ) can be derived if the luminosity distance ( $D_L$ ) of the galaxy is known. As an example, let's consider the optical R band. The standard relation for absolute luminosity in this band is:

$$M_R = m_R - DM(z) - k_R(z) - e_R(z) . \quad (40)$$

The DM term is the distance modulus. It is defined as:

$$DM = 5 \log_{10}(D_L) + 25 , \quad (41)$$

where the luminosity distance is in megaparsecs. The distance can be derived using the redshift of the galaxy, from analyzing its observed spectrum, as in Paper I.

The term  $k_R$  is the k-correction for R band and  $e_R$  is the correction for luminosity evolution. Even though we used samples at low redshifts, yet still, we had to account for the k-correction, for example in the absolute magnitude calculations, usually using software (Blanton et al., 2003). The correction is needed, because the same galaxy spectrum interval observed in a specific fixed passband changes due to redshift, so in practical terms we see different parts of the galaxy spectrum depending on redshift. For example, the light registered in our SDSS  $r$  band filter in the

**Table 3.** The Johnson-Cousins *UBVRI* photometric system (Bessell, 2005). The shapes resemble a contour of a bell, but are not always symmetrical. The bluest filter is limited by the effect of the atmosphere on transmission (Sutton, 2011). A repository of filter information (including transmission curves) is provided by the Spanish Virtual Observatory (Rodrigo et al., 2012; Rodrigo & Solano, 2020).

Standard filters	Effective wavelength ( $\lambda_{\text{eff}}$ )	FWHM ( $\Delta\lambda$ )
	Å	Å
U	3663	650
B	4361	890
V	5448	840
R	6407	1580
I	7980	1540

optical regime (observed-frame) may have been originally emitted in UV (rest-frame of the galaxy). This correction is important when comparing observations of several galaxies, as it “brings” all galaxies to the same (usually  $z=0$ ) redshift. The effect is larger with higher redshift. Hogg et al. (2002) comprehensively presents this subject in a pedagogical manner.

From the absolute magnitude  $M_R$ , the luminosity in the optical R band ( $L_R$ ) can then be derived,

$$M_R = -2.5 \times \log_{10} \left( \frac{L_R}{L_{\text{std}}} \right), \quad (42)$$

where the standard luminosity ( $L_{\text{std}}$ ) can be obtained from the specific reference object in that magnitude system.

## 5.2 Spectroscopy

A further step is to obtain a spectrum of an object. The spectroscopy shows the flux of an object at each wavelength, allowing the study of individual spectral lines, calculating redshift, and much more. Spectral lines could be emission or absorption features.

Technically, the spectrum is obtained by splitting the incoming light into individual wavelengths. In Paper I, the ALFOSC instrument uses a diffraction grating method to achieve this. However, spectroscopy usually requires special instruments and is more time consuming than imaging.

There are several methods to obtain a spectroscopy of an object. The two methods used here are the *longslit spectroscopy* in Paper I and the *multiobject spectroscopy* (MOS) in Paper II. In the first case, a long slit is centered on an object, so only through the narrow window of the slit the light can pass through. The MOS observations were done using multiple slitlets so that several objects in a field could be observed at once. To obtain a calibrated spectrum, besides observing on target, various calibrations are performed as well for wavelength and flux calibration.

The spectra of elliptical galaxies and spiral galaxies are different. The spectrum of an elliptical galaxy is dominated by the old stellar population. The elliptical galaxy spectrum has numerous deep absorption lines from cool giant stars (M, K) and the 4000-Å break (Sparke & Gallagher, 2007). The 4000-Å break (*Balmer break*) is a characteristic of older stellar populations. This feature in the spectrum is observed as a “jump by a factor of  $\sim 2$  in the spectra” (Schneider, 2006). It is generally due to which type of Hydrogen transitions are possible and species abundances (Emerson, 1997). The most conspicuous absorption lines are Ca II doublet  $\lambda\lambda$  3934, 3969, G band  $\lambda$ 4300, Mg b  $\lambda$ 5155, and Na D  $\lambda$ 5894. No indicators of SF, such as emission lines are present (typically).

The spiral galaxies have emission lines in their spectra due to the on-going SF, such as the Hydrogen Balmer lines ( $H\alpha$   $\lambda$ 6564,  $H\beta$   $\lambda$ 4861,  $H\gamma$   $\lambda$ 4340) as well as

forbidden lines [O II]  $\lambda 3737$  and [O III]  $\lambda\lambda 4959, 5007$ . The optical-UV spectra of Type I quasars are dominated by broad emission lines, such as H $\alpha$   $\lambda 6564$ , [Mg II]  $\lambda 2799$ , [C III]  $\lambda 1909$ , [C IV]  $\lambda 1549$ , and Ly $\alpha$   $\lambda 1216$  (Beckmann & Shrader, 2013).

Forbidden spectral lines are produced “when an electron jumps from an upper energy level to a lower level” (Ridpath, 2018). The term “forbidden” refers to the distinction that these less probable transitions are not observed on the Earth (under normal conditions), but are possible in space where the gas density is sufficiently low. The square brackets are used as notation to indicate forbidden lines, e.g., [O III] line is a forbidden line of oxygen, doubly ionized (Dyson, 1997).

### Instrument sensitivity

To get the correct flux values of the spectrum, the calibration needs to consider the instrument’s *sensitivity function*,  $S_\nu$ , which affects the measurements as follows:

$$F = \int_0^\infty S_\nu F_\nu \nu \, d\nu, \quad (43)$$

where  $\nu$  is the frequency. Note, this is accounted for after all of the other effects are removed (bias, dark, flat, etc). For example, the sensitivity function of the human retina (as an instrument) peaks at  $\lambda \sim 550$  nm, which is the yellowish green color. The sensitivity  $S$  of a spectrometer as a function of wavelength is determined by observing a standard star with a known flux distribution, and then by applying the derived sensitivity function to calibrate the flux data from the observed galaxy (Example in Figs. 32, 33). This step allows the spectra to have physically meaningful values on the flux axis.

### 5.2.1 Estimating the luminosity of an emission line

The above concepts were applied in analyzing emission line fluxes in Papers I and II, and here we give a short overview of the main steps for the case of the [O II] 3727 Å emission line (but which can be applied to others). After the final calibrated spectra were obtained, for some objects, their optical spectra had a prominent [O II] 3727 Å emission line (in the bluer part of the spectrum), such as in Fig. 34.

In Paper I, for example, we used the SPLOT tool of IRAF (Tody, 1986, 1993) to measure the flux within the emission line (without the continuum). This method is based on fitting the emission line with a Gaussian (example in the top diagram of Fig. 34). The fit results are given in a text file and include the central wavelength and the flux value along with several other measurements.

The spectroscopic redshift was estimated using the RVSAO tools based on all the available robust emission and absorption lines (Kurtz et al., 1992; Kurtz & Mink, 1998). Then within the concordance cosmology framework, we calculated the luminosity distance,  $D_L$ , in megaparsecs, for that object (§2.3). These two measurements



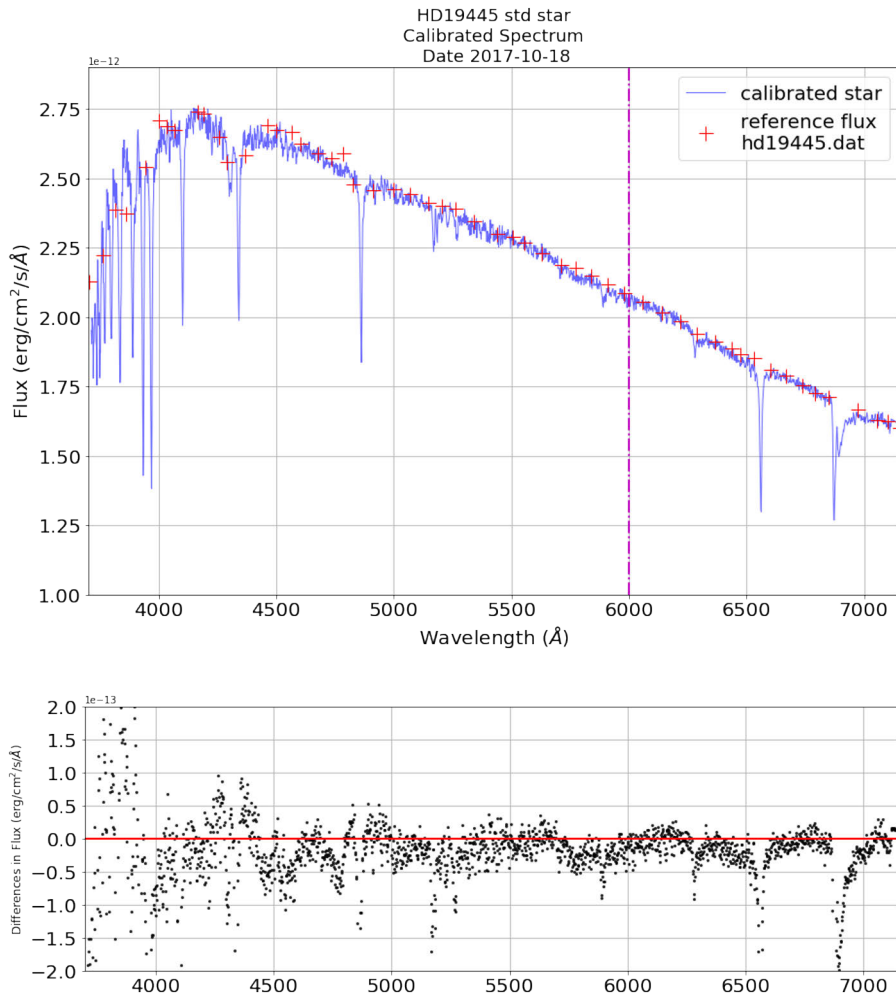


**Figure 32.** As part of testing the quality of the reduction, in Paper I, we perform flux calibration check. In this particular plot we check the spectrum of the standard star (calibrated, 1D, blue curve) by overplotting it with the reference values (red crosses). The middle panel shows the differences in flux (black dots).

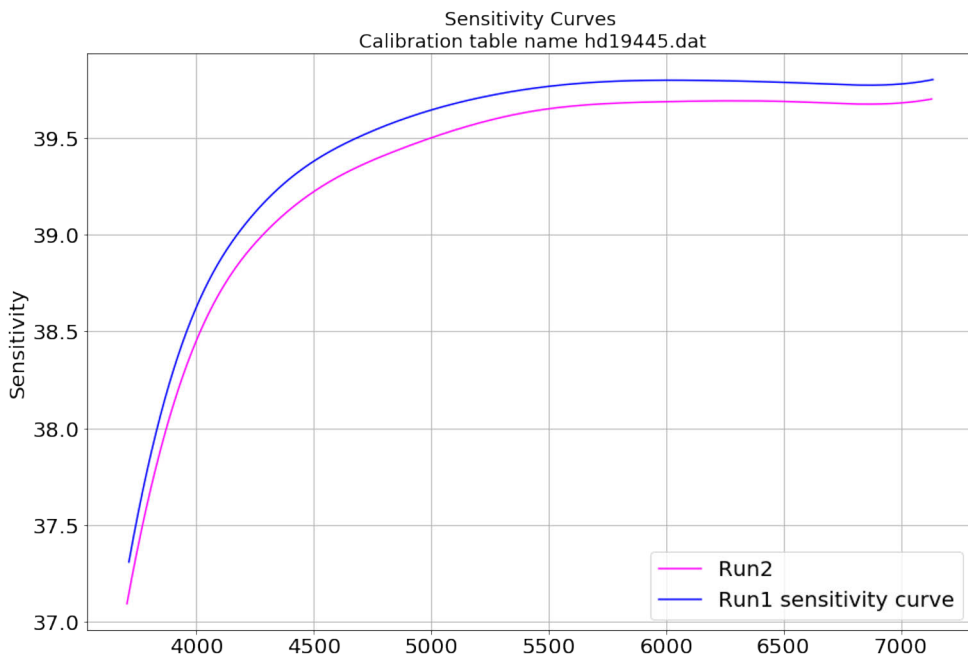
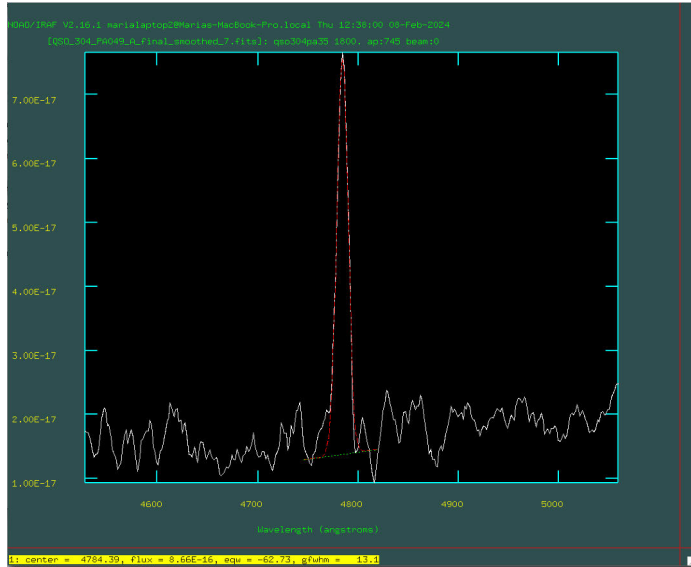


**Figure 33.** In Paper I, we observed targets on various dates (different runs). A standard star was observed for each run. We check for consistency the sensitivity curves (different colors) of the same standard star observed on different dates.



### Object A-304

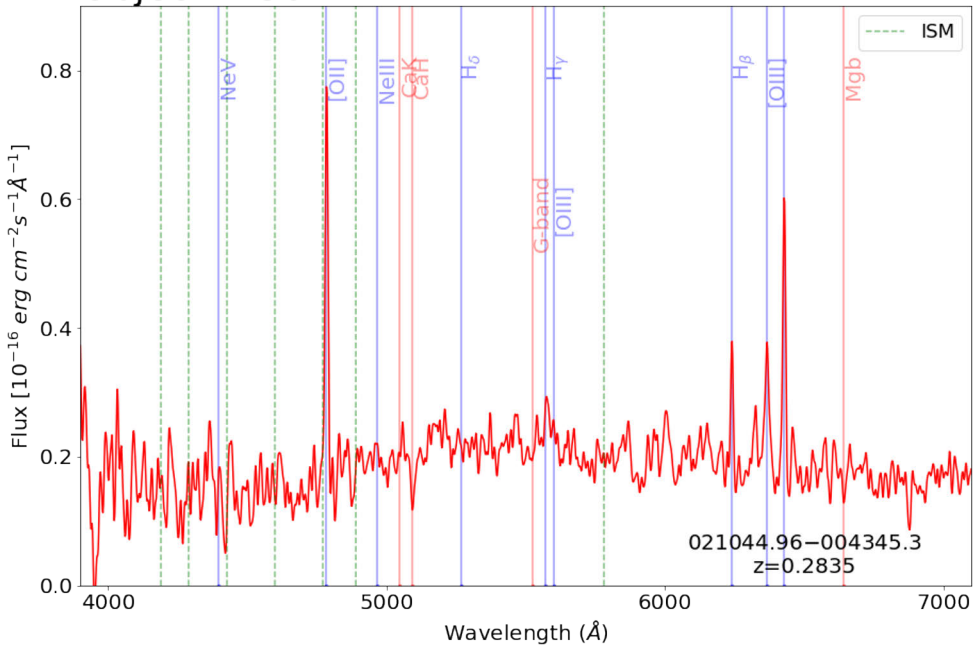


**Figure 34.** *Top.* This picture illustrates the observed calibrated spectrum in white and the Gaussian fit to the emission line in dashed red line. Produced by SPLIT tool. *Bottom.* In this plot, the spectrum of a quasar (red curve) is overlaid with expected emission lines (blue vertical lines), absorption lines (red), and ISM lines (green dashed). Note the prominent [O II] 3727 Å emission line.

were used to convert the measured fluxes to luminosities. We take care to keep the units consistent for all quantities, using conversions when needed. The luminosities of the emission line thus obtained can be used in the next steps to estimate the SFR values for the object.

## 5.2.2 Measuring SFR from [O II] emission lines

In Paper I it is not possible to use the robust  $H\alpha$  indicator to estimate the SFR because it was shifted to redder wavelengths and not present in the spectra. An alternative approach was used based on the [O II] emission line. This approach is fully discussed in Kennicutt (1998) and Gilbank et al. (2010). Here we highlight the main points. The same methods were used in Paper II.

### Stellar mass estimates

First, the galaxy stellar mass can be estimated using procedures from Bell et al. 2003; Kauffmann et al. 2003b,a; Gilbank et al. 2010, which are based on SDSS imaging of a large sample of  $z < 0.1$  galaxies. It is Equation (1) in the Gilbank+2010 paper:

$$\log_{10}(M_{\star}/M_{\odot}) = 0.480(g - r)_0 - 0.475M_z - 0.08, \quad (44)$$

where the rest-frame SDSS  $g - r$  color is used, and the  $M_z$  is the rest-frame absolute  $z$  band magnitude. In essence, this formula is constructed based on an empirical method, using the SDSS  $z$  band luminosity and SDSS  $g - r$  color: other color combinations give larger scatter, as noted by Gilbank et al. (2010). While we employed this method for Paper I, stellar mass can be estimated using other methods, such as in Paper IV with spectral energy distribution (SED) analysis. The calculated stellar mass then is used in the SFR equation given below (Equation 46).

### SFR estimates

Next, the intensity of [O II] 3727 Å line is used as an approximate SFR tracer. When present, Balmer emission line luminosities are good indicators of current SFR in galaxies (Gallagher et al., 1989). However, Balmer lines are not always available, when  $H\alpha$  line is out of the visible window,  $z > 0.5$  (Kennicutt, 1998). For blue galaxies, the flux of  $H\beta$  emission line is well correlated to the flux of [O II] emission line. This emission line is produced by photoionization from OB stars and hence is a measure of the recent SFH.

Besides the fact that [O II] forbidden line doublet is present in high redshift optical spectra, it is usually also a *strong* emission line (Kennicutt, 1998). However, one disadvantage is that the [O II] luminosity is not directly coupled to the ionizing luminosity, since it is a forbidden line. Its excitation depends on the properties of

the gas (abundance, ionization state). Kennicutt (1998) provides a formula (equation 3 in their paper) for SFR calculation with a way to correct for extinction (at  $H\alpha$ ). Kennicutt (1998) equation for [O II]-SFR is based on the average between the calibrations done with blue irregular galaxies (Gallagher et al., 1989) and normal and peculiar galaxies (Kennicutt, 1992). It is as follows:

$$\text{SFR}_0 / (M_\odot \text{ yr}^{-1}) = L([\text{O II}]) / 3.80 \times 10^{40} \text{ erg s}^{-1} . \quad (45)$$

The [O II]-SFR estimate is less precise than the  $H\alpha$ -based estimate of SFR (Kennicutt, 1998). The observed [O II] luminosity,  $L[\text{O II}]$ , was estimated from NOT spectra in Paper I.

### Correction to SFR estimates

Gilbank et al. (2010, 2011) examined the [O II]-SFR empirical relation using the SDSS DR7 data (Abazajian et al., 2009) in the local Universe. Specifically, the data sample used was from the deeper Stripe 82 region ( $275 \text{ deg}^2$ ), so that the stellar mass range of galaxies was the lowest possible in the survey. The sample consisted of  $\sim 50\,000$  galaxies, within the redshift range  $0.032 < z < 0.2$ , and considered over a wide mass range ( $8.5 < \log M_\star < 12.0$ ). They further verify the accuracy of this empirical calibration by cross-comparison with other SFR indicators, in particular with  $H\alpha$ , because uncertainties may be present due to stellar mass (Phillipps, 2005). Through this comparison, it was identified that a correction was needed, which was modeled well with a tanh function (*tanh-correction*, Fig. 35).

Hence, in Paper I, to estimate the SFR, equation 8 was employed from Gilbank et al. 2010, 2011. Gilbank's equation provides an empirical correction via a mass-term to the Kennicutt (1998) equation for [O II]-SFR, correcting for the dust extinction and metallicity:

$$\text{SFR}_{\text{emp,corr}} = \frac{\text{SFR}_0}{a \tanh[(x - b)/c] + d} . \quad (46)$$

Here,  $x$  is a mass-dependent term:

$$x = \log_{10}(M_\star / M_\odot) , \quad (47)$$

and  $a = -1.424$ ,  $b = 9.827$ ,  $c = 0.572$ ,  $d = 1.700$ . The Kroupa initial mass function (IMF) is assumed. Furthermore, the specific SFR,  $\text{sSFR} = \text{SFR}/M_\star$ , can also be then calculated.

Thus, by measuring the [O II] luminosity and by calculating the stellar mass of the galaxy, it is possible to estimate the SFR for that galaxy (the cited papers in the above method explain their limitations, e.g., in the estimation of the obscured star formation). In particular, to understand the uncertainties, it is important to remember

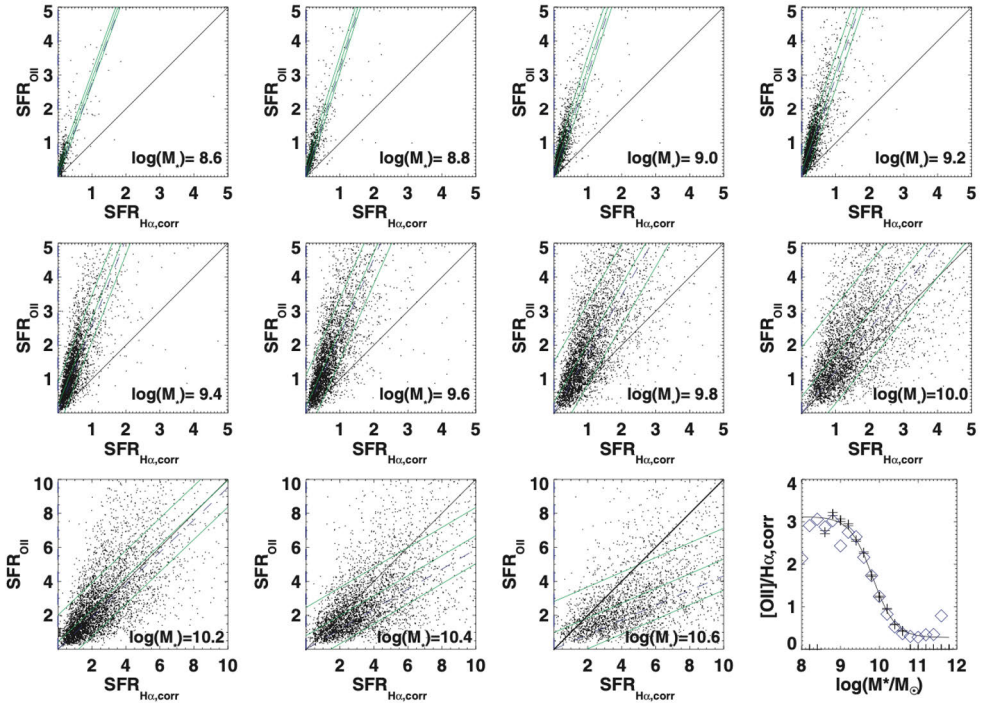


**Figure 35.** The cross-comparison of [O II]-SFR and  $H\alpha$ -SFR simple indicators. Source: Figure 3 from Gilbank et al. (2010). Each subplot represents a stellar mass bin. The x-axis gives the  $H\alpha$ -SFR, corrected with Balmer decrement. The y-axis shows the values for [O II]-SFR for the same set of galaxies (dots). The black solid line is plotted as a reference, to show the line where the two indicators would hold the same values. The green lines represent the best-fitting line and  $1\sigma$  uncertainty. The blue dashed line represents the “slope adopted in the best-fit fitting function”, used to construct the correction term via the tanh function. The final panel shows the mass-dependent best-fitting ratio of the SFR indicators (black points with error bars); the adopted tanh correction as green line. The blue diamonds show the ratio of the SFR density from [O II] to total SFR.

that [O II] indicator was calibrated using the  $H\alpha$  locally.  $H\alpha$ -SFR is dependent on the assumed IMF, for example (Mo, 2010). Metallicity and dust extinction may change with mass and redshift and need to be accounted especially for high-mass galaxies, where the Kennicutt (1998) equation for [O II]-SFR needs a correction as given by Gilbank et al. (2010). It is a good practice to compare SFR estimates done using data from other wavelengths as well (when possible).

### 5.3 Infrared observations

The IR domain is divided into three sub-sections: the NIR interval 1–5  $\mu\text{m}$ , the MIR of 5–30  $\mu\text{m}$ , and the far-IR (FIR) 30–300  $\mu\text{m}$ . The corresponding specific temperatures of the blackbody radiation curve peaks are  $T\sim 2000$ , 300, and 50 K respectively. The FIR is followed by the millimeter and radio regime, as the wavelength increases. There are three main photometric bands in the NIR: J, H, and K (Table 4 and Fig. 36).

An important aspect of observing is the Earth’s atmosphere. Sky is very bright in the IR wavelengths and may change rapidly, thus a careful sky background subtraction is needed. Certain observational techniques are used to skirt this issue when collecting data. For example, the HAWK-I wide-field IR imager (ESO) allows obtaining images with multiple short exposures as well as dithering, which are then combined, thus allowing to obtain greater S/N value.

Actually, the atmosphere absorbs light; the atmosphere blocks large sections of the electromagnetic radiation from space: gamma rays, X-rays, UV, most of the IR, and long wavelength radio waves. To observe in these regimes, space observatories are used (Fig. 36). IR instruments usually require cooling agents. This is to lower the thermal noise of the instrument itself. Thus, for space instruments especially, when the cooling agent runs out, the telescope cannot provide data anymore.

The applications of the IR are, for example, to observe processes at low temperatures. IR observations also allow studying regions obscured by dust (high extinction). It is important to study the IR, because some galaxies have their radiation peak in the IR, including some quasars, for example, dusty starburst galaxies, e.g., M82, LIRGs,

**Table 4.** Standard NIR bands (Heidt, 2022). The  $W_{\text{eff}}$  values pertain to the United Kingdom Infrared Deep Sky Survey (UKIDSS, Lawrence et al., 2007) characteristics and are given here as an example. The design of the NIR passband shapes is limited by the fact that several large regions are affected by the absorption from the atmospheric water vapor.

Band	Central wavelength	Effective Filter Width
	$\lambda_c$ $\mu\text{m}$	$W_{\text{eff}}$ $\mu\text{m}$
J	1.3	0.150
H	1.6	0.279
K	2.2	0.305

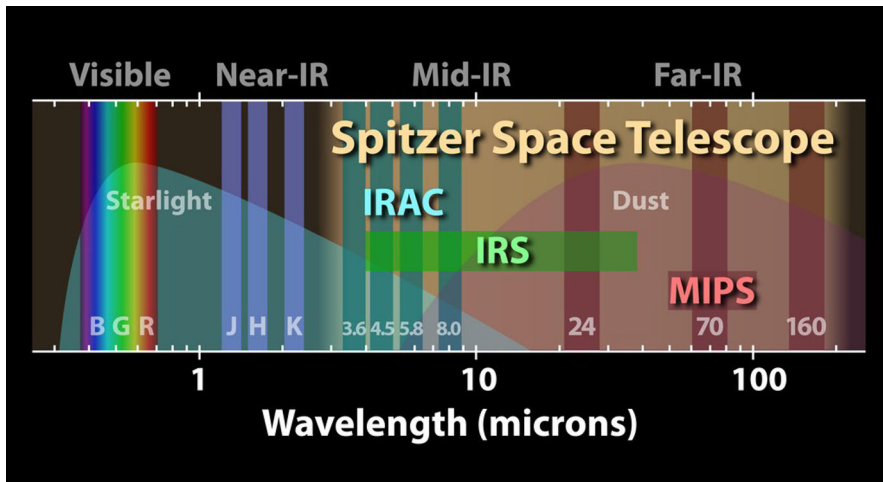


**Figure 36.** The *Spitzer* space observatory covered MIR and FIR, while the *JWST* has instruments for NIR and MIR. In this illustration, the vertical bars show the bands, from visible (B,G,R) to NIR (J,H,K) to MIR (3.6, 4.5, 5.8, 8.0  $\mu\text{m}$ ) to FIR (24, 70, 160  $\mu\text{m}$ ). The shaded regions of starlight (bluegreen) and dust (brown) are overlaid on the respective bands. The *Spitzer* instruments are labeled over the bands they cover (IRAC, IRS, MIPS). These longer wavelengths covered by *Spitzer* (about 3–160  $\mu\text{m}$ ) are best observed from space and are dominated by dust emission. Image Credit: NASA.

ULIRGs. The optical emission may be elevated in dusty starburst galaxies, but the IR emission is stronger. IR emission also includes dust emission, thus we can directly study the dust properties in the galaxy. Plus, distant galaxies may be observed in the IR because the intrinsically optical emission is redshifted to longer wavelengths.

The NIR also may have a stronger signature of AGN host galaxy star light (compared to the non-stellar emission). At higher redshifts, it is the IR images of quasars that are often used to study the morphology of the quasar hosts (e.g., Sanghvi et al., 2014). Actually, a multiwavelength study is necessary to get the full picture of the AGN, because AGN emit in all wavelengths significantly.

## 5.4 Surveys

This work used extensively archival data from sky surveys, which are briefly described here. Getting telescope time is expensive and time-consuming. Furthermore, even if observing time has been granted for a proposal, part of the time may be lost due to unforeseen circumstances, such as poor weather. Plus, some of the data might not be usable, for example due to unfavorable sky conditions and high sky background. Thus, it is valuable to use archival data by large surveys. The availability of accessible large survey archives are crucial to statistical studies based on galaxy observations. The main surveys used in this thesis are: the Sloan Digital Sky Survey



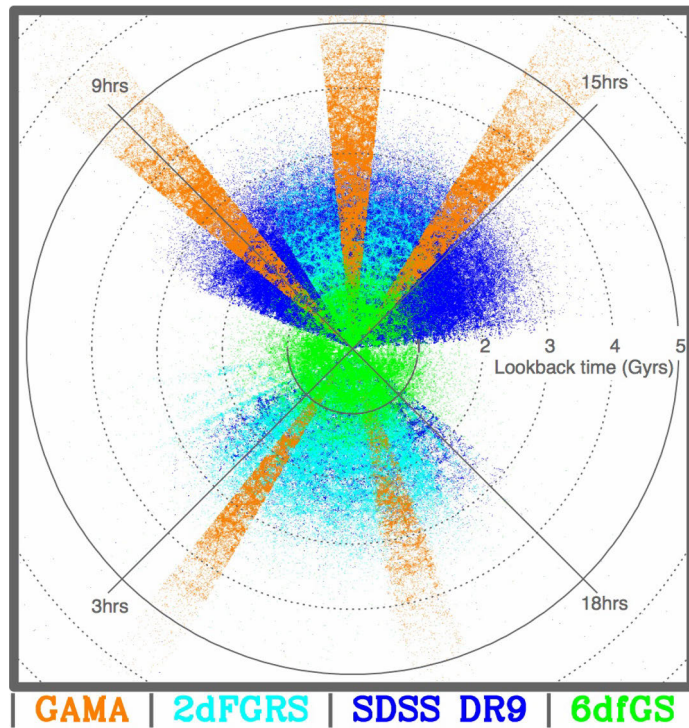


**Figure 37.** Survey Cones. This plot indicates which parts of the Universe the GAMA survey covered (orange). Similar illustration is given to few other known surveys (SDSS in blue, 2dFGRS in cyan, and 6dfGS in green). GAMA survey overlaps with SDSS survey regions, but goes much deeper, up to about 5 Gyr lookback time. It covers five sectors, three of which are equatorial (9hrs, 12hrs, 15hrs). Credit: GAMA survey.

(SDSS, DR18, Almeida et al. 2023) and the Galaxy and Mass Assembly (GAMA) spectroscopic survey (DR4, Driver et al. 2022). In Fig. 37, the survey cones of SDSS and GAMA survey are illustrated in blue and orange colors respectively.

### 5.4.1 Sloan Digital Sky Survey

SDSS is a rich imaging and spectroscopic redshift survey in the visible domain which began in the year 2000. It is based on the observations of a 2.5 m optical telescope at the Apache Point Observatory. This large-scale survey covered 1/3 of the sky area (Northern Hemisphere). The imaging was done in five bands: SDSS  $u$ ,  $g$ ,  $r$ ,  $i$ , and  $z$  (Fig. 31). Many major programs have been carried out based on SDSS data. In particular, for quasar science, we used the SDSS-based catalogs of quasars (Lyke et al., 2020). Furthermore, one area of the sky was imaged deeper, called the Stripe82 (Annis et al., 2014). Samples in Papers I and II are from Stripe82.

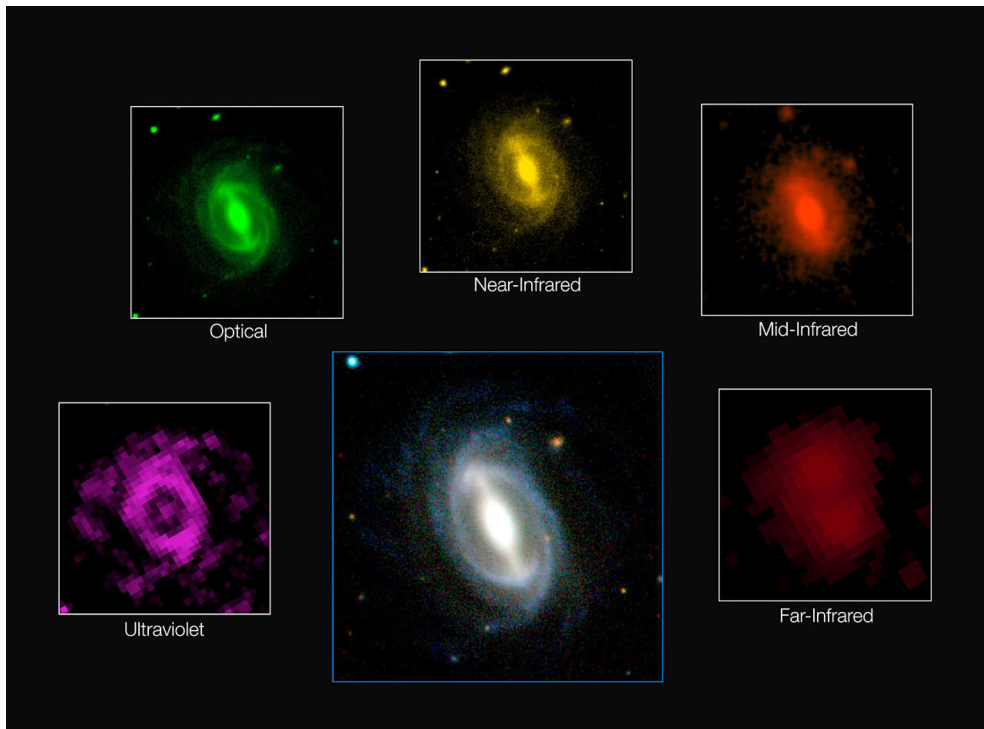


**Figure 38.** GAMA survey provides photometry for 21 bands, ranging from FUV to FIR. Here the same galaxy (bottom center) appears when imaged at different wavelengths covered by GAMA survey (going left to right): UV, optical, NIR, MIR, FIR. The stamp-pictures at different wavelengths also show how different features become emphasized at different regimes of the EMS (note also the resolutions are different). Credit: ICRAR/GAMA and ESO, ESO images.

### 5.4.2 GAMA survey

GAMA is a spectroscopic survey of  $\sim 300\,000$  galaxies in an area of the sky of around  $300\text{ deg}^2$  (Driver et al., 2022; Liske et al., 2015). The observations were performed with the 4 m class Anglo-Australian Telescope (AAT) from 2008–2014. The GAMA project incorporated data from other archives, and with its final data release the GAMA survey provides a rich database of optical spectra and ancillary information, including multi-band photometry from far-UV (FUV) to FIR (Fig. 38).

## 5.5 Spectral energy distribution of galaxies

Data from photometric surveys can be used to gain more insight into astronomical objects. One technique is the construction of the *spectral energy distribution* (SED) of a galaxy which shows the energy amount across different frequencies (or wavelengths). Different phenomena contribute to various parts of the SED graph. Rich surveys in UV, optical, and IR provide the necessary data to use with this technique.

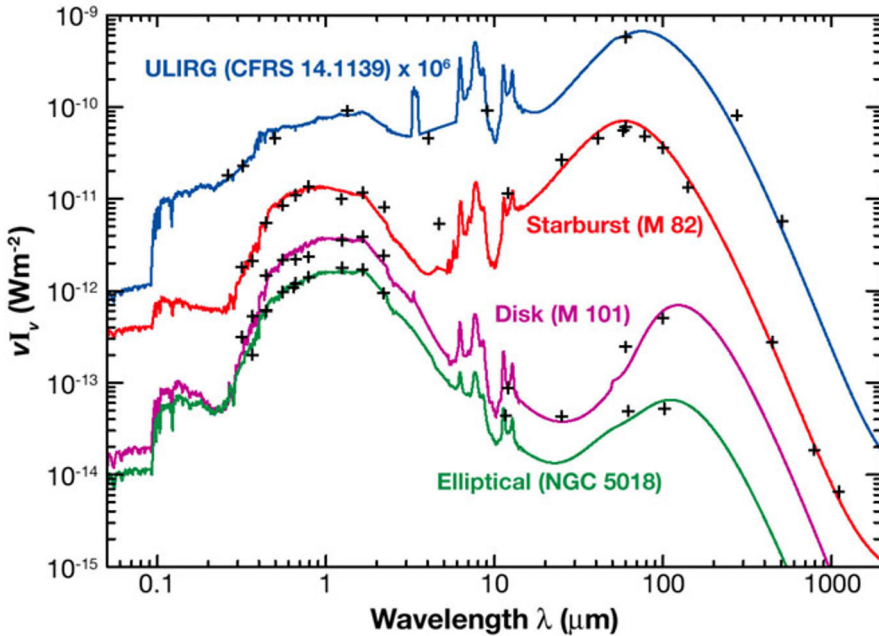


**Figure 39.** Here an example SED (restframe) of ULIRG galaxy (blue) is shown in contrast with the SEDs of various galaxies (Figure 1 from Lagache et al., 2005). The wavelength range is from UV to millimeter. The ULIRG SED shows that the emission in IR dominates over the optical emission. On the other hand, the typical elliptical and spiral galaxies are more prominent in the optical regime. The starburst galaxy SED typically is also bright in the IR, but at a lesser degree than the ULIRG reported here ( $z=0.66$ ).

The UV/optical region of the EMS gets contributions from the young star emissions, while the older stellar populations emit most of their energy in the redder wavelengths (optical). Dust absorbs energy from young stars and then re-emits it at much longer wavelengths. Additionally, dust grain emission peaks in the IR since dust has cooler temperatures.

Some galaxies shine more brightly in the IR than in the optical because of the dust obscuration, e.g., ULIRGs, Fig. 39. AGN contribution can affect all wavelengths. For example, very high energy blazars need to have multiwavelength studies, because they emit strongly in gamma-rays and also in radio. An example of blazar SED study is given in Fig. 40. Here the red line represents a model. In this case several models are tested to fit the observed photometric points. Understanding the SED of blazars is a continued effort in astronomical research.

The advantage of the SED technique is that it uses multiwavelength observations. Also, it is useful when only broadband photometry is present. Plus, for galaxies, the SEDs use general metrics of the stellar populations since often we cannot resolve individual stars in a distant galaxy. From the SED, we can estimate physical properties of galaxies, such as SFR, stellar mass, and dust mass. As an example, I pulled the

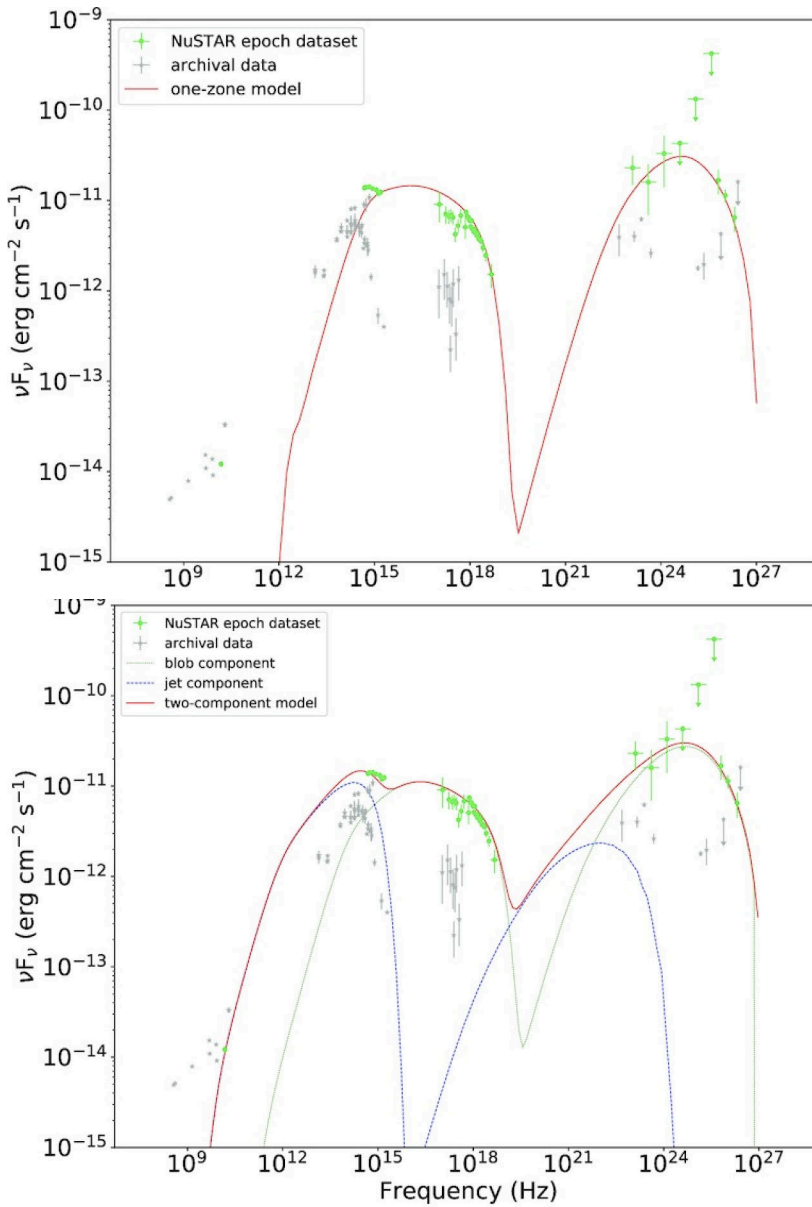


**Figure 40.** Blazar SED examples (Fig. 8 from Acciari et al., 2021). The data points are fitted with two models, represented by a red curve. *Top.* The one-component model. *Bottom.* The two-component model: blob emission (green curve) and jet contribution (blue line). In this case, Acciari et al. (2021) highlights that the one-component model fails to agree with the data in the radio regime and does not capture the optical emission accurately, while the two-component leptonic model agrees with the data more closely.

GAMA survey SEDs for the same galaxies for which the spectra were shown in §3 (Fig. 41). These were produced using the MAGPHYS tool (da Cunha et al., 2008; da Cunha & Charlot, 2011; Liske et al., 2015; Driver et al., 2022).

However, SED technique has also its limits. One problem is that apparently similar looking SEDs may be a result of quite different processes at play (e.g., age-metallicity degeneracy).

The SED construction requires processing a large amount of data. Nowadays several programs exist. In practice, the SED is built originally from several modules. Each module has several parameters associated with it. There are some differences between various programs.

### 5.5.1 CIGALE

For example, CIGALE models multiwavelength observations from FUV to radio. In the case of CIGALE (Boquien et al., 2019) used in Paper IV, in a nutshell, the SFH parameters come from the SFH module which describes the evolution of SFR. Stars are modeled as black bodies (Boquien et al., 2019). The stellar spectrum is computed using a standard library of single stellar populations (SSP), e.g., the Bruzual & Charlot (2003) SSP library. It is here that such important parameters as the stellar IMF and stellar metallicity of the model are provided.

Besides stars, dust also plays a role in building the SED. Dust absorbs starlight (UV-NIR) and then re-emits it in longer wavelengths (MIR, FIR). A separate module accounts for the attenuation laws to extinct the SED. The dust emission modules are responsible for modeling the mentioned re-emission in MIR and FIR regimes. CIGALE is using the energy balance principle to implement how the energy absorbed by dust is re-emitted by the dust at longer IR wavelengths.

CIGALE has an option to include a contribution from the AGN to the galaxy SED and thus can also model X-ray photometric points (Yang et al., 2020, 2022b). We used CIGALE in Paper IV to assess the AGN contribution to quasar host SEDs, since the MAGPHYS fits in the GAMA survey did not include the AGN component.

### 5.5.2 Stellar population synthesis

The SED technique is fascinating<sup>2</sup> since the SED of unresolved stellar populations in galaxies is a product of the various fundamental properties, e.g., stellar IMF, stellar metallicity, dust and gas properties, SFH. In Paper III, I readily used SED-based results from GAMA survey archives. Here I restrict to highlighting just a few fundamental concepts, generously borrowing from the brilliant review paper by Charlie Conroy on the subject (Conroy, 2013). Tinsley (1980) also provides very clear and

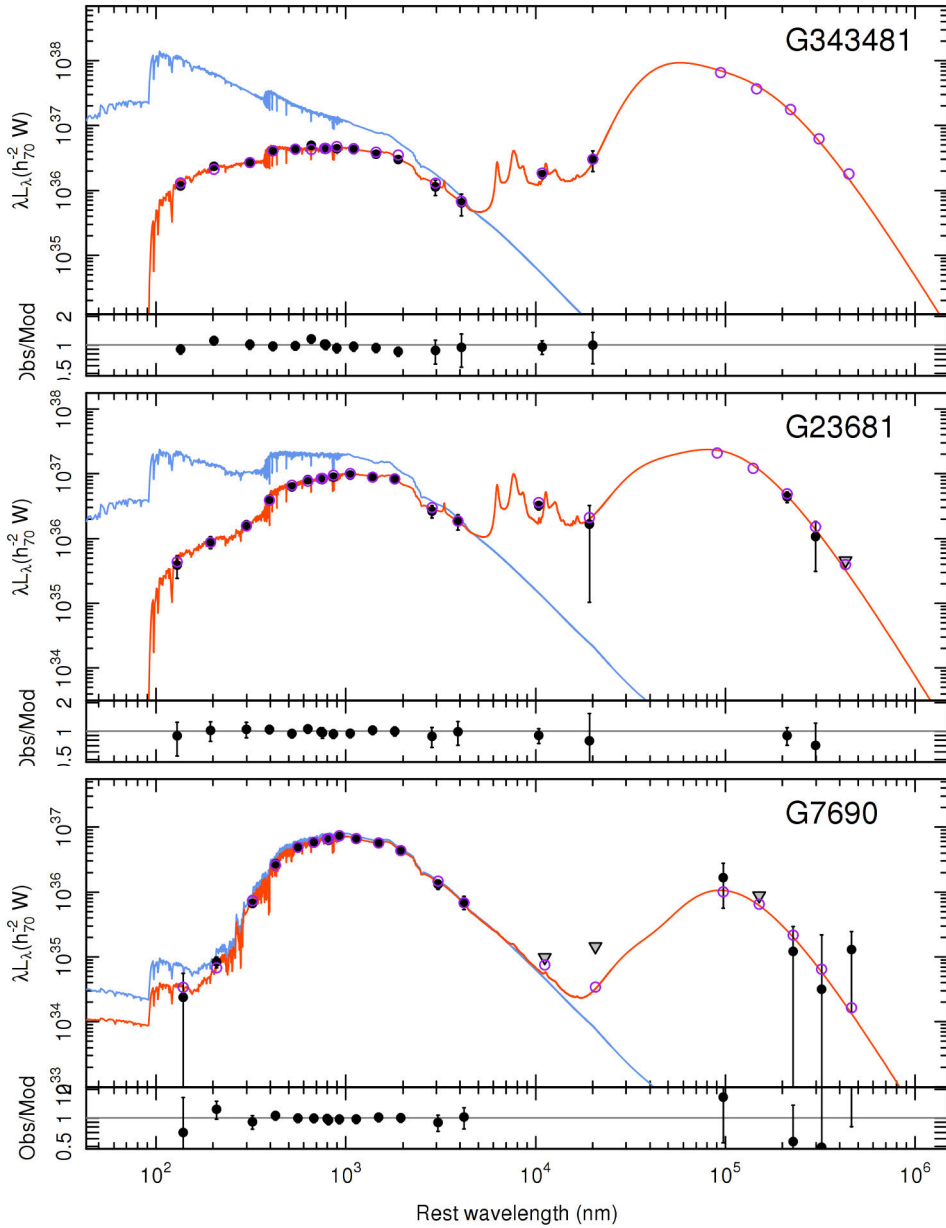


**Figure 41.** SED examples from Paper IV: a starburst galaxy (top), a spiral galaxy (center), and an elliptical galaxy (bottom) from the GAMA survey DR4. In all panels, the orange line represents the best-fit SED, while the blue line models the case where the galaxy has no dust. Colored circles are photometry data points, while the clear circles are model-predicted data points. As in Fig. 39, note the progressively stronger emission (elliptical to disk to starburst hosts) in the longer wavelengths because the dust re-emits light absorbed from young stars. The diagrams are sourced from the GAMA Single Object Viewer tool (Hopkins et al., 2013; Liske et al., 2015; Driver et al., 2022).

didactic explanations of stellar population analysis and the math associated with it.

To model the overall stellar population in a galaxy, the key player in the game is the *stellar population synthesis* (SPS) technique, which allows the construction of *simple stellar populations* (SSPs) and then the *composite stellar populations* (CSPs), as illustrated in Fig. 42 (Conroy & Gunn, 2010; Conroy, 2013), by summing the spectra of the constituent stars (Walcher et al., 2011). The SSP is built upon three components: IMF, isochrones, and stellar spectra. IMF gives the initial distribution of stellar masses for stars in the stellar main sequence. The isochrone is the locus of stars of the same age.

Uncertainties in each ingredient towards the SED model play a significant role, as discussed in Conroy et al. (2009) and are continuously refined by research teams. As an example, with regards to the IMF, one uncertainty exists in the extremes of stellar masses (low and high). Key areas of an uncertain IMF are, for example, the assessment of mass-to-light ratio and interpretation of time evolution of galaxy populations.

### 5.5.3 SED-based properties from GAMA survey

The GAMA survey uses the software MAGPHYS (Multiwavelength Analysis of Galaxy Physical Properties) to interpret the observed data on galaxies (da Cunha et al., 2008; da Cunha & Charlot, 2011; Baldry et al., 2018; Driver et al., 2018). The GAMA survey photometry spans 21 bands from FUV to FIR (Driver et al., 2016; Wright et al., 2016). These data were used in Papers III and IV. How do we go backwards now from the observed SED to galaxy-wide properties?

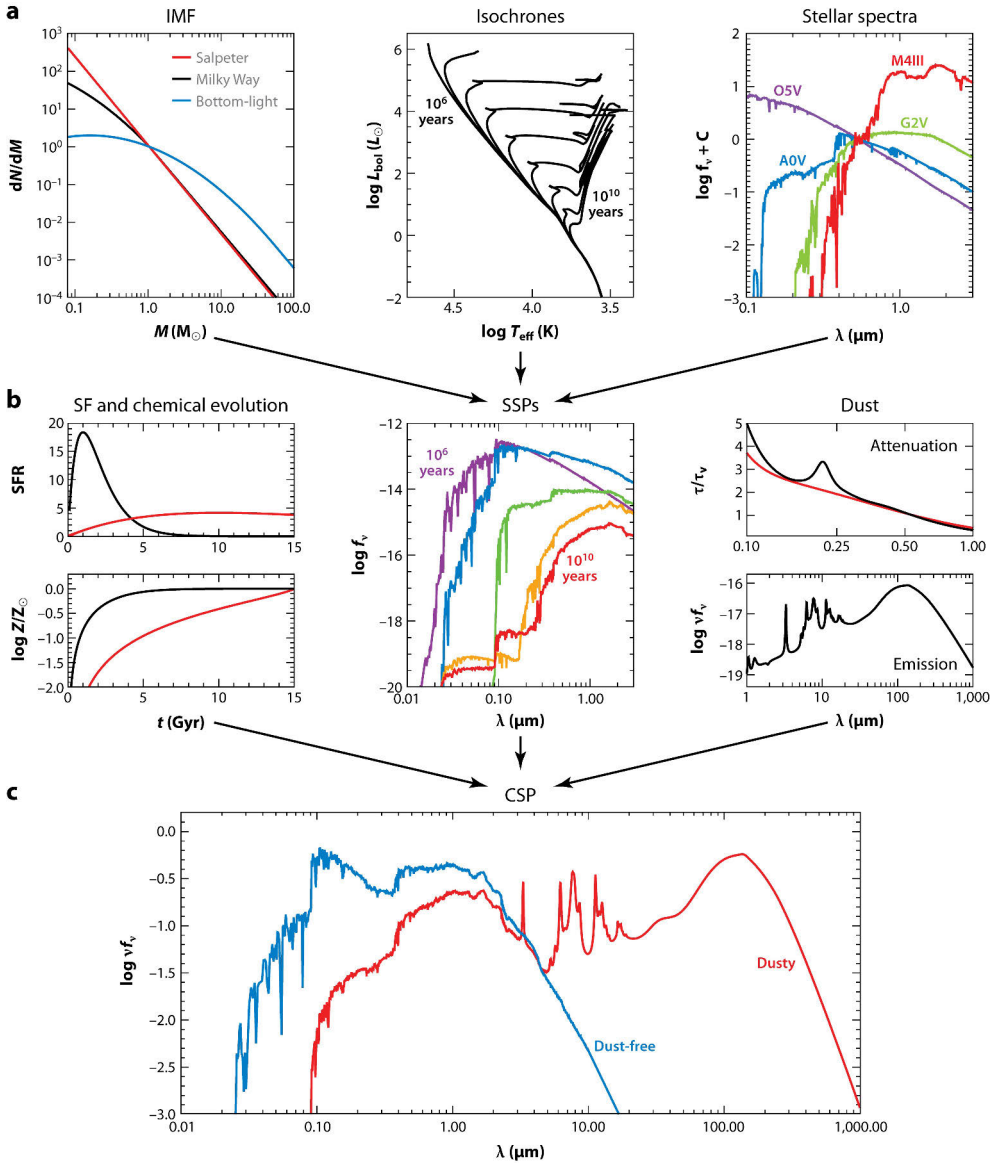
As a first step, a library of model SEDs is built matching the observed galaxy's redshift and photometric bands. Here, the stellar and ISM physical parameter ranges are wide. The detailed computation of the models is beyond the thesis introduction, and the reader is referred to the MAGPHYS documentation.


As a second step, the observed SED is compared (statistically) against the models in the library. In fact, the result does not give just one value for any single physical parameter. Rather, a more complete statistical assessment is given as an output for each parameter by the likelihood distribution and the associated percentiles. For details on the Bayesian approach, the reader again is referred to the statistics textbooks.

Of course, each assumption made may lead to uncertainties. For example, da Cunha et al. (2008) reports that stellar mass estimates can be different with different assumed IMF models. That's why in Paper IV, we provide the full list of used parameters and constraints. Pacifici et al. (2023) provides a comparison of several SED-fitting codes. More data points constrain better the SED model. In particular,

---

<sup>2</sup>It is also fascinating as when the SED techniques were developed, inspiring and audacious astronomers (such as Beatrice Tinsley) made contributions to methods and the original models were done without the sophisticated computers of today.



 Conroy C. 2013. Annu. Rev. Astron. Astrophys. 51:393–455

**Figure 42.** In the stellar population synthesis technique, first the SSP model is constructed, using the building blocks in the top panel: IMF, isochrones, and stellar spectra. The SSPs are scaled up to CSP by taking into account the “building materials” in the middle panel: SFH, chemical evolution, dust attenuation, and emission. The final CSP model is then displayed as the SED across the wavelength range considered. Source: Fig. 1 from Conroy 2013.





**Figure 43.** NOT telescope (Spain). Image Credit: Maria B. Stone.

for this work, since the GAMA survey provides 21 photometric points, it samples the FUV to FIR range well.

## 5.6 Telescopes

Several observatories around the world were used to obtain observations for work included in this thesis. I will briefly describe the telescope and the instruments here.

### 5.6.1 Nordic Optical Telescope

The Nordic Optical Telescope (NOT) is part of the Roque de los Muchachos Observatory, located in La Palma, one of the Canary Islands near the equator (Fig. 43). Its primary mirror is 2.6 m. NOT has optical and IR capabilities.

As part of this dissertation, I used NOT for obtaining optical spectra for several quasars and their neighboring galaxies in Paper I. I employed the ALFOSC instrument, which is an optical spectrograph and camera. NOT is a very user-friendly telescope. The observations were carried out in person by myself and by Kalle



**Figure 44.** GTC telescope in La Palma, Spain (dome on the right). Image Credit: Maria B. Stone.

Karhunen. Some dedicated night time was lost due to poor weather and observing “target-of-opportunity” objects (TOO) such as various transient objects (e.g., a TOO observation of an afterglow reported in GRB Coordinates Network, Circular Service, No. 34731).

## 5.6.2 Gran Tecan

The Gran Telescopio CANARIAS (GTC) is a giant 10 m class telescope (Fig. 44). It is a part of the same observatory as NOT, holding today the title of the largest telescope in optical and IR regimes. Its mirror is composed of 36 hexagonal units. It was used to obtain a set of optical spectra for quasars and their neighbors in Paper I by a collaborator. With such a large mirror, fainter objects can be studied. Thus our team was able to observe higher redshift quasar fields. In general, GTC spectra had a better S/N than with the NOT telescope.



**Figure 45.** NTT telescope at the La Silla Observatory (Chile). Image Credit: ESO/B. Tafreshi (twanight.org).

### 5.6.3 New Technology Telescope

For Paper II, I used the 4 meter class New Technology Telescope (NTT), which is located in the Southern Hemisphere (Fig. 45). It belongs to the La Silla Observatory in Chile. It is operated by the European Southern Observatory (ESO). The climate at the location of the NTT is ideal for astronomical observations due to the low humidity, high elevation, and great seeing. However, the arid high desert is a harsh environment for humans. I had the opportunity to observe five nights in person and a co-author observed another set of nights there. I used the multi-object spectroscopy of quasar fields in Paper II in the optical regime. The instrument used was the ESO Faint Object Spectrograph and Camera 2 (EFOSC2, Buzzoni et al. 1984). A set of normal galaxy fields was also observed as control.

## 6 Summary of the original publications

Millions de ces petites choses que l'on voit  
quelquefois dans le ciel.

A million of those little things that one sees  
sometimes in the sky.

---

“Le Petit Prince”  
Antoine de Saint-Exupéry  
Translated from French

### 6.1 Low-redshift quasars in the SDSS Stripe 82 – II. Associated companion galaxies and signature of star formation

There are two major mechanisms proposed to explain the AGN triggering and fueling of the SMBH activity in the center of galaxies. According to the merger scenario, two galaxies of similar mass interact. Through this interaction gas flows towards the center of the galaxy and is served as fuel for the central engine. The alternative thought is based on secular processes such as bar instabilities and/or minor mergers. In this latter mechanism the presence of a large neighboring galaxy is not required. There are galaxy simulations which model both mechanisms.

In this paper we set out to gain observational information on galaxies around quasars to see whether we can discover evidence in the environments of quasars. We obtained optical spectroscopy data from GTC and NOT for 22 quasar fields at  $z < 0.5$ , which are located in the equatorial region of the sky from Falomo et al. (2014) catalog.

This catalog is based on the SDSS DR7 quasar catalog (Schneider et al. 2010), restricted to low redshift ( $0.1 < z < 0.5$ ) and to the Stripe 82 region of the sky. The Stripe82 region of SDSS has deeper images than the rest of the survey. The Falomo et al. (2014) catalog comprises over 400 Type I quasars, with absolute magnitude  $M_i < -22$ . These quasars are spectroscopically confirmed.

We used longslit spectroscopy to obtain a spectrum of the quasar and of at least one candidate companion galaxy within 15 arcsec of the quasar. The companion spectra provided us with their spectroscopic redshifts. The redshifts were used to

check that the candidate companions are actually physically associated or whether they are chance projections in the same field. We also used the [O II] 3727Å emission line to estimate the SFR of the companions.

We combined our results with the results from previous observations of 12 other quasar fields. We find that 15/24 quasars had a physically associated companion galaxy in their vicinity. Moreover their SFR is moderate, and its distribution in SFR versus stellar mass plot is similar to that of randomly selected galaxies in the field. Our results showed that the quasars do not have a strong influence on the star formation of their associated companion galaxies.

For quasars, we positioned the long slits away from the center to attempt to capture the host galaxy light. Combined with previously published results, we detected host stellar signatures in 11 quasars, mostly showing absorption features of old stellar populations. Three cases exhibited typical signatures of a post-starburst spectrum.

## 6.2 Low-redshift quasars in the SDSS Stripe 82 — III. MOS observations

In this paper, we address the same questions as in Paper I but with an increased sample size, bringing the total number of observed quasar fields to 44 from the Falomo et al. (2014) catalog. Plus, we observe 11 inactive galaxies matched in mass and redshift to the quasar sample, as a control group for comparison. Additionally, we combine our results with all of the available spectra from the SDSS archives.

To obtain the observations, we used the MOS technique with NTT/EFOSC2 (ESO) in the Southern Hemisphere. With MOS technique, we were able to put multiple slitlets at the same time and thus collect optical spectra for several candidate companion galaxies at one observing instance around each quasar (or galaxy). For 12 quasar fields, we collected 76 spectra and for 11 inactive galaxy fields, we collected 53 spectra.

Our results, in combination with previously published data and archival data from SDSS, show that 19 out of 44 quasars have a physically associated galaxy. Compared to the inactive galaxy fields this fraction is not significantly different. On the other hand, the companions of quasars have a higher frequency of star formation signatures (e.g., emission lines) in their optical spectra, unlike those of inactive galaxies, suggesting a moderate link between the quasar activity and star formation processes in nearby galaxies.

### 6.3 Galaxy and Mass Assembly (GAMA): Low-redshift Quasars and Inactive Galaxies Have Similar Neighbors

Galaxy and Mass Assembly (GAMA) survey provides spectroscopic data for over 300 000 galaxies, covering an area of  $\sim 300 \text{ deg}^2$ , restricted to SDSS  $r$  band,  $r < 19.8$  mag, based on observations with the Anglo-Australian Telescope (AAT), which are supplemented by the archival spectra from previous surveys. In addition to spectra, GAMA survey database has a slew of ancillary products, such as 21-band photometry (UV, optical, IR), k-corrections, stellar population properties based on SED analysis with MAGPHYS software.

In this paper, we used the GAMA spectroscopic survey archival data to study the close environment of a large and homogeneous sample of quasar fields, and compared our results to a robust control sample of inactive galaxies.

The quasar data sample has 205 quasar fields and it is limited to the GAMA equatorial regions (Wethers et al., 2022). The quasar classification comes from the largest quasar catalog of Type I quasars (Large Quasar Astrometric Catalogue, LQAC-4, Gattano et al., 2018), where all of the quasars are confirmed by analysis of their optical spectra. Our data sample belongs to a redshift cut of  $0.1 < z < 0.35$ , as at this low- $z$  redshift interval GAMA is spectroscopically highly complete. Each quasar has apparent magnitude in SDSS  $r$  band brighter than the GAMA survey limit. Furthermore, as a control we created 200 Monte Carlo realizations of 205 inactive galaxies, matched in redshift and in stellar mass to the quasar sample. We identified the bright and close neighbors around each quasar (or a matched inactive galaxy) within about 2 Mpc comoving radius.

Each quasar field was analyzed to assess the number of neighbors within that volume. Furthermore, we compare properties for the neighbors: SFR, stellar mass, ages, colors, metallicities, morphologies — based on the ancillary data provided by the GAMA database. We used the two-sample Kolmogorov-Smirnov (KS) test to compare the distributions of properties for the population of quasar neighbors and inactive galaxy neighbors.

We found that there is no significant difference between physical, morphological, and SFH properties of quasar neighbors and inactive galaxy neighbors. Our results favor secular mechanisms and possibly minor mergers to explain AGN triggering.

## 6.4 Galaxy and Mass Assembly (GAMA): The Properties of Quasar Host Galaxies, Star Formation Histories, and Stellar Populations.

As a follow-up work for Paper III, we studied the quasar host galaxy SFH properties for the same sample of AGN. We then contrasted how the quasar hosts compared to the inactive galaxies (matched in redshift and mass) in terms of their SFH and stellar population properties.

To do this, we needed to account for the nuclear emission, since the quasar host light is contaminated with the photons from the SMBH activity. We used the CIGALE SED analysis tool to model the available 21-band photometric data from the GAMA survey for quasar hosts, and included an AGN component in these models. We then computed the quasar host stellar mass, SFR metrics, age, metallicity values.

Our results show that these low- $z$  quasar hosts mainly belong to the MS of SFGs, and the SFH path indicates that the AGN activity and SFR increase happen around the same time frame. Our data supports the secular and minor merger scenarios as triggers of nuclear activity at low redshifts, as it is possible that the star forming region within the galaxy may provide the fuel for the AGN activity.

## 6.5 The author's contribution to publications

### **Paper I. Low-redshift quasars in the SDSS Stripe 82 – II. Associated companion galaxies and signature of star formation**

The author performed the observations with NOT to collect the spectra for quasar fields and reduced the NOT data with IRAF. Further, the author analyzed all of the spectra, created the first draft of the manuscript, and led the paper through review and submission. The author's role is primary.

### **Paper II. Low-redshift quasars in the SDSS Stripe 82 — III. MOS observations**

The author contributed to the data collection step by performing five nights of observations at the La Silla Observatory. Furthermore, the author contributed to performing part of the analysis and drafting, as well as revising the manuscript.

### **Paper III. Galaxy and Mass Assembly (GAMA): Low-redshift Quasars and Inactive Galaxies Have Similar Neighbors**

The author performed the analysis, drafted the manuscript, and led it through the two-stage review process: (i) first with the GAMA collaboration and (ii) with the scientific journal. The author's role is primary.

### **Paper IV. Galaxy and Mass Assembly (GAMA): The Properties of Quasar Host Galaxies, Star Formation Histories, and Stellar Populations.**

The author performed the analysis, contributed to a major part of the writing of the paper, submitted it to a journal, and is leading the paper through the review. The author is one of the two main contributors to the paper.



## 7 Future research

— Well, boy, there's another day of the  
wonderful world gone forever.  
— New day tomorrow, though.

---

“Papa, you are crazy”  
William Saroyan

In this thesis we have studied Type I AGN environments at low redshifts. However, the other classes of AGN, such as the obscured (Type II) AGN constitute the majority of the AGN population. I extended the investigation to Type II AGN, and already one set of observations have been completed at the NOT (P67-022, Principal Investigator: Stone).

Zooming into the host galaxy and studying its morphology also provides an avenue to understand the immediate environment around a quasar. One may ask questions such as, do these low-redshift AGN preferentially reside in spirals or ellipticals (Stone et al. in prep.)? Does this depend on the presence of radio emission, BH properties, luminosity?

Furthermore, it is interesting to look at the environment at different redshifts to see how the role of AGN changes as the Universe evolved. To reach further distances and greater detail in the high- $z$  arena major space observatories such as *JWST* and radio interferometry (e.g., ALMA, VLBI) are used — they pave the way to future discoveries. Similarly, the *Nancy Grace Roman Space Telescope*, formerly known as the *Wide Field First InfraRed Survey Telescope (WFIRST)*, is scheduled to launch in a few years.

Moreover, in this study we observed the bright companions of AGN. The low surface brightness regime is also an unexplored frontier, where dimmer galaxies may provide clues to the formation and evolution processes. Here the Rubin Observatory (Legacy Survey of Space and Time, LSST) programs are set out to provide astronomers with the key data for exploration.

Overall, crucially, to answer the global questions on galaxy formation and evolution, cooperation between multiwavelength observations and comparative studies with simulations are necessary.

# List of References

- Abazajian K. N., et al., 2009, *ApJS*, 182, 543
- Abdurro'uf et al., 2022, *ApJS*, 259, 35
- Abell G. O., Corwin Harold G. J., Olowin R. P., 1989, *ApJS*, 70, 1
- Abraham R. G., van den Bergh S., Glazebrook K., Ellis R. S., Santiago B. X., Surma P., Griffiths R. E., 1996, *ApJS*, 107, 1
- Abramowicz M. A., Fragile P. C., 2013, *Living Reviews in Relativity*, 16, 1
- Acciari V. A., et al., 2021, *MNRAS*, 507, 1528
- Adams T. F., 1977, *ApJS*, 33, 19
- Ahumada R., et al., 2020, *ApJS*, 249, 3
- Aihara H., et al., 2022, *PASJ*, 74, 247
- Alexander D. M., Hickox R. C., 2012, *New A Rev.*, 56, 93
- Almeida A., et al., 2023, *ApJS*, 267, 44
- Annis J., et al., 2014, *ApJ*, 794, 120
- Antonucci R., 1993, *ARA&A*, 31, 473
- Antonuccio-Delogu V., Silk J., 2010, *AGN Feedback in Galaxy Formation*. Cambridge University Press, Cambridge, doi:10.1017/CBO9780511761386
- Astropy Collaboration et al., 2013, *A&A*, 558, A33
- Astropy Collaboration et al., 2018, *AJ*, 156, 123
- Bañados E., et al., 2018, *Nature*, 553, 473
- Babić A., Miller L., Jarvis M. J., Turner T. J., Alexander D. M., Croom S. M., 2007, *A&A*, 474, 755
- Bacon R., et al., 2010, in McLean I. S., Ramsay S. K., Takami H., eds, *Society of Photo-Optical Instrumentation Engineers (SPIE) Conference Series Vol. 7735, Ground-based and Airborne Instrumentation for Astronomy III*. p. 773508, doi:10.1117/12.856027
- Baldry I. K., Glazebrook K., Brinkmann J., Ivezić Ž., Lupton R. H., Nichol R. C., Szalay A. S., 2004a, *ApJ*, 600, 681
- Baldry I. K., Balogh M. L., Bower R., Glazebrook K., Nichol R. C., 2004b, in Allen R. E., Nanopoulos D. V., Pope C. N., eds, *American Institute of Physics Conference Series Vol. 743, The New Cosmology: Conference on Strings and Cosmology*. pp 106–119 (arXiv:astro-ph/0410603), doi:10.1063/1.1848322
- Baldry I. K., et al., 2014, *MNRAS*, 441, 2440
- Baldry I. K., et al., 2018, *MNRAS*, 474, 3875
- Baryshev Y., Teerikorpi P., 2012, *Fundamental Questions of Practical Cosmology*. Vol. 383, Springer, Dordrecht, doi:10.1007/978-94-007-2379-5
- Baugh C. M., Cole S., Frenk C. S., 1996, *MNRAS*, 283, 1361
- Beckmann Volker ., Shradler C., 2013, *Active Galactic Nuclei*. Wiley, Hoboken
- Begelman M. C., Blandford R. D., Rees M. J., 1980, *Nature*, 287, 307
- Bell E. F., de Jong R. S., 2000, *MNRAS*, 312, 497
- Bell E. F., McIntosh D. H., Katz N., Weinberg M. D., 2003, *ApJS*, 149, 289
- Benavides J. A., Sales L. V., Abadi M. G., 2020, *MNRAS*, 498, 3852
- Bessell M. S., 1990, *PASP*, 102, 1181
- Bessell M. S., 2005, *ARA&A*, 43, 293
- Binney J., Merrifield M., 1998, *Galactic Astronomy*. Princeton University Press

- Binney J., Tremaine S., 1987, *Galactic dynamics*. Princeton series in astrophysics, Princeton University Press
- Blandford R., Meier D., Readhead A., 2019, *ARA&A*, 57, 467
- Blanton M. R., et al., 2003, *ApJ*, 594, 186
- Böhm A., Ziegler B. L., 2016, *A&A*, 592, A64
- Boquien M., Burgarella D., Roehlly Y., Buat V., Ciesla L., Corre D., Inoue A. K., Salas H., 2019, *A&A*, 622, A103
- Boris N. V., Sodré L. J., Cypriano E. S., Santos W. A., de Oliveira C. M., West M., 2007, *ApJ*, 666, 747
- Böttcher M., Harris D. E., Krawczynski H., 2012, *Relativistic jets from active galactic nuclei*. Wiley-VCH, Weinheim, Germany
- Bournaud F., 2016, in Laurikainen E., Peletier R., Gadotti D., eds, *Astrophysics and Space Science Library* Vol. 418, *Galactic Bulges*. p. 355 ([arXiv:1503.07660](https://arxiv.org/abs/1503.07660)), doi:10.1007/978-3-319-19378-6\_13
- Bournaud F., Elmegreen B. G., Martig M., 2009, *ApJ*, 707, L1
- Bournaud F., Dekel A., Teyssier R., Cacciato M., Daddi E., Juneau S., Shankar F., 2011, *ApJ*, 741, L33
- Bournaud F., et al., 2012, *ApJ*, 757, 81
- Bowers R. L., Deeming T., 1984b, *Astrophysics*. 1, Stars. Jones and Bartlett, Boston
- Bowers R. L., Deeming T., 1984a, *Astrophysics II : interstellar matter and galaxies*. Jones and Bartlett Publishers Boston, Boston
- Bruzual G., Charlot S., 2003, *MNRAS*, 344, 1000
- Bullock J. S., Boylan-Kolchin M., 2017, *ARA&A*, 55, 343
- Buzzoni B., et al., 1984, *The Messenger*, 38, 9
- Byrd G. G., Chernin A. D., Valtonen M. J., 2007, *Cosmology : foundations and frontiers*. URSS : KomKniga Moscow, Moscow
- Byrd G., Chernin A. D., Teerikorpi P., Valtonen M., 2012, *Paths to Dark Energy: Theory and Observation*, 1. Aufl. edn. De Gruyter Studies in Mathematical Physics Vol. 2, De Gruyter, Germany
- Cappellari M., 2016, *ARA&A*, 54, 597
- Cappellari M., et al., 2011, *MNRAS*, 413, 813
- Caputi K. I., et al., 2017, *ApJ*, 849, 45
- Cardamone C., et al., 2009, *MNRAS*, 399, 1191
- Castellano M., et al., 2022, *ApJ*, 938, L15
- Cattaneo A., et al., 2009, *Nature*, 460, 213
- Chen C.-Y., Hwang C.-Y., Ko C.-M., 2016, *ApJ*, 830, 123
- Chester C., Roberts M. S., 1964, *AJ*, 69, 635
- Cheung E., et al., 2015, *MNRAS*, 447, 506
- Cirasuolo M., Magliocchetti M., Celotti A., Danese L., 2003, *MNRAS*, 341, 993
- Circosta C., et al., 2018, *A&A*, 620, A82
- Cisternas M., Jahnke K., 2015, *Highlights of Astronomy*, 16, 344
- Cisternas M., et al., 2011, *ApJ*, 726, 57
- Cisternas M., Sheth K., Salvato M., Knapen J. H., Civano F., Santini P., 2015, *ApJ*, 802, 137
- Combes F., 2001, in Aretxaga I., Kunth D., Mújica R., eds, *Advanced Lectures on the Starburst-AGN*. p. 223 ([arXiv:astro-ph/0010570](https://arxiv.org/abs/astro-ph/0010570)), doi:10.1142/9789812811318\_0006
- Combes F., 2021, *Active Galactic Nuclei: Fueling and Feedback*. IOP Publishing, Bristol, UK, doi:10.1088/2514-3433/ac2a27
- Combes F., Boisse P., Mazure A., Blanchard A., Seymour M., 1995, *Galaxies and Cosmology*. Springer, Berlin
- Conroy C., 2013, *ARA&A*, 51, 393
- Conroy C., Gunn J. E., 2010, *ApJ*, 712, 833
- Conroy C., Gunn J. E., White M., 2009, *ApJ*, 699, 486
- Conselice C. J., et al., 2004, *ApJ*, 600, L139
- Cowie L. L., Hu E. M., Songaila A., 1995, *AJ*, 110, 1576
- Crain R. A., van de Voort F., 2023, *Annual Review of Astronomy and Astrophysics*, 61, 473

- Dasyra K. M., et al., 2007, *ApJ*, 657, 102
- Davies R. L., Efstathiou G., Fall S. M., Illingworth G., Schechter P. L., 1983, *ApJ*, 266, 41
- Decarli R., Treves A., Falomo R., 2009, *MNRAS*, 396, L31
- Decarli R., et al., 2017, *Nature*, 545, 457
- Decarli R., et al., 2023, *A&A*, 673, A157
- Di Matteo T., Springel V., Hernquist L., 2005, *Nature*, 433, 604
- Djorgovski S., 1991, in Crampton D., ed., *Astronomical Society of the Pacific Conference Series Vol. 21, The Space Distribution of Quasars*. p. 349
- Dodelson S., 2003, *Modern cosmology*. Academic Press, An Imprint of Elsevier, San Diego, California
- Doi M., et al., 2010, *AJ*, 139, 1628
- Draper A. R., Ballantyne D. R., 2012, *ApJ*, 751, 72
- Dressler A., 1980, *ApJ*, 236, 351
- Dressler A., Lynden-Bell D., Burstein D., Davies R. L., Faber S. M., Terlevich R., Wegner G., 1987, *ApJ*, 313, 42
- Driver S. P., Robotham A. S. G., 2010, *MNRAS*, 407, 2131
- Driver S. P., et al., 2016, *MNRAS*, 455, 3911
- Driver S. P., et al., 2018, *MNRAS*, 475, 2891
- Driver S. P., et al., 2022, *MNRAS*,
- Du M., Debattista V. P., Shen J., Ho L. C., Erwin P., 2017, *ApJ*, 844, L15
- Dubois Y., Devriendt J., Slyz A., Teyssier R., 2012, *MNRAS*, 420, 2662
- Dubois Y., et al., 2014, *MNRAS*, 444, 1453
- Dubois Y., et al., 2021, *A&A*, 651, A109
- Dyson J. E. J. E., 1997, *The physics of the interstellar medium*, 2nd ed. edn. The graduate series in astronomy, Institute of Physics Publishing, Bristol
- Eftekharzadeh S., Myers A. D., Hennawi J. F., Djorgovski S. G., Richards G. T., Mahabal A. A., Graham M. J., 2017, *MNRAS*, 468, 77
- Ellison S. L., Patton D. R., Simard L., McConnachie A. W., Baldry I. K., Mendel J. T., 2010, *MNRAS*, 407, 1514
- Ellison S. L., Patton D. R., Mendel J. T., Scudder J. M., 2011, *MNRAS*, 418, 2043
- Ellison S. L., Mendel J. T., Patton D. R., Scudder J. M., 2013, *MNRAS*, 435, 3627
- Ellison S. L., Teimoorinia H., Rosario D. J., Mendel J. T., 2016, *MNRAS*, 458, L34
- Elmegreen B. G., Elmegreen D. M., 2010, *ApJ*, 722, 1895
- Elmegreen D. M., Elmegreen B. G., Rubin D. S., Schaffer M. A., 2005, *ApJ*, 631, 85
- Elmegreen D. M., Elmegreen B. G., Ravindranath S., Coe D. A., 2007a, *ApJ*, 658, 763
- Elmegreen D. M., Elmegreen B. G., Ferguson T., Mullan B., 2007b, *ApJ*, 663, 734
- Elvis M., 2009, *Proceedings of the International Astronomical Union*, 5, 55
- Elvis M., et al., 1994, *ApJS*, 95, 1
- Emerson D., 1997, *Interpreting Astronomical Spectra*. J. Wiley and Sons, Chichester
- Faber S. M., Jackson R. E., 1976, *ApJ*, 204, 668
- Fabian A. C., 2012, *ARA&A*, 50, 455
- Falomo R., Bettoni D., Karhunen K., Kotilainen J. K., Uslenghi M., 2014, *MNRAS*, 440, 476
- Fan X., et al., 2001, *AJ*, 122, 2833
- Fan X., et al., 2006, *AJ*, 132, 117
- Fan X., Bañados E., Simcoe R. A., 2023, *Annual Review of Astronomy and Astrophysics*, 61, 373
- Fanidakis N., et al., 2012, *MNRAS*, 419, 2797
- Farina E. P., Falomo R., Treves A., 2011, *MNRAS*, 415, 3163
- Ferrarese L., 2002, *ApJ*, 578, 90
- Ferrarese L., Merritt D., 2000, *ApJ*, 539, L9
- Ferrarese L., et al., 2006, *ApJ*, 644, L21
- Florez J., et al., 2020, *MNRAS*, 497, 3273
- Floyd D. J. E., Kukula M. J., Dunlop J. S., McLure R. J., Miller L., Percival W. J., Baum S. A., O'Dea C. P., 2004, *MNRAS*, 355, 196

- Fogasy J., Knudsen K. K., Lagos C. D. P., Drouart G., Gonzalez-Perez V., 2017, *A&A*, 597, A123
- Förster Schreiber N. M., Wuyts S., 2020, *Annual Review of Astronomy and Astrophysics*, 58, 661
- Fujita Y., 2023, *MNRAS*, 518, 4551
- Galilei G., 1655, *Sidereus nuncius magna, longeque admirabilia spectacula pandens ... quae a Galileo Galileo*, doi:10.3931/e-rara-2845.
- Gallagher J. S., Bushouse H., Hunter D. A., 1989, *AJ*, 97, 700
- Gao F., et al., 2017, *ApJ*, 834, 52
- Gattano C., Andrei A. H., Coelho B., Souchay J., Barache C., Taris F., 2018, *A&A*, 614, A140
- Gebhardt K., et al., 2000, *ApJ*, 539, L13
- Giavalisco M., Steidel C. C., Macchetto F. D., 1996, *ApJ*, 470, 189
- Gilbank D. G., Baldry I. K., Balogh M. L., Glazebrook K., Bower R. G., 2010, *MNRAS*, 405, 2594
- Gilbank D. G., Gladders M. D., Yee H. K. C., Hsieh B. C., 2011, *AJ*, 141, 94
- Graham A. W., Erwin P., Caon N., Trujillo I., 2001, *ApJ*, 563, L11
- Green P. J., Myers A. D., Barkhouse W. A., Aldcroft T. L., Trichas M., Richards G. T., Ruiz Á., Hopkins P. F., 2011, *ApJ*, 743, 81
- Grier C. J., et al., 2012, *ApJ*, 755, 60
- Gunn J. E., Peterson B. A., 1965, *ApJ*, 142, 1633
- Gupta A., Mathur S., Kingsbury J., Das S., Krongold Y., 2023, *Nature Astronomy*, 7, 799
- Haines C. P., Clowes R. G., Campusano L. E., Adamson A. J., 2001, *MNRAS*, 323, 688
- Hamill P., 2010, *Intermediate dynamics*. Jones and Bartlett Publishers Sudbury, Mass., Sudbury, Mass.
- Häring N., Rix H.-W., 2004, *ApJ*, 604, L89
- Harrison C., 2014, PhD thesis, Durham University, UK
- Harrison C. M., 2017, *Nature Astronomy*, 1, 0165
- Heidt J., 2022, *Astronomy in the Near-Infrared - Observing Strategies and Data Reduction Techniques*. *Astrophysics and Space Science Library* Vol. 467, *Ap&SS*, doi:10.1007/978-3-030-98441-0
- Hennawi J. F., et al., 2006, *AJ*, 131, 1
- Hennawi J. F., et al., 2010, *ApJ*, 719, 1672
- Henry R. B. C., Worthey G., 1999, *PASP*, 111, 919
- Hickox R. C., Alexander D. M., 2018, *ARA&A*, 56, 625
- Hirschmann M., Dolag K., Saro A., Bachmann L., Borgani S., Burkert A., 2014, *MNRAS*, 442, 2304
- Hogg D. W., 1999, arXiv e-prints, pp astro-ph/9905116
- Hogg D. W., Baldry I. K., Blanton M. R., Eisenstein D. J., 2002, arXiv e-prints, pp astro-ph/0210394
- Hong J., Im M., Kim M., Ho L. C., 2015, *ApJ*, 804, 34
- Hönig S. F., 2019, *ApJ*, 884, 171
- Hopkins P. F., 2012, *MNRAS*, 420, L8
- Hopkins A. M., et al., 2013, *MNRAS*, 430, 2047
- Hovatta T., Lindfors E., 2019, *New A Rev.*, 87, 101541
- Hubble E. P., 1926, *ApJ*, 64, 321
- Hubble E., 1929, *Proceedings of the National Academy of Science*, 15, 168
- Hubble E. P., 1936, *Realm of the Nebulae*. Dover Publications, Inc., 180 Varick Street, New York, N. Y. 10014
- Husemann B., Harrison C. M., 2018, *Nature Astronomy*, 2, 196
- Inayoshi K., Visbal E., Haiman Z., 2020, *ARA&A*, 58, 27
- Jiang F., van den Bosch F. C., 2014, *MNRAS*, 440, 193
- Jones M. H., Lambourne R. J., 2004, *An introduction to galaxies and cosmology*. Cambridge Univ. Press Cambridge, Cambridge
- Kalfountzou E., Civano F., Elvis M., Trichas M., Green P., 2014, *MNRAS*, 445, 1430
- Kartaltepe J. S., et al., 2023, *ApJ*, 946, L15
- Kauffmann G., et al., 2003a, *MNRAS*, 341, 33
- Kauffmann G., et al., 2003b, *MNRAS*, 341, 54
- Kaviraj S., et al., 2017, *MNRAS*, 467, 4739
- Kennicutt R. C. J., 1983, *ApJ*, 272, 54

- Kennicutt Robert C. J., 1992, *ApJ*, 388, 310
- Kennicutt Jr. R. C., 1998, *ARA&A*, 36, 189
- King A., 2008, *New A Rev.*, 52, 253
- Klypin A., Kravtsov A. V., Valenzuela O., Prada F., 1999, *ApJ*, 522, 82
- Knapen J. H., Cepa J., Beckman J. E., Soledad del Rio M., Pedlar A., 1993, *ApJ*, 416, 563
- Kolcu T., et al., 2023, *MNRAS*, 524, 207
- Kormendy J., 1977, *ApJ*, 218, 333
- Kormendy J., Djorgovski S., 1989, *ARA&A*, 27, 235
- Kormendy J., Ho L. C., 2013, *ARA&A*, 51, 511
- Kormendy J., Richstone D., 1995, *ARA&A*, 33, 581
- Krolik J. H., 1999, *Active galactic nuclei : from the central black hole to the galactic environment*. Princeton University Press, Princeton, N.J.
- Kumar P., Johnson J. L., 2010, *MNRAS*, 404, 2170
- Kurtz M. J., Mink D. J., 1998, *PASP*, 110, 934
- Kurtz M. J., Mink D. J., Wyatt W. F., Fabricant D. G., Torres G., Kriss G. A., Tonry J. L., 1992, in Worrall D. M., Biemesderfer C., Barnes J., eds, *Astronomical Society of the Pacific Conference Series Vol. 25, Astronomical Data Analysis Software and Systems I*. p. 432
- Kutner M. L., 2003, *Astronomy: A Physical Perspective*. Cambridge University Press, Cambridge, U.K.
- Lagache G., Puget J.-L., Dole H., 2005, *ARA&A*, 43, 727
- Lambrides E. L., et al., 2021, *ApJ*, 919, 129
- Lawrence A., et al., 2007, *MNRAS*, 379, 1599
- Leipski C., et al., 2014, *ApJ*, 785, 154
- Lemson G., Virgo Consortium t., 2006, arXiv e-prints, pp astro-ph/0608019
- Li W., Inayoshi K., Onoue M., Toyouchi D., 2023, *ApJ*, 950, 85
- Liddle A., Loveday J., 2008, *The Oxford Companion to Cosmology*. Oxford University Press, doi:10.1093/acref/9780198608585.001.0001, <https://www.oxfordreference.com/view/10.1093/acref/9780198608585.001.0001/acref-9780198608585>
- Lietzen H., et al., 2009, *A&A*, 501, 145
- Linder E. V., 1997, *First principles of cosmology*. Addison Wesley Longman Harlow, England, Harlow, England
- Linder E. V., 2003, *Phys. Rev. Lett.*, 90, 091301
- Lindsay S. N., et al., 2014, *MNRAS*, 440, 1527
- Lintott C. J., et al., 2008, *MNRAS*, 389, 1179
- Liske J., 2000, *MNRAS*, 319, 557
- Liske J., et al., 2015, *MNRAS*, 452, 2087
- Longair M., 1998, *Galaxy Formation. Astronomy and Astrophysics Library*, Springer Berlin Heidelberg Berlin, Heidelberg, Berlin, Heidelberg, <https://doi.org/10.1007/978-3-662-03571-9>
- Longair M. S., 2008, *Galaxy formation, 2nd ed. edn. Astronomy and astrophysics library*, Springer, Berlin
- Lyke B. W., et al., 2020, *ApJS*, 250, 8
- Lynden-Bell D., 1969, *Nature*, 223, 690
- Madau P., Dickinson M., 2014, *ARA&A*, 52, 415
- Madau P., Ferguson H. C., Dickinson M. E., Giavalisco M., Steidel C. C., Fruchter A., 1996, *MNRAS*, 283, 1388
- Maiolino R., et al., 2024, *Nature*, 627, 59
- Menci N., Gatti M., Fiore F., Lamastra A., 2014, *A&A*, 569, A37
- Mihos C., 2003, arXiv e-prints, pp astro-ph/0305512
- Mo H., 2010, *Galaxy formation and evolution*. Cambridge University Press, Cambridge
- Moore B., Katz N., Lake G., Dressler A., Oemler A., 1996, *Nature*, 379, 613
- Moore B., Lake G., Quinn T., Stadel J., 1999, *MNRAS*, 304, 465
- Morris M., Serabyn E., 1996, *ARA&A*, 34, 645

- Mortlock D. J., Webster R. L., Francis P. J., 1999, *MNRAS*, 309, 836
- Moster B. P., Somerville R. S., Newman J. A., Rix H.-W., 2011, *ApJ*, 731, 113
- Mou G., et al., 2023, *Nature Communications*, 14, 781
- Naab T., Ostriker J. P., 2017, *ARA&A*, 55, 59
- Nadler E. O., Benson A., Driskell T., Du X., Gluscevic V., 2023, *MNRAS*, 521, 3201
- Natarajan P., Pacucci F., Ricarte A., Bogdán Á., Goulding A. D., Cappelluti N., 2024, *ApJ*, 960, L1
- Nelson S., 2008, *Nature*, 455, 36
- Nelson D., et al., 2015, *Astronomy and Computing*, 13, 12
- Netzer H., 2013, *The Physics and Evolution of Active Galactic Nuclei*. Cambridge University Press, Cambridge
- Nilsson K., et al., 2018, *A&A*, 620, A185
- Orban de Xivry G., Davies R., Schartmann M., Komossa S., Marconi A., Hicks E., Engel H., Tacconi L., 2011, *MNRAS*, 417, 2721
- Pacifici C., et al., 2023, *ApJ*, 944, 141
- Padovani P., et al., 2017, *A&A Rev.*, 25, 2
- Peebles P. J. E., 1982, *ApJ*, 263, L1
- Peebles P. J. E., 1993, *Principles of Physical Cosmology*. Princeton University Press
- Peebles P. J., Ratra B., 2003, *Reviews of Modern Physics*, 75, 559
- Peng C. Y., Ho L. C., Impey C. D., Rix H.-W., 2002, *AJ*, 124, 266
- Peng C. Y., Ho L. C., Impey C. D., Rix H.-W., 2010, *AJ*, 139, 2097
- Perlmutter S., et al., 1999, *ApJ*, 517, 565
- Péroux C., Howk J. C., 2020, *ARA&A*, 58, 363
- Peterson B. M., 1997, *An Introduction to Active Galactic Nuclei*. Cambridge University Press
- Peterson B. M., 2012, *An introduction to active galactic nuclei*. Cambridge University Press
- Peterson B. A., Bolton J. G., 1973, *Astrophys. Lett.*, 13, 187
- Phillipps S., 2005, *The Structure and Evolution of Galaxies*. John Wiley and Sons, Ltd
- Piattella O., 2018, in *Springer, Cham, Switzerland. UNITEXT for physics*. Springer, Cham, Switzerland
- Planck Collaboration et al., 2020, *A&A*, 641, A1
- Predehl P., et al., 2020, *Nature*, 588, 227
- Predehl P., et al., 2021, *A&A*, 647, A1
- Pringle J. E., 1981, *ARA&A*, 19, 137
- Ramos Almeida C., Ricci C., 2017, *Nature Astronomy*, 1, 679
- Rantala A., Johansson P. H., Naab T., Thomas J., Frigo M., 2019, *ApJ*, 872, L17
- Rees M. J., 1999, in Holt S., Smith E., eds, *American Institute of Physics Conference Series Vol. 470, After the Dark Ages: When Galaxies were Young (the Universe at  $2 < Z < 5$ )*. pp 13–23, doi:10.1063/1.58643
- Rees M. J., Ostriker J. P., 1977, *MNRAS*, 179, 541
- Renzini A., 2006, *ARA&A*, 44, 141
- Reyes R., et al., 2008, *AJ*, 136, 2373
- Ridpath I., 2018, *A dictionary of astronomy, third edition edn*. Oxford University Press [Oxford], [Oxford], <https://doi.org/10.1093/acref/9780191851193.001.0001>
- Riess A. G., et al., 1998, *AJ*, 116, 1009
- Roberts M. S., Haynes M. P., 1994, *ARA&A*, 32, 115
- Robson I., 1996, *Active galactic nuclei*. John Wiley and Sons, Praxis Publishing
- Rodrigo C., Solano E., 2020, in *XIV.0 Scientific Meeting (virtual) of the Spanish Astronomical Society*. p. 182
- Rodrigo C., Solano E., Bayo A., 2012, *SVO Filter Profile Service Version 1.0, IVOA Working Draft 15 October 2012*, doi:10.5479/ADS/bib/2012ivoa.rept.1015R
- Romanishin W., 2002, *An Introduction to Astronomical Photometry Using CCDs*, <https://www1.phys.vt.edu/~jhs/phys3154/CCDPhotometryBook.pdf>

- Roos M., 2015, *Introduction to Cosmology*. New York Academy of Sciences Ser, John Wiley & Sons, Incorporated Newark, Newark, <https://public.ebookcentral.proquest.com/choice/PublicFullRecord.aspx?p=7104233>
- Rossiter M. W., 2012, *Women scientists in America : forging a new world since 1972*. Johns Hopkins University Press Baltimore, Md., Baltimore, Md.
- Roth G. D., 1975, *Astronomy: a handbook..* Springer-Verlag, Berlin
- Rowan-Robinson M., 2000, *MNRAS*, 316, 885
- Salpeter E. E., 1955, *ApJ*, 121, 161
- Salpeter E. E., 1964, *ApJ*, 140, 796
- Sandrinelli A., Falomo R., Treves A., Farina E. P., Uslenghi M., 2014, *MNRAS*, 444, 1835
- Sandrinelli A., Falomo R., Treves A., Scarpa R., Uslenghi M., 2018, *MNRAS*, 474, 4925
- Sanghvi J., Kotilainen J. K., Falomo R., Decarli R., Karhunen K., Uslenghi M., 2014, *MNRAS*, 445, 1261
- Sarkar K. C., 2024, *A&A Rev.*, 32, 1
- Satyapal S., Ellison S. L., McAlpine W., Hickox R. C., Patton D. R., Mendel J. T., 2014, *MNRAS*, 441, 1297
- Sawala T., et al., 2016, *MNRAS*, 457, 1931
- Scannapieco E., Silk J., Bouwens R., 2005, *ApJ*, 635, L13
- Schawinski K., et al., 2014, *MNRAS*, 440, 889
- Schindler S., 1999, arXiv e-prints, pp astro-ph/9909042
- Schneider P., 2006, *Extragalactic Astronomy and Cosmology*. Springer
- Scoville N., et al., 2007, *ApJS*, 172, 38
- Scudder J. M., Ellison S. L., Torrey P., Patton D. R., Mendel J. T., 2012, *MNRAS*, 426, 549
- Seyfert C. K., 1943, *ApJ*, 97, 28
- Shakura N. I., 2014, *Physics Uspekhi*, 57, 407
- Shakura N. I., Sunyaev R. A., 1973, *A&A*, 24, 337
- Shapley H., 1938, *Nature*, 142, 715
- Sheth K., et al., 2008, *ApJ*, 675, 1141
- Silk J., Rees M. J., 1998, *A&A*, 331, L1
- Silk J., Di Cintio A., Dvorkin I., 2014, in *Proceedings of the International School of Physics 'Enrico Fermi' Course 186 'New Horizons for Observational Cosmology' Vol. 186*. pp 137–187 (arXiv:1312.0107), doi:10.3254/978-1-61499-476-3-137
- Silverman J. D., et al., 2011, *ApJ*, 743, 2
- Singh A., et al., 2023, *ApJ*, 953, 64
- Smethurst R. J., et al., 2024, *MNRAS*, 527, 10855
- Smith M. G., Wright A. E., 1980, *MNRAS*, 191, 871
- Söchting I. K., Clowes R. G., Campusano L. E., 2001, in Clowes R., Adamson A., Bromage G., eds, *Astronomical Society of the Pacific Conference Series Vol. 232, The New Era of Wide Field Astronomy*. p. 123 (arXiv:astro-ph/0111115)
- Söchting I. K., Clowes R. G., Campusano L. E., 2002, *MNRAS*, 331, 569
- Söchting I. K., Clowes R. G., Campusano L. E., 2004, *MNRAS*, 347, 1241
- Somerville R. S., Davé R., 2015, *ARA&A*, 53, 51
- Somerville R. S., Lee K., Ferguson H. C., Gardner J. P., Moustakas L. A., Giavalisco M., 2004, *ApJ*, 600, L171
- Sparke L. S., Gallagher John S. I., 2007, *Galaxies in the Universe: An Introduction*. Cambridge Univ. Press, Cambridge
- Springel V., et al., 2005, *Nature*, 435, 629
- Stone M. B., 2017, Master's thesis, San Jose State University, California
- Straughn A. N., Ryan R. E., Cohen S. H., Hathi N. P., Windhorst R. A., Pasquali A., 2004, in *American Astronomical Society Meeting Abstracts*. p. 94.17
- Straughn A. N., Cohen S. H., Ryan R. E., Hathi N. P., Windhorst R. A., Jansen R. A., 2005, in *American Astronomical Society Meeting Abstracts*. p. 22.14



Su M., Slatyer T. R., Finkbeiner D. P., 2010, *ApJ*, 724, 1044

Sutton E. C., 2011, *Observational Astronomy*. Cambridge University Press, Cambridge

Tanaka I., Yamada T., Aragón-Salamanca A., Kodama T., Miyaji T., Ohta K., Arimoto N., 2000, *ApJ*, 528, 123

Tanihata I., Toki H., Kajino T., 2023, *Handbook of nuclear physics*. Springer Nature reference, Springer Singapore, Singapore, doi:10.1007/978-981-19-6345-2, <https://www.vlebooks.com/vleweb/product/openreader?id=none&isbn=9789811963452>

Thomas J., Saglia R. P., Bender R., Erwin P., Fabricius M., 2014, *ApJ*, 782, 39

Thompson L. A., 2011, arXiv e-prints, p. arXiv:1108.4864

Tinsley B. M., 1980, *Fund. Cosmic Phys.*, 5, 287

Tody D., 1986, in Crawford D. L., ed., *Society of Photo-Optical Instrumentation Engineers (SPIE) Conference Series Vol. 627, Instrumentation in astronomy VI*. p. 733, doi:10.1117/12.968154

Tody D., 1993, in Hanisch R. J., Brissenden R. J. V., Barnes J., eds, *Astronomical Society of the Pacific Conference Series Vol. 52, Astronomical Data Analysis Software and Systems II*. p. 173

Tohill C., Ferreira L., Conselice C. J., Bamford S. P., Ferrari F., 2021, *ApJ*, 916, 4

Toomre A., Toomre J., 1972, *ApJ*, 178, 623

Trimble V., 1995, *PASP*, 107, 1133

Truebenbach A. E., Darling J., 2018, *ApJ*, 868, 69

Tully R. B., Fisher J. R., 1977, *A&A*, 54, 661

Tully R. B., Pierce M. J., Huang J.-S., Saunders W., Verheijen M. A. W., Witchalls P. L., 1998, *AJ*, 115, 2264

Urry C. M., Padovani P., 1995, *PASP*, 107, 803

Valtonen M. J., et al., 2008, *Nature*, 452, 851

Vogelsberger M., et al., 2014a, *MNRAS*, 444, 1518

Vogelsberger M., et al., 2014b, *Nature*, 509, 177

Vogelsberger M., Marinacci F., Torrey P., Puchwein E., 2020, *Nature Reviews Physics*, 2, 42

Volonteri M., Habouzit M., Colpi M., 2021, *Nature Reviews Physics*, 3, 732

Walcher J., Groves B., Budavári T., Dale D., 2011, *Ap&SS*, 331, 1

Wang F., et al., 2021, *ApJ*, 907, L1

Wenger M., et al., 2000, *A&AS*, 143, 9

Wethers C. F., et al., 2022, *ApJ*, 928, 192

White S. D. M., Rees M. J., 1978, *MNRAS*, 183, 341

Wolf M. J., Sheinis A. I., 2008, *AJ*, 136, 1587

Wright E. L., 2006, *PASP*, 118, 1711

Wright A. H., et al., 2016, *MNRAS*, 460, 765

Yamanoi H., et al., 2012, *AJ*, 144, 40

Yan H., Ma Z., Ling C., Cheng C., Huang J.-S., 2023, *ApJ*, 942, L9

Yang C., Ge J.-Q., Lu Y.-J., 2019, *Research in Astronomy and Astrophysics*, 19, 177

Yang G., et al., 2020, *MNRAS*, 491, 740

Yang H. Y. K., Ruszkowski M., Zweibel E. G., 2022a, *Nature Astronomy*, 6, 584

Yang G., et al., 2022b, *ApJ*, 927, 192

Yee H. K. C., 1992, in Filippenko A. V., ed., *Astronomical Society of the Pacific Conference Series Vol. 31, Relationships Between Active Galactic Nuclei and Starburst Galaxies*. p. 417

York D. G., et al., 2000, *AJ*, 120, 1579

Zhuang M.-Y., Ho L. C., 2023, *Nature Astronomy*, 7, 1376

da Cunha E., Charlot S., 2011, *MAGPHYS: Multi-wavelength Analysis of Galaxy Physical Properties* (ascl:1106.010)

da Cunha E., Charlot S., Elbaz D., 2008, *MNRAS*, 388, 1595

de Carvalho E., Bernui A., Carvalho G. C., Novaes C. P., Xavier H. S., 2018, *J. Cosmology Astropart. Phys.*, 2018, 064

van den Bergh S., Abraham R. G., Ellis R. S., Tanvir N. R., Santiago B. X., Glazebrook K. G., 1996, *AJ*, 112, 359



**TURUN  
YLIOPISTO**  
UNIVERSITY  
OF TURKU

ISBN 978-951-29-9720-6 (PRINT)  
ISBN 978-951-29-9721-3 (PDF)  
ISSN 0082-7002 (Print)  
ISSN 2343-3175 (Online)